Title
Germinal Center Dark and Light Zone Organization and Cellular Dynamics

Author
Allen, Christopher David Caballero

Publication Date
2007-06-15

Peer reviewed|Thesis/dissertation

Germinal Center Dark and Light Zone Organization and Cellular Dynamics

by

Christopher David Caballero Allen

DISSERTATION

Submitted in partial satisfaction of the requirements for the degree of

DOCTOR OF PHILOSOPHY

in

Biomedical Sciences

in the

GRADUATE DIVISION

of the

UNIVERSITY OF CALIFORNIA, SAN FRANCISCO

This dissertation is dedicated to my parents,

Yvonne Caballero-Allen and Tim Allen,

for giving me the opportunities and encouragement

to become a scientist.

ACKNOWLEDGMENTS

First and foremost, I would like to acknowledge the exceptional mentorship and support of Jason Cyster. Back in 2002 when I first rotated in the lab, Jason took it upon himself to mentor me directly at the bench, which proved to be one of the most influential and challenging experiences that I have ever had as a student. During this rotation and the first few years after I joined the lab, I learned a tremendous amount from Jason's technical prowess, creative experimental design, superior command of the literature, and intense devotion to research. As I grew increasingly independent, Jason continued to devote remarkable amounts of time and energy to meeting with me to discuss data and ideas as well as providing prompt and detailed feedback on my writing and presentations. Jason has also been an outstanding role model as a scientist, in the way in which he develops models based on existing evidence, then tests the models, and finally revises the models based on the new data.

I have also been fortunate to be mentored by my other two thesis committee members: Tony DeFranco and Art Weiss. I've learned a great deal from Tony's vast knowledge of immunology and his thoughtful feedback and curiosity about my research. I've also greatly appreciated Art's expertise, rigorousness, and commitment to mentorship. Both Tony and Art have been very supportive in helping me develop my future plans.

Among the most interesting experiences that I have had as a graduate student have been the interactions with the people in the lab whose desks and benches were in close proximity to mine. Spending most of our waking hours together led to the

formation of strong bonds and provided deep insights into each others' personalities. When our lab was located on the third floor of HSE, I had a unique desk and bench setup where my desk was near that of Karin Reif but my bench was in a bay with Mehrdad Matloubian, Taka Okada, and Charles Lo. I came to greatly appreciate Karin's understated humor and meticulous organization during that time. She and I also tended to be the 'late-comers' to the lab each day. Once Mehrdad grew tired of trying to kick me out of his bay, I deeply enjoyed his unique sense of humor, his perspective on life, and the friendship that we developed. I don't think I have ever seen anyone work as hard as Mehrdad did in those days. I was very fortunate to share a bench with Taka during most of my graduate career and to get to know him very well during that time. He has a wonderful personality and unparalleled patience. During his last couple of years in the lab we also had a close collaboration that I'll describe in detail in the Contributions to Presented Work. Charles was always the 'leader' in the lab and I can't even begin to thank him enough for the many lab tasks and social events that he organized. He also tried to encourage me to do things more quickly and look more for bargains when spending money. One can't mention Charles without also thinking about Robin Lesley, the other graduate student a year ahead of me. In a way it was almost as if they were my older siblings. In addition to teaching me a number of experimental techniques and various aspects of B cell biology, Robin had a distinctive personality, always voiced her opinions, and was the one person who really cared when there were problems in the lab.

In later years in the lab I was also fortunate to get to know João Pereira and Trung Pham, who took the place of Mehrdad and Charles, respectively, in the bay. I've greatly enjoyed João's warm personality and the interesting discussions and debates that we have

had. João has a unique ability to question everything. Trung is one of the friendliest people that I have ever met. I have been fascinated by his many talents and positive outlook on life but also by his erratic schedule.

I am deeply indebted to these and all of the other members of the Cyster Lab who have been incredibly supportive and helpful during my time as a graduate student. The lab dynamic has made it a wonderful place to spend most of my time. Two people who deserve special mention for helping me when I started in the lab are Diana Hargreaves and Sanjiv Luther. I also appreciated overlapping briefly with Eric Ekland, for it was watching how he dealt with the immense challenges in his research and in his personal life that taught me about perseverance and helped me keep things in perspective during difficult times. Larry Shiow has been one of the nicest and most talented people that I have ever known and it was a true pleasure getting to know him over the past few years. I am grateful that he has assumed much of Charles' former role in taking care of general lab issues and social events. I also have appreciated Susan Schwab's enthusiasm and vibrant personality. I would not have been able to accomplish as much in the lab were it not for the devoted and talented technicians that I've worked with, including Ying Xu, Matt Lesneski, Caroline Low, Jinping An, and Olivia Lam. Joan Junkin has been our lab 'mother' and I appreciate both the Star Wars and koala-themed personality that she has added to the lab but also her culinary talents, particularly her experimentation with non-dairy desserts that I could enjoy.

I'd also like to thank everyone else that I have known in the UCSF community for friendship, support, and a welcoming environment. I would particularly like to thank current and former BMS students Luke Barron, Vikas Gupta, Janet Lau, Kristy Red-

Horse, Dave Rosen, Yan Ping Qi, Aaron Tooley, and Aaron Tward, as well as my longtime friend and former roommate Jeremy Cholfin. I have also enjoyed years of exposure to Susan Watson's acerbic wit and our shared passion of all things flow cytometric. My time as a student has been made much easier by the staff of the BMS office over the years, including Lisa Magargal, Monique Piazza, Rachel Brebach, Kevin Luong, and Pam Humphrey.

I was privileged to be one of the final recipients of a Howard Hughes Medical Institute predoctoral fellowship. This award covered the costs of my educational expenses and most of my stipend, but also provided extra funds that, among other things, allowed me to attend several conferences and purchase computer equipment and supplies.

On a more personal level, I would not be where I am today without the incredible love and support of my parents and family. My parents worked very hard to give me a wonderful childhood, an excellent education, and the chance to pursue my dreams. Even though they are not scientists, they were instrumental in getting me interested in science and providing me with opportunities to do research, ranging from chemistry sets to science fairs. I will never forget how my mom taught me about changing one variable at a time and making observations as I tried to ‘cure’ my goldfish and how my dad drove me halfway across the city in the afternoons so that I could do research on fruit flies at Cal State San Marcos. I also deeply appreciate the enthusiasm and encouragement of my grandma, my great aunt Dorothy, and my aunt Martha.

Finally, I have been extremely fortunate to have the unwavering support of Lisa Kelly. She has been there for me during both wonderful and difficult times and words cannot express how she has brought extraordinary meaning and joy to my life.

CONTRIBUTIONS TO PRESENTED WORK

All work described in this thesis was performed under the direct supervision and guidance of Dr. Jason G. Cyster. Additional contributions to specific chapters will be described below.

Chapter 2 was published as Allen CDC, Ansel KM, Low C, Lesley R, Tamamura H, Fujii N, and Cyster JG. (2004). Germinal center dark and light zone organization is mediated by CXCR4 and CXCR5. *Nat Immunol.* **5**(9): 943-52. Epub 2004 Aug 1. The manuscript is reproduced here in accordance with the policies of the Nature Publishing Group. I performed all of the experiments presented in the figures as well as all quantifications described in the text. I also prepared all of the figures and I wrote the manuscript together with Jason. Before I embarked on this project, Dr. K. Mark Ansel, a former graduate student in the lab, had spent considerable effort working on the role of CXCR5 and its ligand CXCL13 in GC organization. In doing so, he made several important observations but also experienced many technical challenges and other experimental difficulties that in combination had a substantial influence on the experimental approaches that I used and saved me considerable amounts of time. Mark had also helped with some early observations of a phenotype for CXCR4-deficient mice in GC organization and tested whether this phenotype was a result of CXCR4 deficiency in T cells which are described in the text of this chapter. Dr. Robin Lesley also contributed to the latter set of experiments early on as a graduate student in the lab. Caroline Low was our animal technician at the time and she performed most of the mouse screening and helped with the generation of fetal liver chimeras, but also

contributed to the study in unique ways that went beyond her regular duties. Her prior experience with the implantation of Alzet osmotic pumps was a major factor in our decision to pursue this approach to administer an inhibitor of CXCR4 to mice and thus allowed us to demonstrate the effects of acute CXCR4 inhibition on GC organization. In addition, Caroline provided expertise in the handling of rats which were essential for the SDF immunohistochemistry presented in Figure 5. Drs. Hirokazu Tamamura and Nobutaka Fujii generously provided large amounts of the CXCR4 inhibitor used to generate the data for Figure 2. Other individuals who contributed to this study are listed on the specific acknowledgments page for this chapter.

Chapter 3 was published as Allen CDC, Okada T, Tang HL, and Cyster JG. (2007). Imaging of germinal center selection events during affinity maturation. *Science* **315**(5811): 528-31. Epub 2006 Dec 21. The manuscript is reproduced here in accordance with *Science* policy. This work was done in complete collaboration with Dr. Takaharu Okada while he was a postdoctoral fellow in the lab, and combined Taka's expertise in two-photon microscopy and the analysis of T and B cell interactions with my experience in GC analysis and expertise in flow cytometry. We appeared as co-first authors in the publication and Taka also appeared as co-corresponding author with Jason. Taka and I performed the vast majority of experiments together, which not only made the work more efficient but also prompted fruitful discussions about the data and experimental design. I prepared Figures 2 and 3 for publication while Taka did the major work in preparing Figures 1 and 4. I prepared all 9 of the supplementary figures, although Taka did much of the data analysis presented in Figures S5 and S7. I wrote most of the manuscript, with input from Taka on the section describing B-T interactions and with editing and revision

by Jason. Dr. H. Lucy Tang generated the VDJ9/κ5 HyHEL10 heavy chain knock-in and light chain transgenic mice that were essential for these studies. Other individuals who contributed to this study are listed on the specific acknowledgements page for this chapter.

Germinal Center Dark and Light Zone Organization and Cellular Dynamics

By Christopher David Caballero Allen

ABSTRACT

The germinal center (GC) is an important site for the generation and selection of B cells bearing high-affinity antibodies during an immune response. The GC is organized into two main compartments termed dark and light zones. However, despite extensive anatomical definition of these zones, the mechanisms by which GC compartmentalization and selection occur have remained poorly defined.

First, we considered the possible role of chemokines as GC organizers. We show here that GC organization into dark and light zones was absent in mice deficient in the chemokine receptor CXCR4. GC B cells migrated toward the CXCR4 ligand SDF-1, which was more abundant in the dark zone than in the light zone. B cells in the dark zone expressed more CXCR4 than B cells in the light zone, and CXCR4-deficient B cells were excluded from the dark zone in the context of a wild-type GC. These findings suggest that CXCR4 promotes dark zone localization in response to SDF-1. In contrast, CXCR5 helped direct cells to the light zone, which is rich in the CXCR5 ligand CXCL13. Deficiency in CXCL13 was associated with aberrant positioning of the light zone.

To gain insight into the GC cell migration and interaction dynamics during selection, we imaged GCs in intact mouse lymph nodes by two-photon microscopy. We

observed that GC B cells were highly motile and exhibited a dendritic morphology with long cell processes. GC B cell motility was partially dependent on the chemokine CXCL13. GC B cells transited between dark and light zones and divided in both zones, yet the cells resided in the light zone for only a few hours. GC B cells formed few stable contacts with GC T cells despite frequent encounters, and GC T cells were seen to carry dead GC B cell blebs.

On the basis of these observations, we conclude that GC organization into dark and light zones is a chemokine-driven process. We also suggest a new model for selection in which competition for T cell help plays a more dominant role than previously appreciated.

TABLE OF CONTENTS

LIST OF TABLES

Chapter 2

LIST OF FIGURES

Chapter 2

Chapter 3

LIST OF FIGURES
(continued)

Chapter 3

CHAPTER 1

Introduction

T-dependent Antibody Responses

Secondary lymphoid organs, such as the spleen, lymph nodes, and tonsils, are specialized structures that are highly organized to generate an immune response (reviewed in Cyster, 1999; Vinuesa and Cook, 2001). These organs are strategically positioned to detect infection in a variety of body tissues. For example, peripheral lymph nodes receive lymphatic drainage from the skin. B and T cells, which generate antibody and cell-mediated effector responses, respectively, home to specific compartments within secondary lymphoid organs, known as B cell follicles and T cell zones (reviewed in Cyster, 1999). These respective areas are rich in specialized accessory cells that can capture and present foreign antigen. Follicular dendritic cells (FDCs) in B cell follicles are thought to be mesenchymally-derived stromal cells that express receptors that allow the efficient capture of unprocessed antigen in the form of immune complexes (reviewed in Cyster *et al.*, 2000; Kosco-Vilbois, 2003; Szakal *et al.*, 1989). FDCs have been shown to be potent activators of B cells (reviewed in Kosco-Vilbois, 2003). The T zone is rich in hematopoietically-derived classical dendritic cells (DCs) that efficiently take up and process antigen into peptides and then present these peptides on MHC molecules to the T cells (reviewed in MacLennan *et al.*, 1997). Some DCs may also maintain antigen in intact form and present antigen to B cells as they migrate into the secondary lymphoid organs (Qi *et al.*, 2006). Naïve B and T cells migrate rapidly within their respective zones in secondary lymphoid organs in a fashion that resembles random motion but appears to follow the path of resident stromal cells (Bajenoff *et al.*, 2006; Miller *et al.*, 2002). Naïve B and T cells exhibit a wide range of specificities for foreign antigens and frequently

recirculate among secondary lymphoid organs via the blood. This process results in rapid surveying of the body for infection.

Antibody responses against foreign antigens can be subdivided into two major classes, known as T-independent and T-dependent antibody responses (reviewed in Bachmann and Zinkernagel, 1997). T-independent antibody responses can be generated by B cells in the absence of T cell help, and typically occur upon immunization or infection with antigens that provide polyclonal B cell activation or consist of repetitive determinants on a large polysaccharide backbone (reviewed in Bachmann and Zinkernagel, 1997; Mond *et al.*, 1995). These T-independent responses are thought to be generated by distinct subsets of B cells, such as the marginal zone B cells in the spleen that are positioned close to the marginal sinus and sample the blood for infectious bacteria (Martin *et al.*, 2001). In contrast, follicular B cells are typically involved in T-dependent antibody responses, in which contact with cognate antigen-specific helper T cells is required.

In T-dependent antibody responses, soon after infection or immunization, as few as 1 in 100,000 naïve B and T cells that are specific for the foreign antigen(s) exhibit a marked change in their migratory behavior within the secondary lymphoid organ(s) that drain the site of immunization or infection (reviewed in Cyster, 1999; MacLennan *et al.*, 1997). These rare antigen-specific B and T cells come together at the boundary between B cell follicles and T cell zones and engage in long interactions leading to the generation of an immune response (Garside *et al.*, 1998; MacLennan *et al.*, 1997; Okada *et al.*, 2005). The mechanisms responsible for determining the fate of the activated B cells remain controversial, although various studies suggest that the affinity of the B cell

receptor for the foreign antigen as well as the costimulatory signals received from T cells may be involved (Benson *et al.*, 2007; Dal Porto *et al.*, 1998; Dal Porto *et al.*, 2002; Paus *et al.*, 2006; Shih *et al.*, 2002). Activated B cells typically adopt one of two fates: 1) movement into extrafollicular areas followed by proliferation and terminal differentiation into short-lived plasma cells that secrete antibodies or 2) movement into the B cell follicles followed by proliferation and the establishment of germinal centers (GCs) (Jacob *et al.*, 1991a; Liu *et al.*, 1991b). A common clonal origin of short-lived plasma cells in extrafollicular foci and GC B cells in follicles was established by sequencing of the immunoglobulin variable-diversity-joining (VDJ) rearrangements from microdissected cell clusters, which showed that rare VDJ rearrangements could be found in cells isolated from nearby extrafollicular foci and GCs but not from those at distant sites (Jacob and Kelsoe, 1992).

Several decades ago, it was observed that the average affinity of serum antibody for a given foreign antigen increases over time after immunization (Eisen and Siskind, 1964). This process was later termed affinity maturation and shown to be due to somatic mutations in the antibody variable genes in the antibody-secreting plasma cells (reviewed in Tarlinton and Smith, 2000). Subsequent work showed that most short-lived plasma cells in extrafollicular foci lack somatic mutations, whereas a high frequency of somatic mutations was evident in GC B cells, suggesting that a hypermutation mechanism is activated in GC B cells (Berek *et al.*, 1991; Jacob *et al.*, 1991b). These somatic mutations were clustered in the complementarity-determining regions (CDRs) that encode the amino acids of antibodies that form the interface with cognate antigens. A high ratio of amino acid replacement to silent mutations was observed, indicating that selection had

taken place. In addition, many of the GC B cells picked out from individual GCs appeared to be clonally related, and indeed some GCs appeared to be dominated by cells derived from a single clone. These observations suggested that the affinity maturation of the antibody response occurs in GCs, through the process of clonal proliferation, somatic hypermutation and selection. GCs do not appear to be absolutely required for affinity maturation, however, as mice deficient in GCs do exhibit measurable affinity maturation with certain types of immunization (Futterer *et al.*, 1998; Koni and Flavell, 1999; Matsumoto *et al.*, 1996; Wang *et al.*, 2000). Therefore, the GC is thought to be a site specialized for efficient affinity maturation of the antibody response.

As the immune response progresses, the extrafollicular foci of plasma cells wane, whereas long-lived plasma cells and memory B cells begin to appear (reviewed in Tarlinton and Smith, 2000). Many of these long-lived plasma cells then home to the bone marrow, where they secrete antibody for several weeks or longer. Notably, the antibody variable genes in long-lived plasma cells and memory B cells exhibit a high degree of somatic mutations that show evidence of selection, suggesting that these cells were derived from GCs (reviewed in McHeyzer-Williams *et al.*, 2006; Tarlinton and Smith, 2000). Further evidence for the GC origin of long-lived plasma cells and memory B cells was provided by a recent study that carefully tracked the appearance of these cells in the blood (Blink *et al.*, 2005). High affinity mutations in antibody variable genes were found to emerge in parallel in antigen-specific cells in the spleen, blood, and bone marrow, suggesting a common origin for these cells. Interestingly, however, there was a slight delay in the appearance of high affinity mutations in the blood compared with the spleen,

strongly arguing that these cells emerged from GC B cells in the spleen after differentiation into plasma cells or memory B cells.

Taken together, these findings suggest that plasma cells in the extrafollicular foci that appear shortly after immunization produce the low affinity antibodies that are observed early in the immune response. Over time the somatic hypermutation and selection process in the GC generates long-lived plasma cells that lodge in the bone marrow and secrete high affinity antibodies, resulting in the affinity maturation of the antibody response observed decades ago. The GC also generates memory B cells that recirculate through secondary lymphoid organs and survey for subsequent exposures to the same foreign antigen. Reintroduction of the same foreign antigen by subsequent infection or booster immunization results in rapid differentiation of memory B cells into large numbers of bone-marrow tropic plasma cells, resulting in a marked increase in the serum antibody specific for the foreign antigen within a few days. This process provides rapid protection from infection and helps to maintain long-term production of high affinity antibodies to prevent subsequent re-infection.

GC Organization and Function

The GC was first described in 1884 by Flemming, who observed a site of large lymphocytes undergoing mitosis in the follicles of lymph nodes and other secondary lymphoid organs and proposed this site to be a major source of all lymphocytes in the body (reviewed in Nieuwenhuis and Opstelten, 1984). Flemming's work prompted intense study of the GC by a variety of groups, although his original proposed function for the GC was eventually disproven. In the 1930s, through the careful study of cross-

sections of cat lymph nodes, Rölich observed that the GC could be subdivided into two main compartments, the dark zone and the light zone, based on their histological appearance (Röhlich, 1930; Röhlich, 1933). In the dark zone, lymphocytes were closely packed, whereas in the light zone much of the space was occupied by reticular cells.

The light zone appears to be strategically positioned in secondary lymphoid organs toward the source of foreign antigens (Congdon, 1962; Millikin, 1966). In the spleen, the light zone pole of the GC is proximal to the marginal sinus where blood-borne antigens enter the tissue. In lymph nodes, the light zone is positioned close to the subcapsular sinus, which receives afferent lymphatic drainage from the skin, mucosa, and viscera. In gut Peyer's patches, the light zone is oriented towards the intestinal lumen. The mechanisms by which antigens reach the FDC network in the light zone need much more investigation, but it has been suggested that antigens are carried by specialized antigen-transporting cells (Martinez-Pomares *et al.*, 1996; Nieuwenhuis and Opstelten, 1984; Szakal *et al.*, 1983) or marginal zone B cells (Ferguson *et al.*, 2004), or that soluble antigen might freely diffuse into the follicle (Pape *et al.*, 2007).

Through extensive fixed tissue analysis and *in vitro* studies, a classical model was described 13 years ago for the mechanism of GC organization and function (MacLennan, 1994). GC B cells in dark and light zones were defined as centroblasts and centrocytes, respectively. Centroblasts were named based on the observation of large, mitotically active cells in the dark zone that lacked surface immunoglobulin (Ig). These cells were proposed to undergo a rapid process of proliferation and somatic hypermutation of their antibody variable region genes. Centroblasts were then suggested to exit the cell cycle, reexpress surface Ig, and become smaller centrocytes that traveled to the light zone. This

process was proposed to result in the generation of centrocytes expressing surface antibodies with a wide range of affinities for a given antigen. Centrocytes were then proposed to compete for binding to antigen in the form of immune complexes bound to FDCs in the light zone. Several in vitro studies provided evidence that recognition of antigen on FDC, along with other FDC-specific molecules, may promote survival of selected B cell clones (Kosco *et al.*, 1992; Li and Choi, 2002; Petrasch *et al.*, 1991). Integrins were suggested to contribute to centrocyte adhesion to FDC, as integrin ligands were found to be abundant on FDC in the light zone and in vitro culture of centrocytes with these integrin ligands also promoted survival (Koopman *et al.*, 1994). The presence of "tingible body" macrophages that have phagocytosed large numbers of GC B cells that were recently in cycle, suggests that most B cells die during this selection process (MacLennan, 1994). Selected centrocytes could then present antigen to helper T cells in the light zone, which could enhance survival or promote differentiation into antibody-secreting plasma cells or memory B cells. Indirect experimental results and theoretical modeling also suggested that some centrocytes might return to the dark zone to complete an additional round of mutation and selection (Kelsoe, 1996; Kepler and Perelson, 1993).

Cell Migration in the GC

The movement of GC B cells from the dark zone to the light zone was demonstrated by several groups (Hanna, 1964; Koburg, 1966; Liu *et al.*, 1991b). In these studies, cells were labeled in S phase of the cell cycle with thymidine analogs, such as ^{3}H-thymidine or bromodeoxyuridine (BrdU). Enrichment of labeled cells in the dark zone after several hours was followed by the appearance of these cells in the light zone.

However, the signals required for centroblasts to move to the light zone as they differentiate into centrocytes, as well as the signals needed for centrocytes to return to the dark zone or exit the GC, remain undefined. The trafficking of these cells between the dark zone and light zone compartments might depend on general cues that have been defined for lymphocyte movement within secondary lymphoid organs. In recent years, small chemoattractant proteins known as chemokines have been shown to regulate the position of lymphocytes, such as the establishment of distinct B and T cell compartments, within several organs including the spleen and lymph nodes (reviewed in Cyster, 1999).

The idea that chemoattractants may be present in the GC is supported by several older studies indicating that transferred GC B cells home to GCs in recipient animals. In one study, for example, it was found that intravenously transferred GC B cells from a rabbit appendix were found in GCs of the spleen in recipients three hours after transfer (Opstelten *et al.*, 1981). A similar result was not reported for LN GCs, which may be due to lack of L-selectin expression by GC B cells (Reichert *et al.*, 1983). Indeed, one group transferred GC B cells directly into afferent lymphatics and showed that they homed to LN GCs within several hours (Deenen *et al.*, 1984).

Further supporting the notion that chemokines may be involved in the GC process, gene-targeted mice deficient in the chemokine CXCL13 or its receptor CXCR5 displayed defects in GC size, position, and compartmentalization (Ansel *et al.*, 2000; Forster *et al.*, 1996; Voigt *et al.*, 2000). In the spleen, rather than forming in B-cell follicles, GCs formed in the T-cell and dendritic-cell rich area known as the periarteriolar lymphoid sheath (PALS), proximal to the central arteriole. Immunohistochemical analysis indicated that these GCs were small in size by staining GC B cells with the lectin

peanut agglutinin (PNA). Staining of the FDC network with the antibody FDC-M2 or an antibody against complement receptor 1 suggested that these GCs lacked compartmentalization into dark and light zones. A similar phenotype was observed in GCs in the lymph nodes, although the position of these GCs was more normal, inside of B-cell rich areas. However, it was unclear whether the GC defects observed in CXCL13 and CXCR5 deficient mice were secondary to other abnormalities, such as a lack of B cell follicles and primary FDC.

GC B cells were also shown to express the chemokine receptor CXCR4, which binds the ligand stromal cell derived factor 1 (SDF-1) also known as CXCL12 (Bleul *et al.*, 1998; Casamayor-Palleja *et al.*, 2002; Forster *et al.*, 1998; Roy *et al.*, 2002). However, in standard *in vitro* chemotaxis assays the GC B cells failed to migrate (Bleul *et al.*, 1998; Casamayor-Palleja *et al.*, 2002; Corcione *et al.*, 2000; Corcione *et al.*, 2002; Roy *et al.*, 2002). These data led some to conclude that GC B cells are sessile.

Here, we have examined the roles of chemokine receptors in GC B cell positioning and GC organization, through a variety of approaches including the analysis of gene-targeted mice. In addition, we have performed the first real-time imaging studies of GC B cell migration *in vivo*, which have provided novel insights in to the selection mechanism in GCs.

CHAPTER 2

Germinal center dark and light zone organization is mediated by CXCR4 and CXCR5

This chapter was published as:

Allen CDC, Ansel KM, Low C, Lesley R, Tamamura H, Fujii N, and Cyster JG. (2004). Germinal center dark and light zone organization is mediated by CXCR4 and CXCR5. *Nat Immunol.* **5**(9): 943-52. Epub 2004 Aug 1.

Abstract

Germinal center (GC) dark and light zones segregate cells undergoing somatic hypermutation and antigen-driven selection, yet the factors guiding this organization are unknown. We report that GC organization was absent in mice deficient in the chemokine receptor CXCR4. Centroblasts expressed high amounts of CXCR4 and GC B cells migrated toward SDF-1 (CXCL12), which was more abundant in the dark zone than the light zone. CXCR4-deficient cells were excluded from the dark zone in the context of a wild-type GC. These findings establish that GC organization depends on CXCR4 sorting centroblasts into a dark zone. In contrast, CXCR5 helped direct cells to the light zone and deficiency in CXCL13 was associated with aberrant light zone localization.

Introduction

The organization of the germinal center (GC) was described over 70 years ago by Röhlich, who observed that GCs had two distinct poles or zones, which he termed the dark and light zones based on their histological appearance (Röhlich, 1930). These histological differences are now known to be associated with important functional differences. B cells in the dark zone, termed centroblasts, undergo rounds of rapid proliferation and somatic hypermutation of their antibody variable genes. The centroblasts then become smaller, non-dividing centrocytes and undergo selection in the light zone based upon the affinity of their surface antibody for the inducing antigen (MacLennan, 1994). In addition to centrocytes, the light zone contains helper T cells and a network of follicular dendritic cells (FDCs) that sequester antigen (Kelsoe, 1996; MacLennan, 1994). Centrocytes that fail to bind sufficient antigen or to receive T cell help undergo apoptotic cell death and are cleared from the GC by tingible body macrophages (MacLennan, 1994), whereas centrocytes that successfully bind antigen and receive T cell help survive and exit the GC as long-lived plasma cells or memory B cells (Berek *et al.*, 1991; Kelsoe, 1996; MacLennan, 1994; McHeyzer-Williams and Ahmed, 1999).

GCs develop in a stereotypic manner within B cell follicles during the first week of T-dependent immune responses. After an initial period of rapid B cell proliferation in the follicle, the dark zone develops proximal to the T cell zone or medullary cord region and the light zone emerges at the distal pole (Liu *et al.*, 1991b). Once these zones are established, the proliferating centroblasts in the dark zone continuously renew the centrocytes in the light zone. Evidence for the movement of proliferating cells from the

dark zone to the light zone is provided by several kinetic analyses of cells labeled with ^{3}H-thymidine or 5-bromo-2'-deoxyuridine (BrdU) (Koburg, 1966; Liu *et al.*, 1991b; MacLennan, 1994). There is also data suggesting that selected centrocytes can return to the dark zone for further rounds of division and somatic mutation (Kelsoe, 1996).

Despite the extensive anatomical description of GC dark and light zones and the evidence that B cells move between these compartments, the mechanisms responsible for achieving this polarity in the GC remain a mystery. The adhesion molecules ICAM-1 and VCAM-1 have been reported to be expressed in the GC and can mediate attachment of GC B cells to FDCs *in vitro* via the integrins LFA-1 and VLA-4 (Freedman *et al.*, 1990; Koopman *et al.*, 1991), but there is no evidence as yet for their *in vivo* role in GC organization. Mice lacking the chemokine CXCL13 (BLC, BCA-1) or its receptor, CXCR5, display defects in GC size and position (Ansel *et al.*, 2000; Forster *et al.*, 1996; Voigt *et al.*, 2000) but it has been unclear whether these defects are secondary to the failure to develop primary follicles and FDCs in these mice or whether they reflect a role for CXCL13 within the GC. The chemokine receptor, CXCR4, is expressed on human and mouse GC B cells (Bleul *et al.*, 1998; Bowman *et al.*, 2000; Casamayor-Palleja *et al.*, 2002; Forster *et al.*, 1998; Roy *et al.*, 2002) and on human GC T cells (Estes *et al.*, 2002). However, in several *in vitro* studies (Bleul *et al.*, 1998; Casamayor-Palleja *et al.*, 2002; Corcione *et al.*, 2000; Roy *et al.*, 2002), GC B cells have been found to exhibit poor chemotactic responses to the only known CXCR4 ligand, SDF-1 (CXCL12), leading some to conclude that GC B cells have an intrinsic lack of motility.

In this study we have explored the mechanisms responsible for GC organization. We demonstrate using genetic and pharmacological approaches that CXCR4 is essential

for GC dark and light zone segregation. When GC B cells are rescued from rapid *in vitro* apoptosis by *bcl-2* overexpression we find that they exhibit robust chemotactic responses to SDF-1 and CXCL13. SDF-1 is found to be expressed within GCs and to be in higher abundance in the dark zone compared to the light zone. Furthermore, we show that CXCR4 is upregulated on centroblasts compared to centrocytes and is required for centroblast localization in the dark zone. In contrast, we demonstrate that CXCR5 helps direct cells to the CXCL13-positive light zone but that it is not essential for light and dark zone segregation. However, CXCL13 and CXCR5 are required to determine the correct position of the light zone within the GC.

Results

CXCR4 is required for dark and light zone segregation

To determine whether CXCR4 was required for GC organization, we generated fetal liver (FL) chimeras by transferring wild-type (*Cxcr4*$^{+/+}$) or *Cxcr4*$^{-/-}$ FL cells into lethally irradiated recipient mice. After reconstitution, these chimeras were immunized intraperitoneally (i.p.) with sheep red blood cells (SRBC), a strong GC-inducing antigen, and the spleens were analyzed eight days later at the peak of the GC response (Shinall *et al.*, 2000). In order to visualize the dark and light zones of each GC, we immunohistochemically analyzed several cross-sections spanning more than 200 μm of depth for each spleen. In *Cxcr4*$^{+/+}$ FL chimeras, GCs showed enriched staining for CD35^{+} FDCs in the light zone, whereas in *Cxcr4*$^{-/-}$ FL chimeras, GCs showed no evidence of CD35^{+} FDC polarity; instead, the FDC network extended throughout the GC (**Fig. 1a**).

To assess whether this phenotype might represent a broad requirement for CXCR4 in GC organization, we immunized *Cxcr4*$^{-/-}$ and *Cxcr4*$^{+/+}$ FL chimeras with subcutaneous (s.c.) antigen in adjuvant and then analyzed draining lymph nodes 10-14 days later. GCs in the lymph nodes of *Cxcr4*$^{-/-}$ FL chimeras also showed disrupted organization, as assessed by staining the FDC network with CD35 and FDC-M2 antibodies (**Fig. 1b**). Examination of lymph nodes also enabled tracking of CD23, a marker selectively expressed on FDCs in the light zone of lymph node GCs (MacLennan, 1994; Maeda *et al.*, 1992), as seen in *Cxcr4*$^{+/+}$ FL chimeras (**Fig. 1b**, left panel). In contrast, this marker was expressed throughout the GC in *Cxcr4*$^{-/-}$ FL chimeras (**Fig. 1b**, right panel). In addition, the chemokine CXCL13, which is normally present in the GC light zone (Cyster *et al.*, 2000), was found throughout the GC in *Cxcr4*$^{-/-}$ FL chimeras

(data not shown), possibly contributing to the disrupted GC organization. Taken together, these data suggest that CXCR4 is required to form distinct dark and light zones.

In addition to analysis of the FDC network, the distribution of GC B cells was assessed by treating immunized chimeras with BrdU. A five hour treatment time was found to be optimal for preferential labeling of centroblasts in the dark zone in mouse GCs (data not shown), consistent with a previous kinetic analysis of rat GCs (Liu *et al.*, 1991b). GCs in *Cxcr4*$^{+/+}$ FL chimeras showed numerous BrdU^{+} cells in the dark zone and only a small number of labeled cells in the light zone (**Fig. 1b,** left panel), whereas GCs in *Cxcr4*$^{-/-}$ FL chimeras had BrdU^{+} cells uniformly distributed throughout the GC (**Fig. 1b**, right panel). By analyzing each GC in serial sections for the distribution of BrdU^{+} centroblasts and CD23^{+} FDCs, dark and light zones were identified in less than 7% of CXCR4-deficient GC compared to greater than 75% of wild-type GC.

The requirement for CXCR4 in the GC was specific for dark and light zone segregation, as other aspects of the structure, such as size and position, were not dependent on CXCR4. Flow cytometric analysis showed that the frequency of GC B cells was similar in *Cxcr4*$^{+/+}$ and *Cxcr4*$^{-/-}$ FL chimeras (**Fig. 1c**). Even in cases in which the reconstitution of B cells was poor in *Cxcr4*$^{-/-}$ FL chimeras, the frequency of GC B cells was similar to controls (data not shown), consistent with previous reports that GC size is independent of the total number of B cells in an animal (Vonderheide and Hunt, 1990). CXCR4 deficiency also did not affect the frequency of proliferating centroblasts in the GC, determined by BrdU labeling (**Fig. 1d**). These findings further support the hypothesis that CXCR4 is specifically required for proper dark and light zone segregation of the GC.

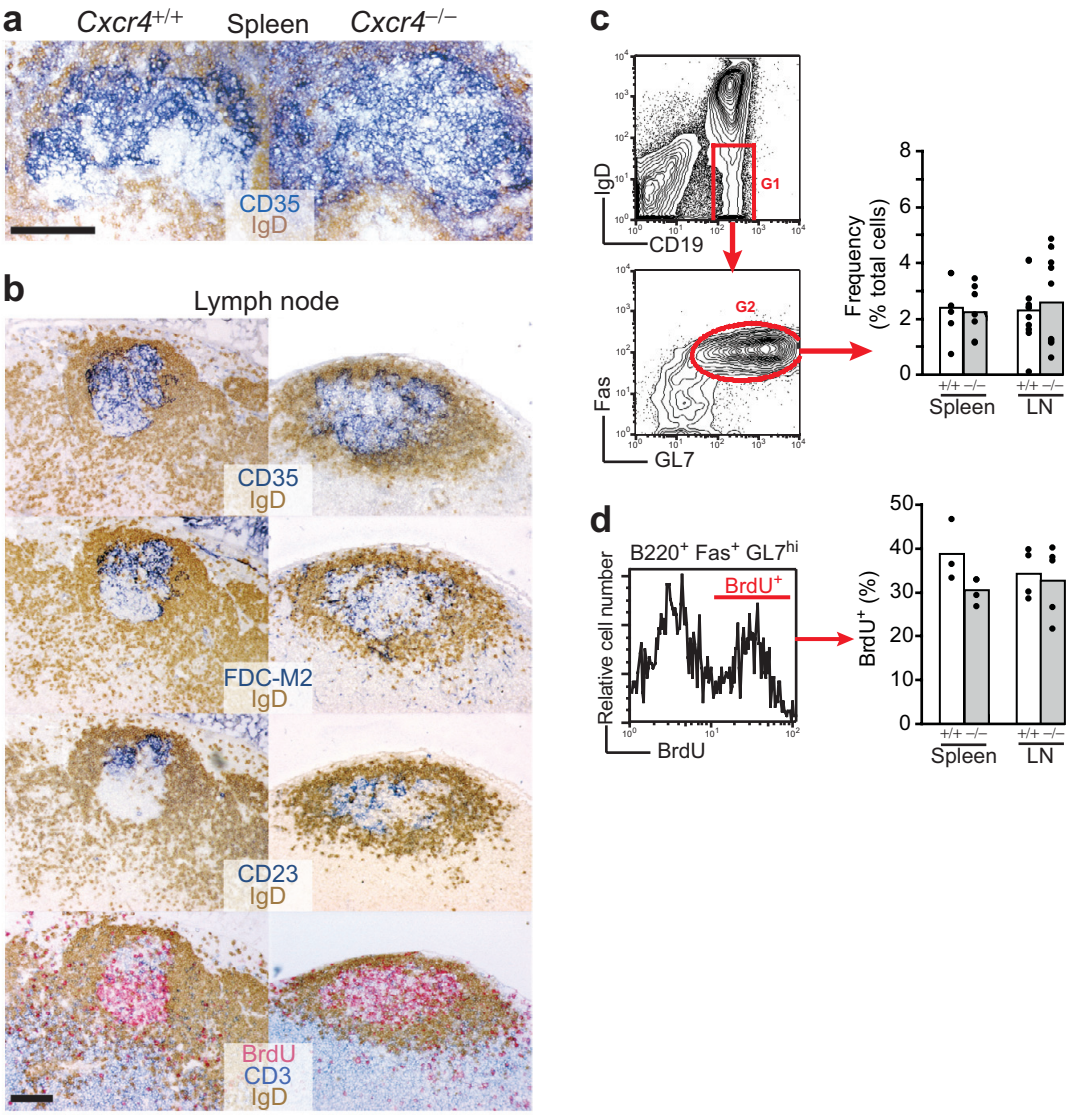

Figure 1. CXCR4 deficiency results in GC disorganization. (**a**) Immunohistochemistry of spleen GCs from immunized *Cxcr4*$^{+/+}$ or *Cxcr4*$^{-/-}$ FL chimeras. Cryostat sections were stained with antibodies to CD35 to reveal the FDC network and IgD to show the IgD^{-} GC surrounded by the IgD^{+} follicular mantle zone. Each panel is representative of GCs analyzed in four chimeras in two independent experiments. Scale bar, 100μm. (**b**) Immunohistochemistry of lymph node GCs from immunized *Cxcr4*$^{+/+}$ or *Cxcr4*$^{-/-}$ FL chimeras after five-hour *in vivo* labeling with BrdU. Cryostat sections were stained with antibodies to IgD to show the surrounding follicular mantle zone; CD35, FDC-M2, or CD23 to detect the FDC network; CD3 to detect T cells; and BrdU to detect proliferating centroblasts that had incorporated BrdU, as indicated. Panels show serial sections of a single GC, and are representative of GCs analyzed in three to six draining lymph nodes each from eight (CD35, CD23), four (BrdU), or two (FDC-M2) chimeras of each type. Scale bar, 100μm. (**c**) Enumeration of GC B cell frequency as % of total organ cells by flow cytometry. GC B cells were identified as CD19^{+} IgD^{-} GL7^{hi} Fas^{+} cells (shown as 5% probability contour plots) or B220^{+}, GL7^{hi}, PI^{-} cells (two to three data points); these gating schemes gave similar frequencies. (**d**) Frequency of BrdU^{+} GC B cells determined by flow cytometry after five-hour *in vivo* labeling with BrdU. For (c) and (d), data points represent individual chimeras from two to three experiments. LN, lymph node.

To rule out the possibility that the disrupted GC organization in *Cxcr4*$^{-/-}$ FL chimeras might be due to long-term defects in bone marrow development of hematopoietic cells, the CXCR4 inhibitor 4F-benzoyl-TE14011 (Tamamura *et al.*, 2003) was administered to immunized normal mice for seven days. Immunohistochemical analysis revealed that GCs in these inhibitor-treated mice resembled GCs in *Cxcr4*$^{-/-}$ FL chimeras. In spleen GCs, identification of centroblasts by BrdU labeling and visualization of FDCs by CD35 and FDC-M2 staining showed an absence of dark and light zone segregation (**Fig. 2**). Analysis of lymph node GCs by staining for CD35 and CD23 demonstrated a similar loss of GC organization after inhibitor treatment (data not shown). Taken together, these results indicated that both genetic ablation and pharmacological inhibition of CXCR4 disrupted GC compartmentalization, establishing that CXCR4 is required for proper GC organization.

CXCR4 expression by B cells regulates GC organization

Although the origin of FDCs remains controversial, substantial evidence indicates that these cells are radiation-resistant (Cyster *et al.*, 2000) and would therefore be wild-type in *Cxcr4*$^{-/-}$ FL chimeras. To test whether expression of CXCR4 on B cells was required for GC organization, we purified B cells from *Cxcr4*$^{+/+}$ or *Cxcr4*$^{-/-}$ FL chimeras and transferred them into B-cell deficient (μMT) recipient mice that were then immunized s.c. Immunohistochemical analysis of the responding lymph nodes in the recipients revealed that FDC and CXCL13 light zone polarity was typically absent in the GC when only B cells lacked CXCR4 (**Fig. 3**). To test whether expression of CXCR4 on T cells was required for GC organization, mixed irradiation chimeras were constructed by

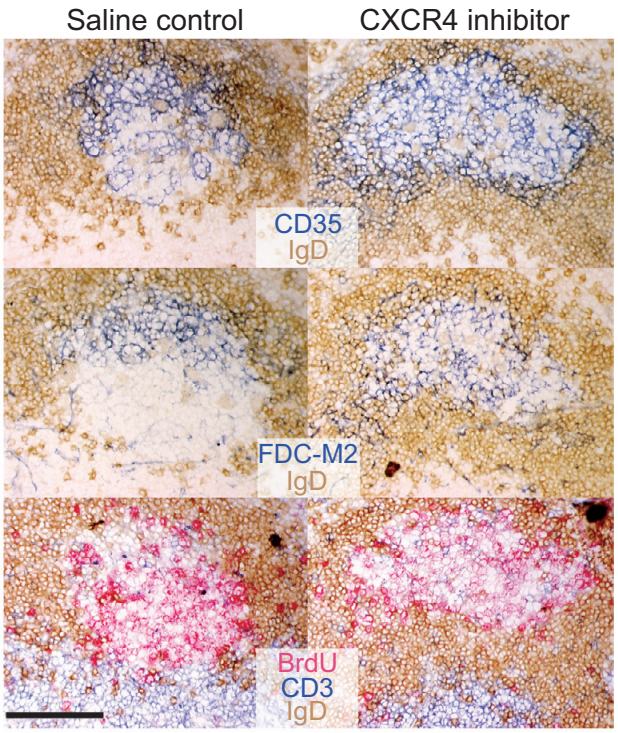

Figure 2. Treatment with a CXCR4 inhibitor results in GC disorganization.
Immunohistochemistry of spleens from wild-type B6 mice immunized i.p. with SRBC on day 0, implanted s.c. with Alzet pumps containing saline (vehicle) or the CXCR4 inhibitor 4F-benzoyl-TE14011 on day 1, and analyzed five hours after BrdU injection on day 8. Panels show serial cryostat sections of a single GC stained with the indicated antibodies. Data are representative of GCs analyzed in two mice from each group. Scale bar, 100μm.

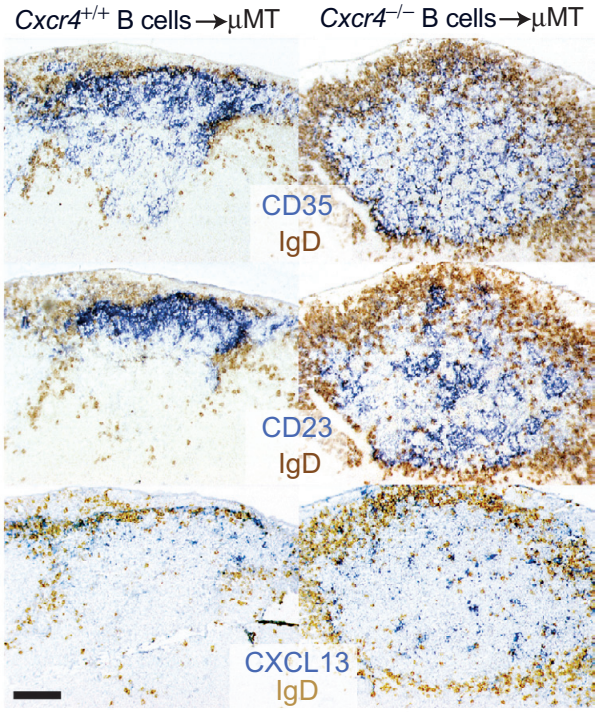

Figure 3. Deficiency of CXCR4 in B cells disrupts FDC and CXCL13 polarity in the GC. *Cxcr4*$^{+/+}$ or *Cxcr4*$^{-/-}$ B cells were purified from the spleens of FL chimeras and then transferred into B-cell deficient mice (μMT), which were immunized s.c. 10–11 days after transfer, and analyzed 10 days after immunization. Lymph node GCs were analyzed by immunohistochemistry of cryostat sections stained with the indicated antibodies. Panels show serial sections of a single GC, and are representative of GCs analyzed in four mice from each group in two experiments. Scale bar, 100μm.

transferring 90% *Tcrb*$^{-/-}$ *Tcrd*$^{-/-}$ bone marrow and 10% *Cxcr4*$^{-/-}$ FL into *Rag1*$^{-/-}$ hosts, such that the majority of the cells would be wild-type, but T cells could only be derived from the *Cxcr4*$^{-/-}$ FL. In these chimeras, immunohistochemical analysis showed normal CD23 light zone polarity (data not shown). These data identify an essential role for CXCR4 on B cells, but not T cells, for normal GC organization and they indicate that B cells regulate the position of FDCs and CXCL13 within the GC.

Enhanced chemotaxis of GC B cells to SDF-1

Previous studies have indicated that human tonsil GC B cells express CXCR4 (Bleul *et al.*, 1998; Casamayor-Palleja *et al.*, 2002; Roy *et al.*, 2002). Flow cytometric analysis of chemokine receptor surface expression on mouse GC B cells (**Fig. 4a**) showed that the majority of GC B cells expressed 5–20-fold more CXCR4 than follicular B cells. In contrast, expression of CXCR5 was similar or weakly elevated (approximately 2-fold) and expression of CCR7, a receptor for T zone chemokines, was similar or slightly reduced compared with follicular B cells (**Fig. 4a**). Although several studies had failed to observe a significant chemotactic response of freshly isolated GC B cells to lymphoid chemokines, including SDF-1 (Bleul *et al.*, 1998; Casamayor-Palleja *et al.*, 2002; Corcione *et al.*, 2000; Roy *et al.*, 2002), it seemed possible that this was due to the propensity of isolated GC B cells to rapidly undergo apoptosis (MacLennan, 1994). Indeed, in transwell migration assays with cells from immunized spleens we observed that greater than half of the GC B cells disappeared during the three-hour assay, presumably by clearance mechanisms for apoptotic cells, and that the vast majority of remaining cells stained positive for Annexin-V and/or propidium iodide (PI) (data not

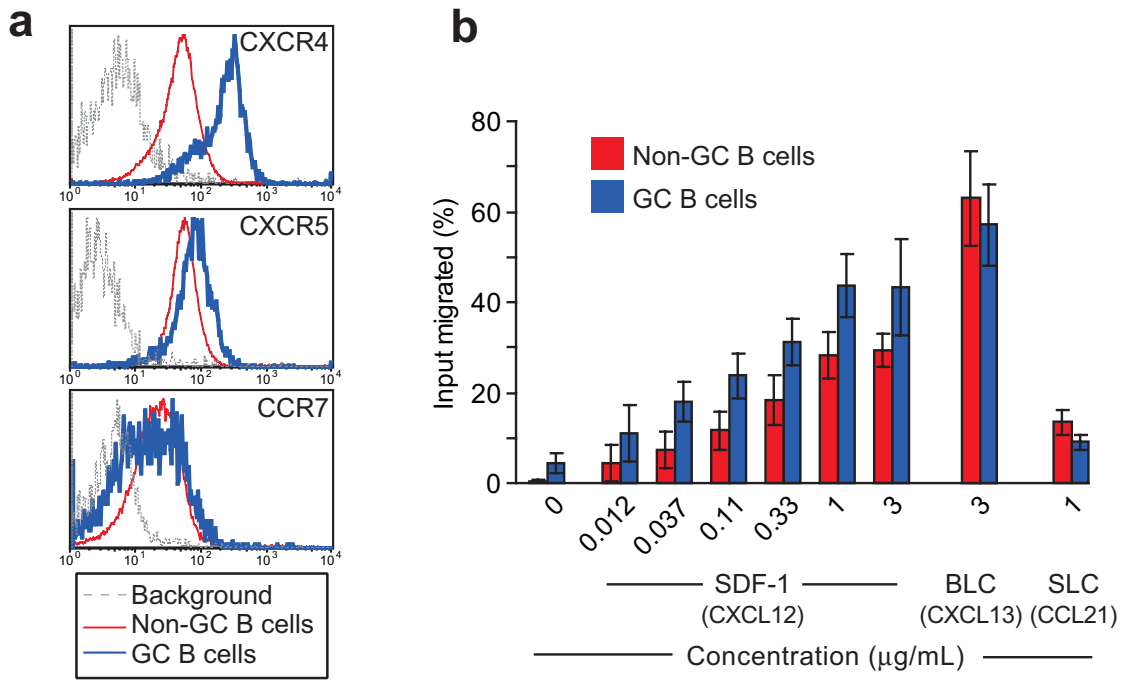

Figure 4. GC B cells upregulate CXCR4 and exhibit enhanced chemotaxis to SDF-1. (**a**) Flow cytometric analysis of chemokine receptors, as indicated, for GC B cells, non-GC B cells, or the following background controls: CXCR4, *Cxcr4*$^{-/-}$ GC B cells; CXCR5, *Cxcr4*$^{-/-}$ *Cxcr5*$^{-/-}$ GC B cells; or CCR7, wild-type GC B cells stained with human LFA-3-Fc. Plots are representative of both spleen and lymph node data from the following immunized animals: CXCR4, 56 mice in 20 experiments; CXCR5, 21 mice in nine experiments; CCR7, three mice in three experiments. (**b**) Transwell migration assay of spleen cells from immunized Eμ-*bcl-2*-22 transgenic mice. Shown are data from four experiments with a similar overall magnitude of response, and are representative of eight experiments. Bars show the mean ± s.d. GC B cells show significantly elevated responsiveness to SDF-1 ($p<0.05$, 0.012 μg/mL to 1 μg/mL) and significantly reduced responsiveness to CCL21 ($p<0.05$) compared with non-GC B cells by the student's paired T-test. In both panels, GC B cells were gated on a combination of the following markers: B220^{+}, CD19^{+}, GL7^{hi}, Fas^{+}, and/or IgD^{-}, whereas non-GC B cells were gated with a combination of B220^{+}, CD19^{+}, GL7^{lo}, Fas^{-}, and/or IgD^{+}. In some experiments, dead cells were excluded by PI staining.

shown). To overcome this rapid cell death, we used cells from mice overexpressing the anti-apoptotic gene *bcl-2* under control of the Ig μ enhancer (Eμ-*bcl-2*-22 mice) (Strasser *et al.*, 1991). These mice have been reported to have relatively normal GC size and morphology (Secord *et al.*, 1995; Smith *et al.*, 2000) and our analysis of GCs in spleens from immunized and BrdU-labeled Eμ-*bcl-2*-22 mice showed distinct centroblast and FDC clusters, consistent with normal dark and light zone segregation (**Supplementary Fig. 1)**. In transwell migration assays, transgenic *bcl-2* expression reduced the frequency of apoptotic GC B cells to less than 20% (data not shown). In contrast with previous findings, *bcl-2* transgenic GC B cells exhibited enhanced migration to SDF-1 relative to follicular B cells, whereas migration to CXCL13 was similar and migration to a CCR7 ligand, CCL21 (SLC), was modestly reduced (**Fig. 4b**). Therefore, of the lymphoid chemokines and receptors, GC B cells have increased responsiveness to SDF-1 and increased surface expression of CXCR4, providing a further indication of a role for this chemokine-receptor pair in the GC.

SDF-1 expression in the dark zone

SDF-1 mRNA expression has previously been detected by *in situ* hybridization in the splenic red-pulp (Hargreaves *et al.*, 2001), lymph node medullary cords (Hargreaves *et al.*, 2001), and in cells associated with high endothelial venules (HEVs) (Okada *et al.*, 2002), but not in the GC (Bleul *et al.*, 1998; Hargreaves *et al.*, 2001). Immunohistochemical analysis with two polyclonal SDF-1 antibodies revealed a similar distribution of SDF-1 protein but failed to detect SDF-1 within the GC (data not shown), consistent with two reports that SDF-1 protein was not detected in human tonsil and

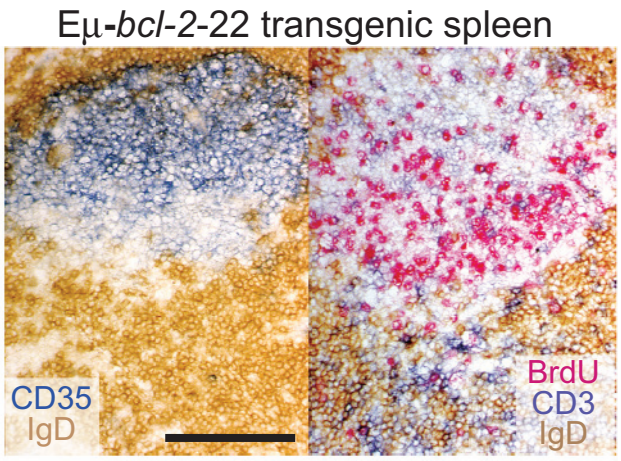

Supplementary Figure 1. GCs in Eμ-*bcl-2*-22 transgenic mice have normal dark and light zone polarity. Immunohistochemistry of a GC from the spleen of an immunized and BrdU-pulsed Eμ-*bcl-2*-22 transgenic mouse. Panels show serial cryostat sections of the same GC stained with the indicated antibodies. Note the presence of distinct CD35-rich (light zone) and BrdU-rich (dark zone) regions in the GC. Panels are representative of GCs from three mice. Scale bar, 100μm.

lymph node GCs (Casamayor-Palleja *et al.*, 2001; Krug *et al.*, 2002). However, as the above findings provided strong functional evidence that SDF-1 was present in GCs, we tested whether another reagent, the monoclonal antibody K15C (Amara *et al.*, 1999), was more sensitive in detecting SDF-1 than the polyclonal reagents. Because K15C is a mouse antibody, we analyzed SDF-1 expression in lymphoid tissue from immunized rats. K15C gave more intense staining in lymph node medullary cords and HEV than the polyclonal reagents and also showed reactivity in T cell zones and B cell follicles (**Fig. 5a**, left panel). More importantly, K15C staining was detected within GCs and in cases where GC dark and light zones could be clearly delineated by BrdU staining, the K15C signal was more intense in the dark zone compared to the light zone (**Fig. 5a**, upper right panel). Staining specificity was confirmed by analysis of adjacent sections incubated with K15C in the presence of an SDF-1 peptide that encompasses the K15C epitope, hence acting as a blocking peptide (**Fig. 5a**, lower right panel). These observations prompted us to further test whether SDF-1 mRNA could be detected within GCs. For this purpose we used laser capture microdissection to isolate dark and light zones as well as neighboring compartments from sections of mouse lymph nodes (**Fig. 5b**). Quantitative RT-PCR analysis on RNA prepared from the captured tissue fragments revealed that, although the abundance was low, SDF-1 mRNA was present within the GC, with higher expression in the dark zone compared to the light zone (**Fig. 5b**). SDF-1 mRNA expression in the follicle and T zone was similar and higher than in the GC, and the highest expression was detected within medullary cords (**Fig. 5b**), an overall pattern that was similar to the K15C staining for SDF-1 protein. In contrast, CXCL13 mRNA was present in higher amounts in the light zone than the dark zone, and was most abundant in follicles, consistent with

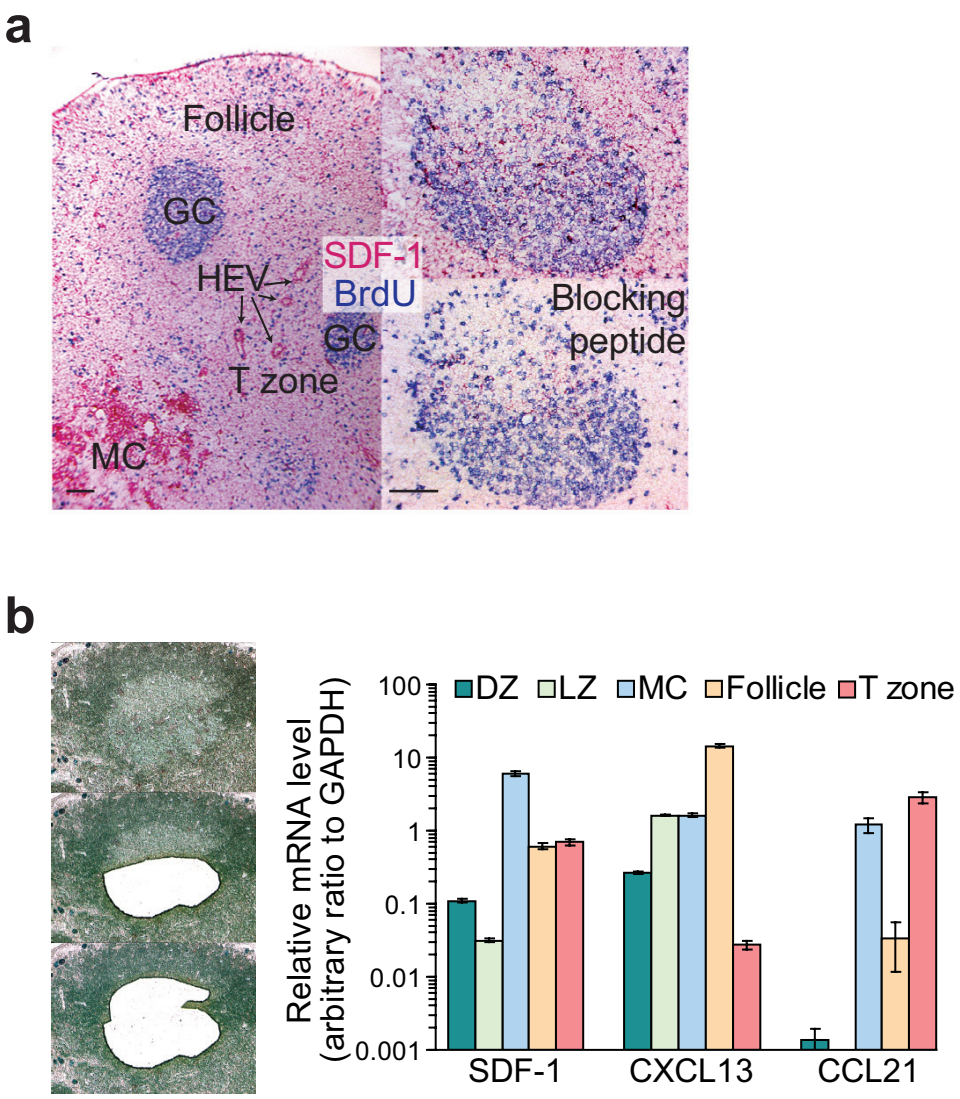

Figure 5. Detection of SDF-1 protein and mRNA within the GC. (**a**) Representative immunohistochemistry of cryostat sections of immunized rat lymph nodes stained with anti-BrdU and K15C anti-SDF-1 with or without the blocking peptide as indicated. The left panel shows a low power view. Note that the GCs were not polarized in this plane of view. The right panel shows serial cryostat sections in which a GC shows dark and light zone polarity as identified by BrdU labeling of centroblasts in the dark zone. Data are representative of two experiments with tissue from three rats. Scale bars, 100μm. (**b**) Analysis of SDF-1 mRNA expression by laser capture microdissection and quantitative RT-PCR. GC dark and light zones were identified in immunized mouse lymph nodes by the respective density of methyl green staining, in which the dense cluster of large centroblasts in the dark zone gave darker staining than the loosely associated, smaller, centrocytes in the light zone (upper panel). Representative laser capture microdissection is shown (sequentially captured regions appear white) of a dark zone (middle panel) and light zone (lower panel). Quantitative RT-PCR analysis of mRNA expression in triplicate from one experiment is shown in the bar graph (mean ± s.d.). Similar data for SDF-1 and CXCL13 were obtained in three experiments (two experiments for the T zone). (DZ, dark zone; LZ, light zone; MC, medullary cord).

previous *in situ* hybridization studies (Cyster *et al.*, 2000). Transcripts for the T zone chemokine, CCL21, were readily detected in tissue fragments isolated from the T zone but were almost undetectable within the GC dark and light zones (**Fig. 5b**). In summary, these findings demonstrate that SDF-1 is expressed within the GC and is present at higher amounts in the dark zone compared to the light zone.

Dark zone localization is dependent on CXCR4

Based upon our findings regarding SDF-1 distribution, we reasoned that CXCR4 might function to promote centroblast localization in the dark zone. Immunohistochemical analysis revealed that CXCR4 expression was higher in the dark zone than in the light zone (**Fig. 6a**), suggesting that CXCR4 was specifically upregulated on centroblasts. This finding was confirmed by labeling proliferating centroblasts *in vivo* with BrdU, then separating $CXCR4^{lo}$ and $CXCR4^{hi}$ subsets of GC B cells by fluorescence activated cell sorting (**Fig. 6a**), and analyzing the subsets by flow cytometry to determine the percentage of $BrdU^{+}$ cells. This experiment showed that the $CXCR4^{hi}$ subset was enriched in $BrdU^{+}$ cells compared with the $CXCR4^{lo}$ subset. Therefore, high CXCR4 expression correlates with the centroblast stage of GC B cell maturation.

The observation that CXCR4 expression was higher on centroblasts than on centrocytes was consistent with the hypothesis that SDF-1 is involved in positioning centroblasts in the dark zone. To further probe this possibility, we examined the position of $Cxcr4^{-/-}$ GC B cells in the context of a wild-type GC. Purified $Cxcr4^{-/-}$ or $Cxcr4^{+/+}$ B cells expressing the congenic marker CD45.1 were co-transferred with $Cxcr4^{+/+}$ CD45.2 cells into B-cell-deficient mice, at a ratio such that the majority of the cells were $Cxcr4^{+/+}$

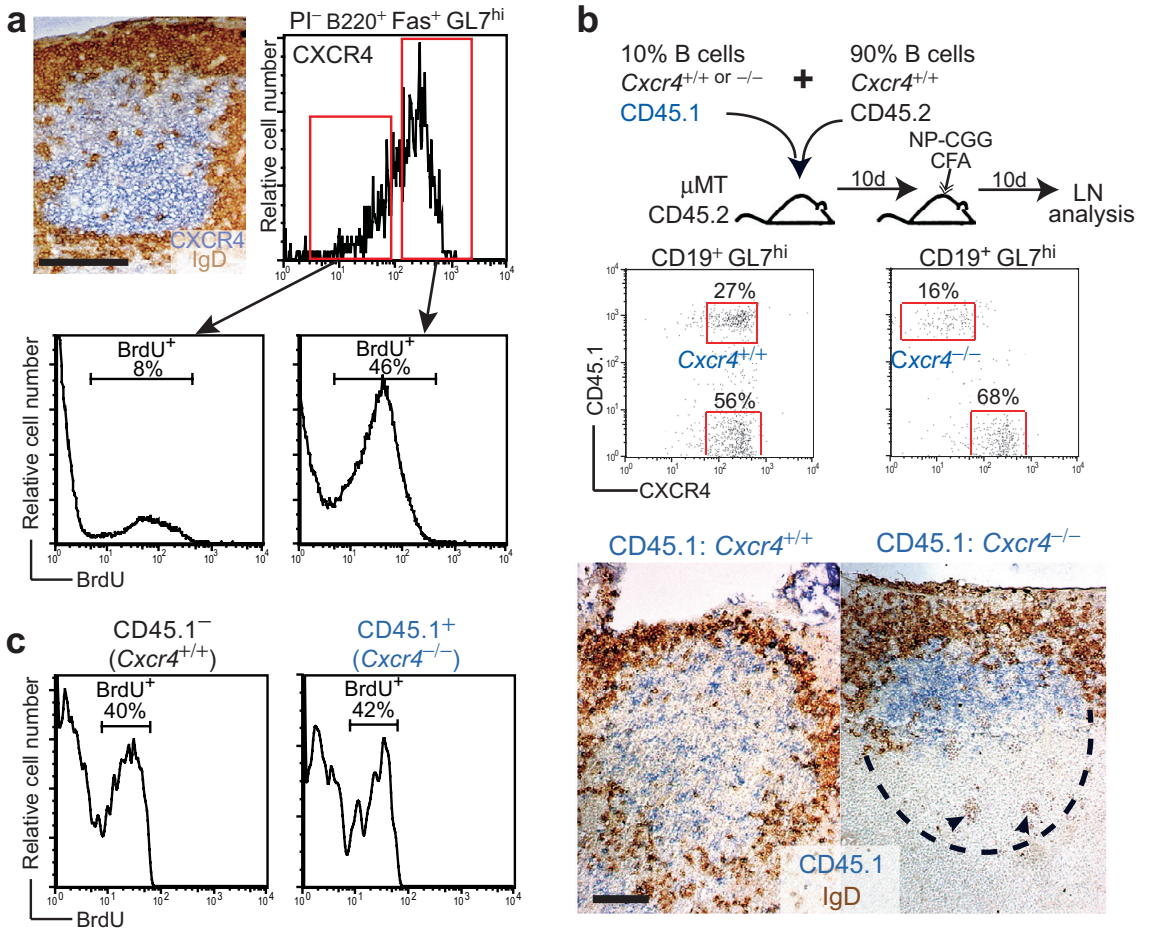

Figure 6. CXCR4 is upregulated on centroblasts and is required for dark zone localization. (**a**) CXCR4 is expressed in the dark zone by proliferating centroblasts. The first panel shows immunohistochemistry of a cryostat section of an immunized mouse lymph node, stained with the indicated antibodies, and is representative of four experiments. No CXCR4 staining was seen in the lymph nodes of *Cxcr4*$^{-/-}$ FL chimeras (data not shown). In the remaining panels, GC B cells (PI^{-} B220^{+} Fas^{+} GL7^{hi}) were sorted into CXCR4^{lo} and CXCR4^{hi} subsets after five-hour *in vivo* labeling with BrdU, then permeabilized, and analyzed by flow cytometry to determine the percentage of BrdU^{+} cells. Cells were sorted from the spleens of six immunized mice, and the data are representative of two experiments. (**b**) CXCR4 is required for centroblasts to localize to the dark zone. To visualize the position of *Cxcr4*$^{-/-}$ B cells in a wild-type GC, a mixture of CD45.1 (*Cxcr4*$^{+/+}$ or *Cxcr4*$^{-/-}$) and CD45.2 (*Cxcr4*$^{+/+}$) B cells were transferred into B-cell deficient mice (µMT) according to the scheme depicted. Flow cytometric analysis shows the actual percentage of GC B cells (CD19^{+} GL7^{hi}) that were CD45.1^{+} in the responding lymph nodes. The position of CD45.1^{+} cells in each GC was assessed by immunohistochemistry. The boundaries of the GCs (indicated in the right panel with dashes), were determined by staining adjacent sections with GL7 and anti-IgD (data not shown). To further assist with visualization of the GC region, arrowheads identify some tingible body macrophages found in the GC. Panels are representative of five GCs each from a set of transfers. The same result has been observed in two additional experiments with mixed FL chimeras. Scale bars, 100µm. (**c**) Flow cytometric analysis of the frequency of BrdU^{+} GC B cells in the mesenteric lymph nodes of a mixed chimera (CD45.1 *Cxcr4*$^{-/-}$ FL and CD45.2 *Cxcr4*$^{+/+}$ BM) that was immunized i.p. and BrdU-pulsed. Histograms were gated on B220^{+} GL7^{hi} and CD45.1^{+} or CD45.1^{-} cells, as indicated. Data are representative of four chimeras in two experiments.

(**Fig. 6b**). After immunization, immunohistochemical analysis revealed that CD45.1^{+} *Cxcr4*$^{-/-}$ B cells accumulated in the light zones of wild-type GCs (**Fig. 6b**, right panel) but were absent from the dark zone, whereas CD45.1^{+} *Cxcr4*$^{+/+}$ B cells in control recipients were evenly distributed in dark and light zones as expected (**Fig. 6b**, left panel). The absence of *Cxcr4*$^{-/-}$ B cells in the dark zone of wild-type GCs was also observed in mixed chimeras that were generated by mixing CD45.1 *Cxcr4*$^{-/-}$ FL with CD45.2 *Cxcr4*$^{+/+}$ bone-marrow (data not shown). BrdU labeling indicated that a similar frequency of *Cxcr4*$^{-/-}$ and *Cxcr4*$^{+/+}$ GC B cells in these mixed chimeras were undergoing cell division (**Fig. 6c**), suggesting that both *Cxcr4*$^{-/-}$ centroblasts and centrocytes were localized in the light zone. These data establish an intrinsic requirement for CXCR4 in the dark zone localization of centroblasts.

CXCR5 determines the position of dark and light zones

The GCs in mice deficient in CXCR5 or its ligand CXCL13 have reduced size and atypical distribution (Ansel *et al.*, 2000; Voigt *et al.*, 2000), yet the function of this receptor-ligand pair in the GC has been unknown. Because CXCL13 mRNA and protein were concentrated in the GC light zone (Cyster *et al.*, 2000) (**Figs. 3 and 5b**) and GC B cells were able to migrate toward CXCL13 (**Fig. 4b**), CXCL13 and CXCR5 appeared likely to direct GC B cells to the light zone. We tested this possibility by transferring a mixture of purified CD45.1 *Cxcr5*$^{-/-}$ B cells and CD45.2 *Cxcr5*$^{+/+}$ B cells into B-cell-deficient recipients, and analyzing the distribution of CD45.1^{+} cells in the GCs formed after immunization. *Cxcr5*$^{-/-}$ B cells were typically excluded from wild-type GCs (data not shown); however by transferring larger numbers of these cells and analyzing

numerous GCs, it was observed that they occasionally participated in wild-type GCs. In these GCs, the *Cxcr5*$^{-/-}$ cells accumulated in the dark zone, adjacent to the T zone, and were absent from the light zone (**Fig. 7a**, right panel). These findings support the conclusion that CXCR5 and CXCL13 contribute to attracting GC B cells to the light zone.

Unexpectedly, however, immunohistochemical analysis of the small GCs that developed in the lymph nodes of immunized and BrdU-pulsed *Cxcl13*$^{-/-}$ mice revealed separate BrdU^{+} and CD23^{+} regions, indicating the presence of dark and light zones, in greater than 66% of GCs (42/64) (**Fig. 7b**). The relative positions of these zones were atypical, such that the light zone seemed to have a random orientation rather than being located distal to the T zone (**Fig. 7b**; arrows indicate positions of light zones). Indeed, in many cases (19/64), CD23 staining was brightest at the center of the GC and was surrounded by a ring of BrdU^{+} centroblasts (**Fig. 7b**). Similar findings were made by analysis of GCs in *Cxcr5*$^{-/-}$ mice (data not shown). To investigate whether CXCR4 was responsible for the segregation of dark and light zones in the absence of CXCL13 or CXCR5, we analyzed GCs in *Cxcr4*$^{-/-}$ *Cxcr5*$^{-/-}$ double-deficient FL chimeras and in *Cxcl13*$^{-/-}$ or *Cxcr5*$^{-/-}$ mice treated with the CXCR4 inhibitor 4F-benzoyl-TE14011. For reasons that are unclear, the expression of the FDC marker CD23 was weak in the GCs that formed under both of these conditions such that its distribution could not be assessed, making it difficult to examine dark and light zone segregation (data not shown). However, BrdU labeling alone revealed that centroblasts formed an identifiable dark zone in about 40% (23/61) of GCs analyzed in *Cxcl13*$^{-/-}$ or *Cxcr5*$^{-/-}$ mice, whereas less than 10% (5/51) of GCs showed any polarity when CXCR4 was also deficient (**Fig. 7c** and

data not shown). Overall, these data suggest that CXCR4 provides a dominant cue for GC dark and light zone segregation and that CXCR5 and CXCL13 are required for the correct orientation of these zones.

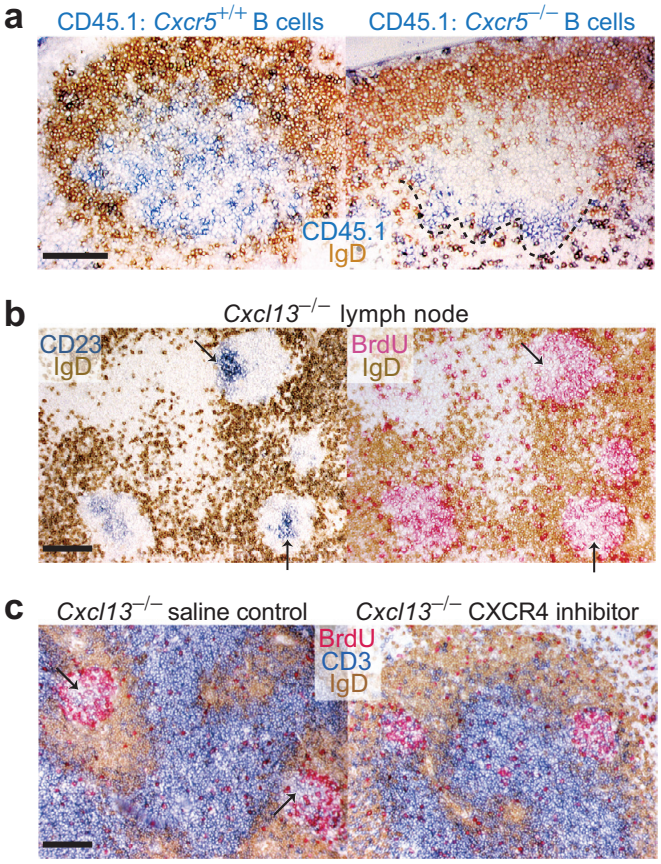

Figure 7. CXCR5 and CXCL13 function in determining light zone position. (**a**) CXCR5-deficient B cells fail to localize within the light zone of predominantly wild-type GCs. A mixture of purified B cells (10% CD45.1 *Cxcr5*$^{+/+}$: 90% CD45.2 *Cxcr5*$^{+/+}$, or 50% CD45.1 *Cxcr5*$^{-/-}$: 50% CD45.2 *Cxcr5*$^{+/+}$) was transferred into B-cell deficient mice, which were then immunized and analyzed by immunohistochemistry as in Fig. 6b. The boundary of the dark zone (indicated with dashes) was identified in serial sections by staining with GL7 and anti-IgD or anti-BrdU, anti-CD45.1, and anti-IgD (data not shown). Similar GCs were observed in at least six recipients of each type in four experiments. (**b**) GCs in *Cxcl13*$^{-/-}$ mice have aberrant light zone position. GCs were analyzed by immunohistochemistry of cryostat sections of lymph nodes present in immunized and BrdU-pulsed *Cxcl13*$^{-/-}$ mice (typically superficial cervical and mesenteric). Panels show immunohistochemistry of serial cryostat sections stained with the indicated antibodies. Note that dense CD23 and BrdU staining is seen in opposing regions in two GCs. The variable position of the light zone is indicated with arrows. Panels are representative of GCs analyzed from at least three lymph nodes each from seven mice in two experiments. (**c**) CXCR4 is required for GC dark and light zone segregation in CXCL13-deficient mice. *Cxcl13*$^{-/-}$ mice were implanted with Alzet pumps containing saline (vehicle) or the CXCR4 inhibitor 4F-benzoyl-TE14011 three days after s.c. immunization, and analyzed on day 10 by immunohistochemistry with the indicated antibodies. Note the presence of BrdU negative regions in some GCs after saline treatment (left panel, indicated by arrows), but the absence of these regions after CXCR4 inhibitor treatment (right panel). Scale bars, 100μm.

Discussion

The above findings identified essential requirements for GC polarization into dark and light zones. GC B cells were found to be highly motile and centroblasts expressed higher amounts of CXCR4 than centrocytes and localized to the GC dark zone in a CXCR4-dependent manner. Consistent with this CXCR4 requirement, SDF-1 was more abundant in the GC dark zone than in the light zone. GC B cells also expressed CXCR5 and responded to CXCL13, a chemokine present in the GC light zone and CXCL13 and CXCR5 were shown to dictate the orientation of GC light and dark zones. In addition, our analysis of mice containing CXCR4-deficient B cells indicated that B cells were involved in regulating the differential distribution of FDCs in GC light and dark zones.

It has previously been suggested that GC B cells do not respond or respond poorly to chemokines, based upon the failure of human tonsil GC B cells to migrate in several *in vitro* studies (Bleul *et al.*, 1998; Casamayor-Palleja *et al.*, 2002; Corcione *et al.*, 2000; Roy *et al.*, 2002). Instead, we found that when mouse GC B cell survival was extended by *bcl-2* overexpression, these cells exhibited robust migratory responses to chemokines. Consistent with an important role for SDF-1 and CXCR4 in the GC, it was observed that GC B cells responded more strongly to SDF-1 and expressed higher amounts of CXCR4 than follicular B cells. In addition, the basal motility of GC B cells was higher than that of follicular B cells when examined in the absence of chemokine. A previous study of mouse Peyer's patch GC B cells also provided evidence that the cells could respond to lymphoid chemokines, although responsiveness to SDF-1 was suggested to be reduced compared to follicular B cells (Bowman *et al.*, 2000), a difference most likely attributable to the effects of the rapid death of unprotected GC B cells *in vitro*. Consistent with

CXCR4 also functioning in human GCs, CXCR4 has been identified on human tonsil GC B cells by flow cytometry and immunofluorescence analysis of tissue sections (Bleul *et al.*, 1998; Casamayor-Palleja *et al.*, 2002; Forster *et al.*, 1998; Roy *et al.*, 2002). Moreover, human follicular lymphoma cells, which are thought to be derived from GC B cells that acquire mutations promoting increased survival, show marked chemotaxis to SDF-1 (Corcione *et al.*, 2000).

Previous studies of SDF-1 distribution have failed to detect SDF-1 mRNA or protein within GCs (Bleul *et al.*, 1998; Casamayor-Palleja *et al.*, 2001; Hargreaves *et al.*, 2001; Krug *et al.*, 2002). By both *in situ* hybridization and analysis of protein distribution with various polyclonal anti-SDF-1 reagents we were also unable to detect SDF-1 within GCs. However, the sensitivity of these techniques was poor and did not exclude the possibility that SDF-1 was present in GCs in low amounts. Indeed, using more sensitive approaches, we detected a broad distribution of SDF-1 mRNA and protein within lymphoid tissues, including within GCs, follicles and T zones. Importantly, although the abundance of SDF-1 within the GC was lower than in the surrounding compartments, SDF-1 amounts within the GC dark zone were higher than in the adjacent light zone. The overlapping SDF-1 mRNA and protein distribution indicated that the chemokine was produced locally. Because we have not detected SDF-1 mRNA within GC B cells (data not shown), we hypothesize that SDF-1 is produced by stromal cells in the dark zone. Taking these findings together with the observation that centroblasts express higher amounts of CXCR4 than centrocytes and that CXCR4 is required for GC B cells to locate within the dark zone of wild-type GCs, we conclude that SDF-1 functions to attract or retain centroblasts within the dark zone.

It is notable that the expression of SDF-1 is higher in the follicular mantle zone than in the adjacent GC light zone, yet the follicular SDF-1 does not appear to reach the light zone. This suggests that SDF-1 is bound tightly at or near sites of production, a scenario that is supported by the similar profiles of SDF-1 mRNA and protein distribution throughout the lymphoid tissue. Alternatively, boundaries may exist between the GC and surrounding compartments that limit the entry of chemokines. An implication of these findings is that chemokine function can be highly localized such that adjacent tissue regions can employ the same chemokine to control distinct positional events.

CXCL13 has an opposing distribution within the GC compared to SDF-1, being more abundant in the light zone than in the dark zone. Consistent with this distribution, our mixed B cell transfer experiments indicate that CXCL13 and CXCR5 function to direct B cells to the light zone. We therefore propose that as centroblasts down-regulate CXCR4 and differentiate into centrocytes, the balance of chemokine responsiveness shifts in favor of CXCL13 and the cells migrate to the light zone. Unexpectedly, CXCL13 was not essential for dark and light zone segregation as the small GCs that developed in CXCL13-deficient mice frequently contained both zones. However, another defect emerged in these animals: correct polarity of the GC was lost such that the light zone was often found in the center of the GC or near the T zone. Therefore, our findings define a role for CXCL13 to promote positioning of the light zone in the pole of the GC distal to the T zone and they indicate that centrocyte separation from centroblasts is not solely mediated by centrocyte migration to CXCL13. Instead, as dark and light zone formation continued to be CXCR4-dependent in the absence of CXCL13 (or CXCR5), it

appears that differential responsiveness to SDF-1 may be sufficient to segregate centroblasts from centrocytes.

Although we establish essential roles for the CXCR4-SDF-1 and CXCR5-CXCL13 receptor-ligand pairs within the GC, our studies also lead us to propose that further guidance factors contribute to GC organization. This hypothesis is supported by the continued formation of GC clusters in mice lacking both CXCR4 and CXCL13 function. Studies performed several decades ago provided evidence that transferred radiolabeled GC B cells home selectively to GCs in recipient animals (Nieuwenhuis and Opstelten, 1984). As neither SDF-1 nor CXCL13 are GC-specific, these observations are best explained by the existence of a GC-specific attractant. A GC specific activity may also help keep GC cells in a tight cluster and prevent them from migrating out of the GC into the adjacent, SDF-1-, CXCL13-, and CCL21-rich compartments.

Although our studies demonstrate the importance of high CXCR4 expression on centroblasts, the mechanism for selective CXCR4 upregulation on these cells remains unclear. Arguing against a transcriptional mechanism, a previous study showed by RNase protection assay that CXCR4 mRNA expression was similar in GC B cells and follicular B cells from immunized mouse lymph nodes (Wehrli *et al.*, 2001) and using real-time PCR we have made similar findings for sorted splenic GC B cells (data not shown). It therefore seems likely that CXCR4 is regulated in GC B cells by post-translational mechanism(s). Consistent with this possibility, several modes of CXCR4 post-translational regulation have been described (Guinamard *et al.*, 1999; Marchese and Benovic, 2001).

The finding that deficiency of CXCR4 specifically in B cells disrupted the organization of GC FDCs indicates that B cells play an essential role in GC organization. In contrast, CXCR4-deficiency in T cells was not found to disrupt GC organization, although we have not excluded an effect of CXCR4 on T cell localization or interactions within the GC. Compared with primary follicle FDCs, GC FDCs in the light zone normally acquire additional markers, including CD23, $Fc_{\gamma}RIIb$, and VCAM-1 (Balogh *et al.*, 2002; Cyster *et al.*, 2000; MacLennan, 1994; Maeda *et al.*, 1992). Our finding that disruption of centroblast and centrocyte segregation resulted in the appearance of $CD23^{+}$ FDCs throughout the GC, rather than selectively in the light zone, suggests that centrocytes in the light zone normally act to promote the development of FDCs with these unique surface markers at that pole.

In conclusion, we have established that CXCR4 upregulation on centroblasts segregates these cells from centrocytes, resulting in the establishment of the GC dark and light zones. CXCL13 and CXCR5 play an important role in the correct positioning of these zones and contribute to recruiting cells to the light zone. The involvement of chemokines and their receptors in guiding cell movements within the GC and the high motility of GC B cells provide a basis for understanding how newly mutated GC B cells achieve efficient encounters with antigen-bearing FDCs and antigen-specific GC T cells. This study places the GC among a growing number of processes within the immune system that are dependent on CXCR4, including B cell development (Egawa *et al.*, 2001; Ma *et al.*, 1998; Zou *et al.*, 1998), T cell development (Ara *et al.*, 2003; Plotkin *et al.*, 2003), lymph node entry (Okada *et al.*, 2002), plasma cell localization (Hargreaves *et al.*, 2001), and neutrophil homing to the bone marrow (Martin *et al.*, 2003). The central role

of CXCR4 and SDF-1 in these diverse processes supports the view that SDF-1 is a 'primordial' chemokine (Bleul *et al.*, 1996). It also suggests another immune function that is likely to be disrupted in patients with Warts, Hypogammaglobulinemia, Infections, Myelokathexis (WHIM) syndrome who carry C-terminal truncation mutations in CXCR4 (Hernandez *et al.*, 2003) and raises new concerns about the effects of global CXCR4 inhibition for anti-retroviral therapy.

Materials and Methods

Mice, rats, and chimeras.

C57BL/6 (B6) and B6-CD45.1 mice were obtained from The Jackson Laboratory or the National Cancer Institutes. B6-SCID (*Prkdc*^{scid} #001913), B6-RAG (*Rag1*^{tm1Mom} #002216), B6-μMT (*Igh-6*^{tm1Cgn} #002288), and B6-TCRβδ$^{-/-}$ (*Tcrb*^{tm1Mom} *Tcrd*^{tm1Mom} #002122) mice were from The Jackson Laboratory and were maintained on water containing 0.25–2 mg/mL tetracycline (Sigma-Aldrich, American Livestock Company, or USB). 129-RAG (*RAG2-M*) mice were from Taconic. *Cxcr4*$^{+/-}$ mice (Zou *et al.*, 1998), were backcrossed at least six generations and *Cxcl13*$^{-/-}$ mice (Ansel *et al.*, 2000), *Cxcr5*$^{-/-}$ mice (Forster *et al.*, 1996), and Eμ-*bcl-2*-22 mice (Strasser *et al.*, 1991) were backcrossed at least 10 generations to the B6 strain. All mice were maintained in transgenic barrier facilities. Sprague-Dawley rats were obtained from Charles River Laboratories and maintained in a conventional facility. Protocols were approved by the University of California, San Francisco, Institutional Animal Care and Use Committee.

FL chimeras were generated as described (Hargreaves *et al.*, 2001) with the following modifications: as an additional method of screening for *Cxcr4* genotype, FL cells were stained with anti-CXCR4 biotin followed by anti-CD45.1 or anti-CD45.2 FITC, anti-B220 PE, and streptavidin APC and analyzed by flow cytometry as described below. Dead cells were excluded with 1 μg/mL PI (Sigma-Aldrich). In most experiments, FL chimeras were generated in B6-SCID, B6-RAG, or 129-RAG recipients to avoid a contribution from residual host lymphocytes. B6-SCID mice were irradiated with a single dose of 400 rads, and B6-RAG mice were irradiated with two doses of 450 rads. After the *Cxcr4*$^{+/-}$ mice were backcrossed more than 10 generations to the B6 strain, it was

necessary to increase the number of *Cxcr4*$^{-/-}$ FL cells transferred to at least 5x10^6 live cells per recipient in order to obtain reasonable B-cell reconstitution frequencies (within three-fold of normal). Data have only been included for chimeras that had a peripheral B cell frequency of at least 6% of total lymphocytes (average, *Cxcr4*$^{+/+}$ FL chimeras, 46%; *Cxcr4*$^{-/-}$ FL chimeras, 18%).

Immunizations and BrdU treatment.

For induction of spleen GCs, mice were immunized i.p. with SRBC (Colorado Serum Company) as described (Shinall *et al.*, 2000), and analyzed eight days later. For induction of lymph node GCs, animals were immunized s.c. with (4-hydroxy-3-nitrophenyl)acetyl-chicken gamma globulin (NP_{21}-CGG or NP_{36}-CGG; Biosearch Technologies) (mice, total of 100–200 μg; rats, total of 1.5 mg) emulsified in complete Freund's adjuvant (CFA; Sigma-Aldrich), in the scruff of the neck, shoulders, flanks, and/or above the tail. Draining lymph nodes (superficial cervical, axillary, brachial, and inguinal) were analyzed 10–14 days later. To label centroblasts, BrdU (Sigma-Aldrich) was administered (mice, 2.5 mg; rats, 7 mg) in phosphate buffered saline (PBS) by i.p. injection, five to six hours before sacrificing the animals.

CXCR4 inhibitor treatment.

Alzet osmotic pumps (seven-day duration, 0.5 μl/hour pumping rate, Model 1007D, Durect Corporation) were loaded with 40 mg/mL of the CXCR4 antagonist 4F-benzoyl-TE14011 (Tamamura *et al.*, 2003) in saline and implanted s.c. in the back according to

the manufacturer's instructions. 0.05–0.1 mg/kg buprenorphine (Sigma-Aldrich) was given s.c. as an analgesic after surgery.

Flow cytometry and cell sorting.

Cell suspensions were prepared from spleens and lymph nodes by mechanical disruption on 70 μm nylon cell strainers (Falcon) in RPMI-1640 medium (cellgro) containing L-glutamine, 2% fetal bovine serum (FBS; Gibco-BRL), antibiotics (50 IU/mL penicillin, 50 μg/mL streptomycin; cellgro), and 10 mM HEPES (cellgro), washed, and kept on ice. For flow cytometry, cells were plated at $5x10^5$–$1x10^6$ cells per well in 96-well U-bottom plates (Falcon), stained for 20–60 minutes on ice with the antibodies listed in **Supplementary Table 1,** in 25 μL of PBS containing 2% FBS, 1 mM EDTA, and 0.1% NaN_3, and washed twice with 200 μL of the same buffer after each step. Data was collected on a Becton Dickinson (BD) FACS Calibur and analyzed with CellQuest Pro (BD) or FlowJo (TreeStar) software. CCR7 was stained with CCL19-Fc as described (Hargreaves *et al.*, 2001), except that binding was detected with biotin-conjugated goat anti-human IgG, Fc_γ fragment specific (Jackson ImmunoResearch). Annexin-V staining for apoptotic cells was with Annexin-V biotin (BD Pharmingen) in buffer containing Ca^{2+} and Mg^{2+} and lacking EDTA. Biotinylated reagents were detected with streptavidin APC (Molecular Probes). In some cases, dead cells were excluded with 1 μg/mL PI.

For cell sorting, cell suspensions were first prepared from spleens in Hank's Balanced Salt Solution (UCSF Cell Culture Facility) containing 0.5% FBS, 0.5% fatty-acid free bovine serum albumin (BSA; Calbiochem), and 200 μg/mL deoxyribonuclease I from bovine pancreas (DNase I; Sigma-Aldrich) and washed. Cells were labeled on ice at

Supplementary Table 1. Antibodies used in flow cytometry.

Target	Clone	Conjugates	Vendor	Dilution Factor
BrdU	3D4	PE	BD Pharmingen	5
CD45R/B220	RA3-6B2	PE	Caltag	100
CD45R/B220	RA3-6B2	PerCP, PE-Cy7, APC, APC-Cy7	BD Pharmingen	75-100
CD19	1D3	PE-Cy7, APC	BD Pharmingen	75-200
CD45.1/Ly5.2	A20	FITC, PE, biotin	BD Pharmingen	100
CD45.2/Ly5.1	104	FITC, biotin	BD Pharmingen	100
CD95/Fas	Jo2	PE-Cy7	BD Pharmingen	100
CXCR4	2B11/CXCR4	biotin	BD Pharmingen	100
CXCR5	2G8	biotin	BD Pharmingen	50
IgD	11-26	PE	Southern Biotechnology	100
T- and B-cell activation antigen	GL7	FITC	BD Pharmingen	300-500

a concentration of $4x10^7$ cells/mL with anti-CXCR4 biotin for 30 minutes and then erythrocytes were lysed by centrifugation at 4°C in a solution of Tris-buffered NH_4Cl. Next, cells were labeled on ice with GL7 FITC, anti-Fas PE-Cy7, streptavidin APC, and anti-B220 APC-Cy7 and washed. Dead cells were excluded with 1 μg/mL PI. Cells were sorted on a Mo-Flo (DakoCytomation).

The percentage of cells that had incorporated BrdU during DNA synthesis was determined by flow cytometry as described (Luther *et al.*, 1997) with the following modifications: $5x10^5$ Jurkat cells were added to each sample to help pellet the cells, and could be excluded during analysis based upon their large scatter characteristics. For mixed chimeras, cells were stained with anti-CD45.1 biotin for one hour. After fixation and permeabilization, cells were stained in PBS containing 0.5% Tween-20 and 2% FBS with a diluted mixture of: GL7 FITC, anti-BrdU PE, anti-Fas PE-Cy7 or anti-B220 PerCP, and anti-B220 APC or streptavidin APC; or in the case of sorted cells that were already surface stained, only anti-BrdU PE.

B-cell purification and transfer.

Spleens were mashed on 70 μm nylon cell strainers, or in later experiments were digested with collagenase and EDTA as previously described for dendritic cells (Ngo *et al.*, 1998), as this enzymatic digestion improved B cell recovery. Splenocytes were washed and resuspended in DMEM medium (cellgro) containing 4.5 g/L glucose, L-glutamine, 10% FBS, 10 mM HEPES, antibiotics, and 50 μg/mL DNase I. Naïve B cells were then purified by a negative selection strategy. Splenocytes were labeled with anti-CD43 biotin (S7, BD Pharmingen) and anti-CD11c biotin (HL3, BD Pharmingen) for 25 minutes on

ice, washed and centrifuged with Tris-buffered NH_4Cl to lyse erythrocytes, and then labeled with streptavidin microbeads (Miltenyi Biotec) for 20 minutes on ice. Labeled cells were depleted by autoMACS (Miltenyi Biotec) according to the manufacturer's instructions, giving a B-cell purity of at least 90% as determined by flow cytometry. T cell contamination was less than 0.75%, although the identity of the remaining cells remained unclear (they did not stain positive for CD3, CD11c, Mac-1, or NK1.1). $1.5x10^7$–$4.5x10^7$ B cells per recipient were transferred by intravenous injection into the tail veins of B-cell deficient mice (μMT).

Immunohistochemistry.

Spleens and lymph nodes were placed in Tissue-Tek OCT compound (Sakura), snap frozen in dry ice/ethanol, and stored at −80°C. For immunohistochemistry, cryostat sections (7 μm) were affixed to multispot (Hendley-Essex) or Superfrost/Plus (Fisher Scientific) microscope slides, dried at room temperature (RT), fixed in cold acetone for 10 minutes, and then dried at RT. Slides were re-hydrated in Tris-buffered saline (TBS) pH 7.6, and then stained at RT in a humidified chamber in TBS containing 0.1% BSA (ICN), 1% normal mouse serum (Sigma-Aldrich), and a diluted mixture of two of the primary antibodies listed in **Supplementary Table 2** for two to three hours at RT. After washing the slides in TBS for 3 minutes with gentle agitation, sections were stained as described above with the secondary antibodies listed in **Supplementary Table 3** for one to two hours. Biotinylated antibodies were detected with streptavidin alkaline phosphatase (Jackson Immunoresearch or Vector Labs). Rat tissue was stained as described above in TBS containing 0.1% BSA and 1% normal rat serum with 20 μg/mL

Supplementary Table 2. Primary antibodies used in mouse immunohistochemistry.

Species	Target	Clone or Designation	Conjugate	Vendor	Dilution factor
Mouse	BrdU	3D4	FITC	BD Pharmingen	5
Armenian hamster	CD3ε	145-2C11	Purified	BD Pharmingen	100
Rat	CD23	B3B4	Biotin	BD Pharmingen	100
Rat	CD35	8C12	Purified	BD Pharmingen	50
Mouse	CD45.1/Ly5.2	A20	Biotin	BD Pharmingen	100
Goat	CXCL13	Polyclonal	Purified	R&D Systems	20
Rat	CXCR4	2B11/CXCR4	Biotin	BD Pharmingen	100
Rat	Complement component C4	FDC-M2	Purified	Gift of M. Kosco-Vilbois	200
Rat	Complement component C4	FDC-M2	Biotin	ImmunoKontact	200
Rat	IgD	11-26c.2a	Purified	BD Pharmingen	50
Sheep	IgD	Polyclonal	Purified	The Binding Site	300
Goat	SDF-1	Polyclonal (C19)	Purified	Santa Cruz Biotechnology	20
Rabbit	SDF-1	Polyclonal	Purified	Torrey Pines Biolabs	30-100
Rat	T-and B-cell activation antigen	GL7	FITC	BD Pharmingen	100-200

Supplementary Table 3. Secondary antibodies used in mouse immunohistochemistry.

Species	Target	Conjugate	Vendor	Dilution factor
Goat	Armenian hamster IgG (H+L)	AP	Jackson Immunoresearch	100
Donkey	Goat IgG (H+L)	Biotin	Jackson Immunoresearch	200
Donkey	Rabbit IgG (H+L)	Biotin	Jackson Immunoresearch	200-500
Donkey	Rat IgG (H+L)	AP	Jackson Immunoresearch	200
Donkey	Rat IgG (H+L)	HRP	Jackson Immunoresearch	150
Donkey	Sheep IgG (H+L)	HRP	Jackson Immunoresearch	300-500
Sheep	Fluorescein (FITC)	AP	Roche	100

AP, alkaline phosphatase; HRP, horse radish peroxidase

K15C, a mouse monoclonal antibody to anti-SDF-1 (Amara *et al.*, 1999), with or without an 8-fold molar excess (2 μg/mL) of the blocking peptide KPVSLSYRSPSRFFE (synthesized by SynPep) for 18 hours at 4°C, then with biotin-conjugated goat anti-mouse IgG, Fc_γ fragment specific (Jackson ImmunoResearch) for two hours at RT, followed by streptavidin ABC alkaline phosphatase (Vector Labs) for one to two hours at RT. Enzyme conjugates were developed as described (Luther *et al.*, 1997) and slides were mounted in Crystal/Mount (biomeda). Images were collected and processed as described (Cinamon *et al.*, 2004).

For detection of cells that had incorporated BrdU in sections, slides were first stained by standard immunohistochemistry as above and then treated as described (Luther *et al.*, 1997), with the following modifications: HCl treatment was for nine minutes, and BrdU detection was with anti-BrdU FITC (3D4, BD Pharmingen) followed by anti-fluorescein AP.

Laser Capture Microdissection and Quantitative RT-PCR Analysis.

Lymph nodes were frozen in OCT as described above. Cryostat sections (7 μm) were affixed to glass foil slides for membrane-based laser microdissection (Leica), allowed to dry for 30 minutes at RT, fixed in 70% ethanol for one minute, washed in distilled water for 30 seconds, stained with 0.6% w/v methyl green (Fluka) for one minute, rinsed in distilled water, dehydrated by a graded ethanol series (70%, 95%, 100%) for one minute each, and allowed to air dry at RT for 7-12 hours. The following regions were isolated by laser capture microdissection on a Leica LS AMD for each experiment: GC dark and light zones (n=40-85), medullary cord regions (n=20-40), primary follicles lacking GCs

(n=30-60), and T cell zones (n=15-30). Microdissected regions were collected in the caps of 0.2 mL thin-walled, RNase-free PCR tubes (Ambion). RNA was isolated using the RNeasy Micro Kit (Qiagen) with on-column DNase treatment according to the manufacturer's instructions. First-strand cDNA was synthesized from RNA with M-MLV RT (Promega) and random primers (Promega) according to the manufacturer's instructions. For quantitative PCR, 4-8% of the cDNA was placed in a final volume of 50 μL containing 1X PCR Buffer II (Applied Biosystems, ABI), 5.5 mM $MgCl_2$ (ABI), 300 μM each dNTP (PCR grade, Invitrogen), 1.25 units of AmpliTaq Gold DNA Polymerase (ABI) and the primers and probes listed in **Supplementary Table 4**. Samples were analyzed on a Prism 7900HT (ABI) with the following thermal-cycler conditions: 50°C for two minutes, 95°C for 10 minutes, and then 40 cycles of 95°C for 15 seconds followed by 60°C for one minute. To quantify the relative amount of starting mRNA in each sample, standard curves were generated for each primer/probe set by preparing serial dilutions of a pooled mixture containing 4% of the cDNA prepared from each microdissected region, in duplicate wells, and analyzed with SDS 2.1 software (ABI). The quantity of target gene determined for each sample was divided by the quantity of a housekeeping gene (GAPDH), giving a relative ratio of mRNA expression.

Chemotaxis Assays.

Cell suspensions were prepared by mechanical disruption of spleens on 70 μm cell strainers (Fisher) and erythrocytes were lysed with Tris-buffered NH_4Cl for 2 minutes at RT. Splenocytes were resuspended at a concentration of $1x10^7$ cells per mL in RPMI-1640 medium containing L-glutamine, antibiotics, 10 mM HEPES buffer, and 0.5% fatty-

Supplementary Table 4. Primer and probe sequences for quantitative real-time PCR.

Target	Primer/ probe	Sequence	Final concentration (nM)
SDF-1	F primer	TGCTGGCCGCGCTCT	300
	R primer	GAGGATTTTCAGATGCTTGACGTT	300
	Probe	FAM-ACGGTAAACCAGTCAGCCTGAGCTACCG-TAMRA	250
CXCL13	F primer	TGGCCAGCTGCCTCTCTC	900
	R primer	TTGAAATCACTCCAGAACACCTACA	900
	Probe	FAM-AGGCCACGGTATTCTGGAAGCCCAT-TAMRA	150
CCL21	F primer	CCCTGGACCCAAGGCAGT	900
	R primer	AGGCTTAGAGTGCTTCCGGG	900
	Probe	FAM-TCCCATCCCGGCAATCCTGTTCTC-TAMRA	200
GAPDH	F primer	GGTCTACATGTTCCAGTATGACTCCAC	300
	R primer	GGGTCTCGCTCCTGGAAGAT	300
	Probe	FAM-CACAGTCAAGGCCGAGAATGGGAAGC-TAMRA	100
For all samples	Passive reference probe	FAM-TTTTTTTTTT-ROX	60

All primers and probes were from Integrated DNA Technologies. F, forward; R, reverse.

acid free BSA. Cells were resensitized for 30–60 minutes at 37°C prior to being plated in 5 μm-pore size, 6.5 mm-diameter Transwell inserts (#93421) in 24-well plates (Corning). 100 μL ($1x10^6$ cells) were added to the upper wells and 580 μL diluted chemokine were placed in the bottom wells at the indicated concentrations, and incubated for three hours at 37°C, 5% CO_2. Migrated cells were enumerated by flow cytometry as described (Ngo *et al.*, 1998). Duplicate wells were analyzed for each concentration of chemokine. Recombinant human SDF-1 was from Peprotech, and recombinant mouse CXCL13 and CCL21 were from R&D Systems.

Acknowledgments

We thank D. Hargreaves, Y. Xu, and M. Lesneski for technical assistance; C. Miller for training in laser capture microdissection; J. Dietrich for surgical expertise; S. Jiang for cell sorting; D. Littman for *Cxcr4*$^{+/-}$ mice; M. Lipp for *Cxcr5*$^{-/-}$ mice, T. Roach for some Eμ-*bcl-2*-22 mice, F. Arenzana-Seisdedos for K15C antibody; J. Lin and other members of the Weiss Lab for Jurkat cells; the Werb lab for the use of equipment and supplies; the UCSF Diabetes Center for use of the ABI Prism 7900HT; S. Luther, T. Okada, and G. Cinamon for advice and comments on the text and figures; and M. Matloubian, C. Lo, and J. Cholfin for helpful discussions.

C.D.C.A. is, and K.M.A. was, a Howard Hughes Medical Institute (HHMI) predoctoral fellow. J.G.C. is a Packard fellow and an HHMI assistant investigator. This work was supported in part by grants from the National Institutes of Health.

CHAPTER 3

Imaging of germinal center selection events during affinity maturation

This chapter was published as:

Allen CDC, Okada T, Tang HL, and Cyster JG. (2007).

Imaging of germinal center selection events during affinity maturation.

Science **315**(5811): 528-31. Epub 2006 Dec 21.

.

Abstract

The germinal center (GC) is an important site for the generation and selection of B cells bearing high affinity antibodies, yet GC cell migration and interaction dynamics have not been directly observed. Using two-photon microscopy of mouse lymph nodes, we revealed that GC B cells are highly motile and extend long cell processes. They transited between GC dark and light zones and divided in both regions, although these B cells resided for only several hours in the light zone where antigen is displayed. GC B cells formed few stable contacts with GC T cells despite frequent encounters, and T cells were seen to carry dead B cell blebs. We use these observations to propose a model in which competition for T cell help plays a more dominant role in the selection of GC B cells than previously appreciated.

Introduction, Results, and Discussion

Germinal centers (GC) represent critical sites within organized lymphoid tissues in which B cell responses to antigen are amplified and refined in specificity. A classical model of GC function holds that B cells in the dark zone undergo rapid rounds of proliferation and somatic hypermutation of their antibody genes, followed by exit from the cell cycle and movement to the light zone, where the B cells undergo selection based on the affinity of their surface antibody for antigen (Kelsoe, 1996; MacLennan, 1994; Manser, 2004; McHeyzer-Williams *et al.*, 2006; Tarlinton, 2006). The selection process is thought to involve competition between GC B cells for capture of antigen in the form of immune complexes displayed on the processes of follicular dendritic cells (FDCs) (Kosco-Vilbois, 2003; MacLennan, 1994; Manser, 2004; Tarlinton, 2006). However, recent experimental evidence and computer simulations have contradicted aspects of this classical model (Haberman and Shlomchik, 2003; Manser, 2004; Meyer-Hermann *et al.*, 2006; Wang and Carter, 2005), and the mechanism by which selection occurs in the GC has remained elusive. One of the challenges in studying GC selection has been a lack of knowledge about the dynamics of GC B cells in their complex physiological milieu.

We developed a system to study the dynamics of GC B cells within intact mouse lymph nodes (LNs) by two-photon microscopy (the system is described in detail in the Supplementary Text). In this system, 1-2% of GC B cells expressed green fluorescent protein (GFP) (Fig. 1A, fig. S1, and fig. S2) and by our measurements were able to undergo the normal processes of class switching, somatic hypermutation, and affinity maturation (fig. S3 and fig. S4). The dynamics of GC B cell motility in explanted LN were compared with two other B cell populations: naïve B cells (representing B cells

prior to antigen encounter) in the follicular mantle that surrounds the GC; and plasma cells (representing post-selected B cells that secrete antibody) in the LN medulla (for details, see the Supplementary Text). GC B cells had highly dynamic shapes in which they extended dendritic processes resembling pseudopods as they moved (Fig. 1B and movie S1) compared with naïve follicular mantle B cells and plasma cells that exhibited a more round phenotype (Fig. 1B). Similar observations were made when GC and follicular mantle B cells were imaged by intravital microscopy of intact LNs (movie S2). Tracking analysis indicated that GC B cells were highly motile, similar to follicular mantle B cells whereas plasma cells showed little motility (Fig. 1C, fig. S5, A to E; fig. S6; and movie S3). GC B cell motility was partially dependent on the chemokine CXCL13 (Fig. 1C and fig. S5; for a detailed discussion, see the Supplementary Text) that is expressed by FDCs (Allen *et al.*, 2004).

On average, GC B cells formed separate clusters from naïve B cells in the follicular mantle (Fig. 1, A and D), giving the impression of distinct regions typically seen in static images, such as those obtained by immunohistochemistry (e.g., fig. S2C). However, examination of the boundary between these regions revealed that the tracks of GC B cells and follicular mantle B cells were overlapping (Fig. 1D and movie S4), indicating that a physical boundary does not demarcate the GC and follicular mantle. Instead, the majority of cells turned after crossing from one region to the other, suggesting that the GC and follicular mantle are segregated by the responses of cells to attractive (or repulsive) cues.

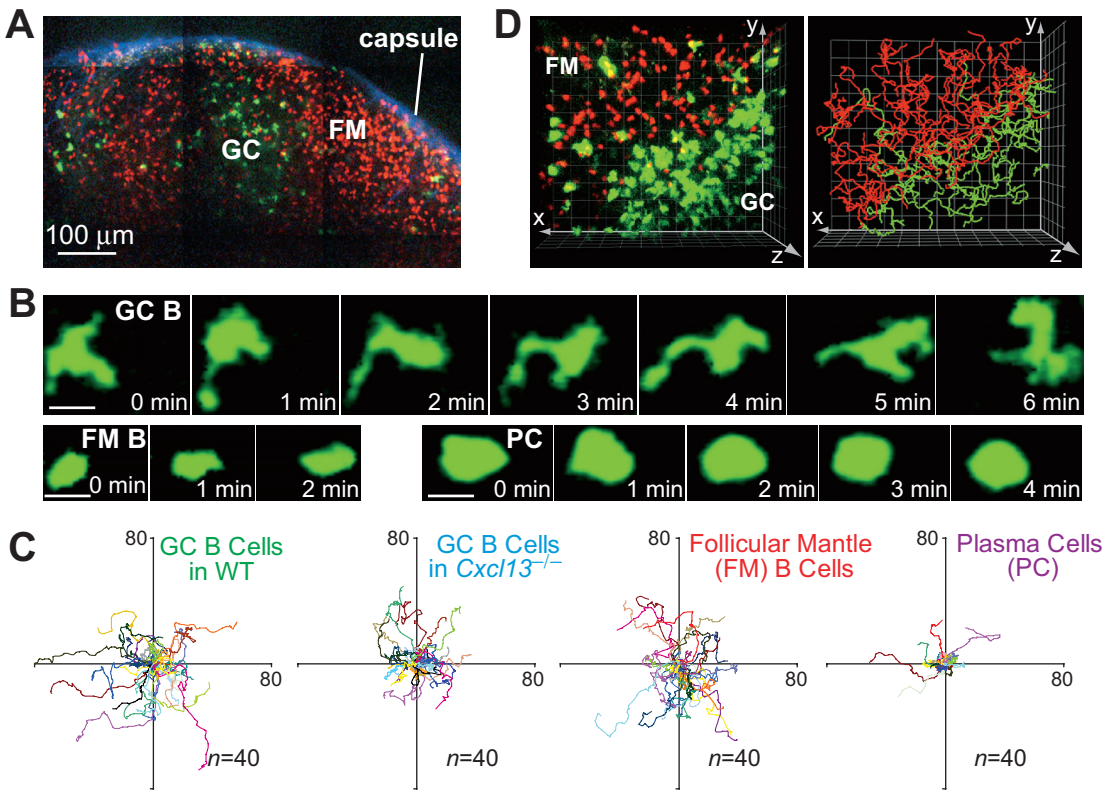

Fig. 1. Dynamics and motility of GC B cells compared with follicular mantle (FM) B cells and plasma cells (PC). (A) An 18 µm maximum intensity z-projection from two-photon microscopy image stacks of a GC and FM in an intact LN. A time-lapse recording corresponding to the center of this region is shown in movie S1. **(B)** Representative time-lapse images from two-photon microscopy showing the morphology of a GC B cell, FM B cell, and PC. The FM B cells in this experiment were naïve GFP^{+} cells that were also labeled with CMTMR, and only the GFP channel is shown in the images. Scale bars, 10 µm. **(C)** Superimposed 15-min tracks of 40 randomly-selected cells of each indicated type in the *xy* plane, setting the starting coordinates to the origin. Units are in µm. WT, wild type. **(D)** Left panel, maximum intensity projection of FM (red) and GC (green) B cells. Right panel, tracks of FM (red) and GC (green) B cells. The gridlines are separated by 20 µm.

The behavior of cells in GC dark and light zones was examined by labeling light zone FDCs *in vivo* with immune complexes containing the fluorescent protein phycoerythrin (PE) (Fig. 2A and movie S5). B cells in dark and light zones were similarly motile (fig. S7). In one hour, most GC B cells appeared to stay within the dark or light zones, although a measurable proportion of total cell tracks (5-8%) showed cell movement along relatively straight paths from one zone to the other, covering substantial distances (Fig. 2, B and C, and movies S6 and S7). These observations extend previous conclusions based on fixed tissue analysis (MacLennan, 1994) that GC B cells migrate from the dark zone to the light zone, and provide direct evidence that GC B cells return from the light zone to the dark zone. Within the light zone, FDC processes appeared to undulate, perhaps due to displacement by migrating GC B cells (movie S5). However, there was little evidence of GC B cell pausing on FDC processes, in contrast to that seen during T cell-DC interactions in the T cell area (Cahalan and Parker, 2006). GC B cells in the light zone followed straighter paths than those in the dark zone (fig. S7, B and C), which may relate to the high concentration of CXCL13 on the FDC processes in the light zone (Allen *et al.*, 2004).

During time-lapse recordings, we occasionally observed cell division in both light (Fig. 3A) and dark zones (Fig. 3B), consistent with other studies that have questioned the classical model that proliferation only occurs in the dark zone (Camacho *et al.*, 1998; Manser, 2004; Wang and Carter, 2005). The relationship between GC B cell position and cell cycle behavior was further analyzed by flow cytometry (for details, see the Supplementary Text), using surface abundance of the chemokine receptor CXCR4 (Fig. 3C) as a marker to delineate cells in dark ($CXCR4^{hi}$) and light ($CXCR4^{lo}$) zones

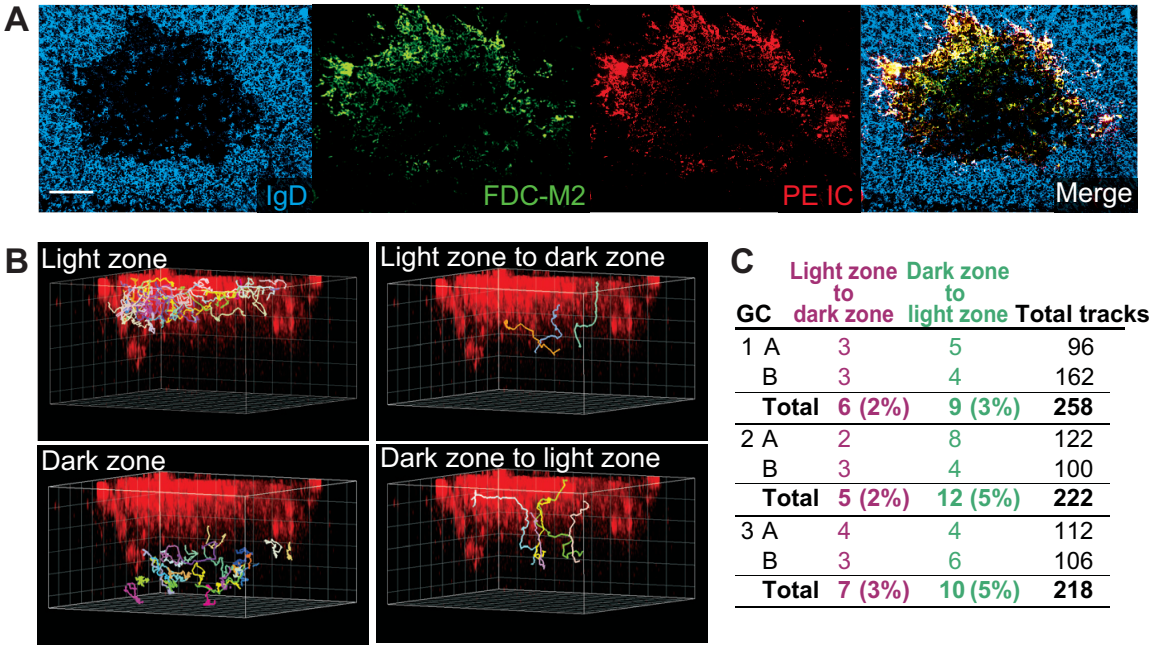

C

GC		Light zone to dark zone	Dark zone to light zone	Total tracks
1	A	3	5	96
	B	3	4	162
	Total	**6 (2%)**	**9 (3%)**	**258**
2	A	2	8	122
	B	3	4	100
	Total	**5 (2%)**	**12 (5%)**	**222**
3	A	4	4	112
	B	3	6	106
	Total	**7 (3%)**	**10 (5%)**	**218**

Fig. 2. GC B cell movement within and between GC dark and light zones.
(A) Immunofluorescence of cryostat sections showing extensive overlap of *in vivo* deposited PE immune complexes (PE IC, red) with FDC-M2 antibody staining (green). The follicular mantle is shown with anti-IgD (blue). Scale bar, 100 µm. **(B)** Representative manual classification of cell tracks into groups with respect to the PE^+ light zone, corresponding to GC 1A in (C). The gridlines are separated by 20 µm. For details of the analysis, see the Materials and Methods. **(C)** Frequency of total cell tracks that showed cells traveling between the light and dark zones in 3 GCs imaged 7 d after immunization. 1 h imaging sessions were subdivided into two segments (A and B) to facilitate analysis.

(Allen *et al.*, 2004). Analysis of DNA content (Fig. 3D) revealed that a similar proportion of GC B cells were in S phase in both dark and light zones (Fig. 3E). A subset of cells were tracked over one complete cell cycle by pulse labeling with 5-bromo, 2'-deoxyuridine (BrdU), a thymidine analog that is incorporated into cells undergoing DNA synthesis (S phase) near the time of BrdU injection (Ryser *et al.*, 1999). Although a similar proportion of GC B cells in dark and light zones were labeled 30 minutes after BrdU injection, after 5 hours, at which time the cells had divided and returned to G1 phase, they accumulated in the dark zone but not in the light zone (Fig. 3, F and G; fig. S8; and fig. S9). These observations indicate that cells that divide in the light zone do not stay resident there—perhaps returning to the dark zone, exiting the GC, or undergoing apoptosis. From 5h to 12h after BrdU injection, the G1 phase cells that had accumulated in the dark zone began to appear in the light zone, suggesting that the light zone is replenished continuously by influx of cells from the dark zone that recently completed a cell cycle (Fig. 3, F and G; fig. S8; and fig. S9). Cells were not seen to reenter S phase until 12 h after they were first labeled with BrdU in S phase (Fig. 3G; and fig. S9, C and D), indicating that the average cell cycle time is 12 h or longer, rather than 6-7 h as was concluded in previous studies (MacLennan, 1994).

T cells are concentrated in the light zone (MacLennan, 1994), and T cell help is thought to be essential for GCs (Manser, 2004; Vinuesa *et al.*, 2000). To understand the mode of B cell-T cell interaction in GCs, we visualized the interactions between GFP^+ GC B cells and CFP^+ GC T cells (movie S8). Most contacts between GC B and T cells were of short duration (Fig. 4A), and only about 4% of GC B cell-T cell encounters led to the formation of stable conjugates, defined here as contacts lasting for more than five

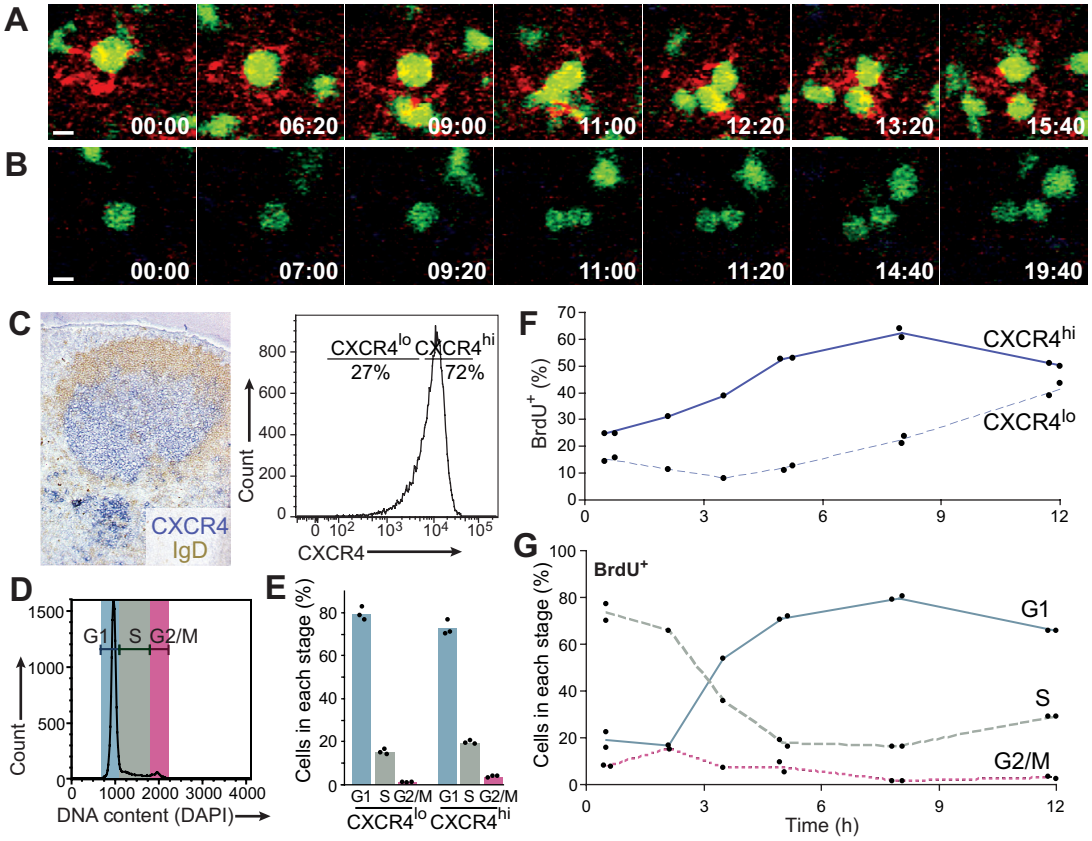

Fig. 3. Cell cycle analysis in dark and light zones. (A and B) Single plane time-lapse images of dividing GC B cells in the light (A) and dark (B) zones. The image sequences begin when the cells have rounded up and stopped moving. Scale bars, 10 µm. Elapsed time is shown as mm:ss. **(C)** CXCR4 is expressed more highly on GC B cells in the dark zone than in the light zone. Left: representative immunohistochemistry of a cryostat section of an immunized mouse LN (antibodies used for staining, bottom right). Right: representative gating of $CXCR4^{lo}$ (light zone) and $CXCR4^{hi}$ (dark zone) GC B cells by flow cytometry. **(D)** Representative cell-cycle analysis of GC B cells by flow cytometric measurement of DNA content. **(E)** Frequency of cells that were in each stage of the cell cycle in the $CXCR4^{lo}$ and $CXCR4^{hi}$ GC B cell subsets. **(F)** Frequency of cells that were $BrdU^+$ in the $CXCR4^{lo}$ or $CXCR4^{hi}$ GC B cell subsets after BrdU injection at 0 h. **(G)** Frequency of cells that were in each stage of the cell cycle among $BrdU^+$ GC B cells. Data points in (E) to (G) represent individual mice. Similar data were obtained in splenic GCs in other experiments. GC B cells in (C) to (G) were gated as in fig. S9A.

minutes (Fig. 4, B and C). In contrast, early in the immune response prior to GC formation, over 50% of contacts between cognate antigen-specific B and T cells led to the formation of stable conjugates (Fig. 4C and movie S9) (Okada *et al.*, 2005). Upon encounters leading to stable interactions with GC B cells, rapidly migrating GC T cells sharply decreased their motility to match B cell motility (Fig. 4D) and conjugates were led by B cells (movie S10), similar to the dynamics of stable B-T conjugates early in the immune response (Okada *et al.*, 2005). The median velocity of GC T cells stably interacting with GFP^+ B cells was below 10 μm/min (Fig. 4E). Only 32% of total GC T cells showed a median velocity below 10 μm/min (Fig. 4E), and the motility coefficient of GC T cells was greater than that of GC B cells (Fig. 4F and fig. S5E), strongly suggesting that the majority of T cells in GCs were not engaged in stable interactions with B cells. As our analyses suggest that each GC B cell encounters as many as 50 T cells per hour and that the majority of GC B cells are capable of binding antigen (fig. S3B), it seems likely that T cell help is limited, not only because there are fewer T cells than B cells, but also due to additional mechanisms suppressing stable B-T interactions in GCs. The threshold for activation of GC T cells appears likely to be higher than that for early activated T cells, providing a mechanism by which high affinity GC B cells could selectively engage in stable B cell-T cell conjugates.

During the selection process in GCs, many GC B cells die and are visible by histology as "tingible bodies" inside macrophages (MacLennan, 1994). Dying GFP^+ GC B cells were observed to undergo fragmentation of their cell body (Fig. 4G), but surprisingly, this occurred outside of macrophages (movie S11). Blebs of dead GFP^+ GC B cells appeared to be taken up by multiple macrophages (movie S11) though some blebs

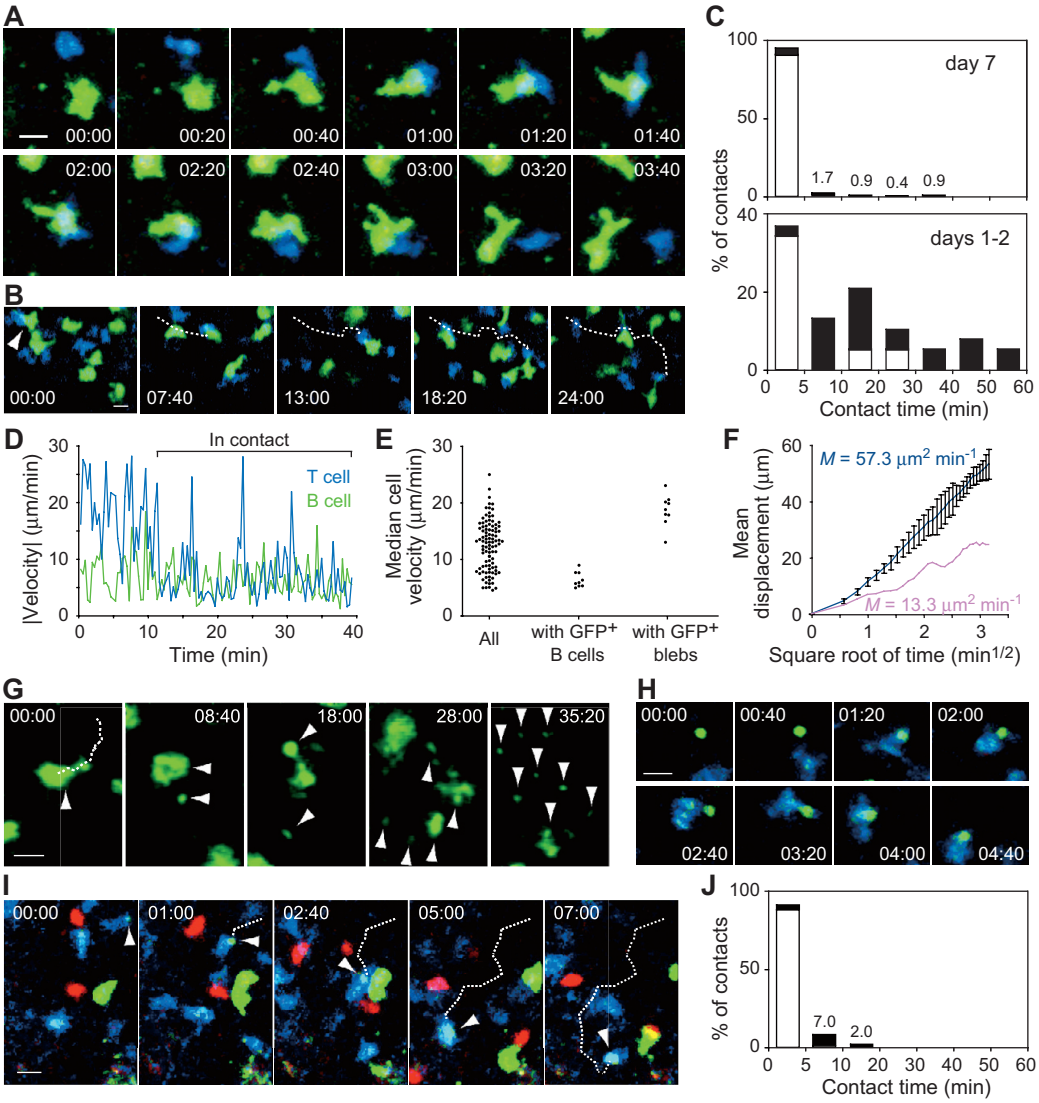

Fig. 4. Dynamics of GC T cell interactions with live GC B cells and dead B cell blebs. **(A and B)** Time-lapse images of a brief contact (A) and a stable conjugate (B, arrowhead and dotted line) of a GC B cell (green) and T cell (blue). **(C)** Contact times between antigen-specific B and T cells at the indicated number of days after immunization. Closed bar segments indicate conjugates that could not be tracked for their entire duration, and therefore are underestimates. Data are from 3 independent experiments. **(D)** Magnitudes of the velocities of a GC B cell and T cell that formed a stable conjugate. **(E)** Median velocity of total GC T cells, GC T cells stably interacting with GFP^+ GC B cells, and GC T cells stably interacting with GFP^+ blebs. **(F)** Displacement of GC T cells plotted against the square root of time. Blue line, mean of 4 imaging data sets from 4 recipient mice; error bars, ± s.d; red line, mean displacement of 7 T cells stably interacting with GC B cells. *M*, motility coefficient (for details of the calculation, see the SOM Materials and Methods). **(G)** A GC B cell undergoing cell death. Dotted line, five minute track of migration preceding the first time point; arrowheads, fragments of the cell. **(H)** A GC T cell (blue) picking up a GC B cell bleb (green). **(I)** A GC T cell (blue) carrying a GC B cell bleb (green, indicated by arrowheads) over a path shown with a dotted line. Some follicular mantle cells (red) are also visible. **(J)** Contact time distribution between GC T cells and GFP^+ GC B cell blebs from 3 independent experiments. Closed bar segments as in (C). For all time-lapse images, elapsed time is shown as mm:ss. Scale bars, 10 μm.

moved rapidly away from the original location of cell death, as if carried by motile cells (movie S2). Indeed, some GFP^+ B cell blebs were attached to and carried by fast migrating CFP^+ T cells (Fig. 4, H and I; and movie S12). All T cells that carried GFP^+ B cell blebs had a median velocity greater than 10 μm/min (Fig. 4E), suggesting that they were not undergoing stable interactions with living B cells. The GFP^+ GC B cells represent only about 1–2% of GC B cells and we observed about 0.5% of T cells carrying GFP^+ blebs; by extrapolation, at least one quarter of the GC T cells may be associated with one or more blebs from dead GC B cells. As a higher frequency of bleb-T cell interactions were stable compared with live B cell-T cell interactions (Fig. 4, C and J), it seems possible that these dead B cell fragments have an impact on the availability of T cell help in GCs, perhaps by causing reduced sensitivity to antigen peptide-MHC complexes on live B cells.

Our findings reveal that GC B cells are highly motile and exhibit a probing behavior as they travel over the antigen-bearing FDC network. The lack of GC B cell pausing during movement throughout the FDC network in the light zone suggests that the selection mechanism does not involve competition for adhesion to FDCs. The rapid movement of B cells in close proximity with each other raises the possibility that high affinity cells remove surface bound antigen from lower affinity cells. The observed migration of GC B cells from light to dark zones is consistent with GC B cells undergoing repeated rounds of mutation and selection within a given GC (Kepler and Perelson, 1993). Our estimate that GC B cells spend only several hours in the light zone suggests a limited amount of time to access helper T cells. Since stable interactions of GC B cells with GC T cells were infrequent, it seems possible that T cell help is a limiting

factor driving selection of higher-affinity B cell clones. *In vitro* studies have shown that T cells responding to antigen-presenting B cells can be sensitive to variations in the affinity of the B cell receptor across several orders of magnitude (Batista and Neuberger, 1998). We propose a selection model in which newly arising mutated GC B cells with higher affinity for antigen obtain and process greater amounts of antigen in a given period of time and then outcompete the surrounding B cells and B cell blebs for the attention of GC T cells.

Supplementary Text

System for visualization of GC B cells by two-photon microscopy

In order to study the dynamics of GC B cells by two-photon microscopy, we developed a system in which a small fraction of GC B cells were fluorescent yet could still undergo the normal processes of class switching, somatic hypermutation, and affinity maturation. We generated a mouse with B cells specific for a model protein antigen, avian lysozyme, so that we could adoptively transfer a small number of lysozyme-specific B cells to normal mice and then recruit them into GCs by immunization with lysozyme. A rearranged immunoglobulin VDJ heavy chain segment from HyHEL10, an antibody to hen egg lysozyme (HEL) (Lavoie *et al.*, 1992), was targeted to the endogenous heavy-chain locus (fig. S1A). These 'knock-in' mice, denoted VDJ9, were bred to HyHEL10 VJ light chain transgenic (κ5) mice, and the resulting VDJ9/κ5 progeny had a high frequency of B cells that bound to HEL (fig. S1B). VDJ9/κ5 mice were then crossed to mice ubiquitously expressing GFP, and a small number of VDJ9/κ5 GFP B cells were cotransferred with a majority of VDJ9/κ5 non-GFP B cells to recipients (fig. S2A). As HyHEL10 has a very high affinity for HEL ($K_a \approx 5 \times 10^{10}$ M^{-1}), we instead chose duck egg lysozyme (DEL) for immunization, to which HyHEL10 has a much lower affinity ($K_a \approx 10^7$ M^{-1}) (Lavoie *et al.*, 1992), thereby more closely modeling a primary immune response. Because the endogenous T cell response to DEL was found to be poor in preliminary experiments (data not shown), we conjugated DEL to ovalbumin (OVA) and cotransferred OT-II $CD4^+$ T cells specific for OVA (Barnden *et al.*, 1998) with the VDJ9/κ5 B cells (fig. S2A). In the draining LNs of DEL-OVA immunized recipients, we found that most of the transferred VDJ9/κ5 B cells were driven into GCs (fig. S2, B and

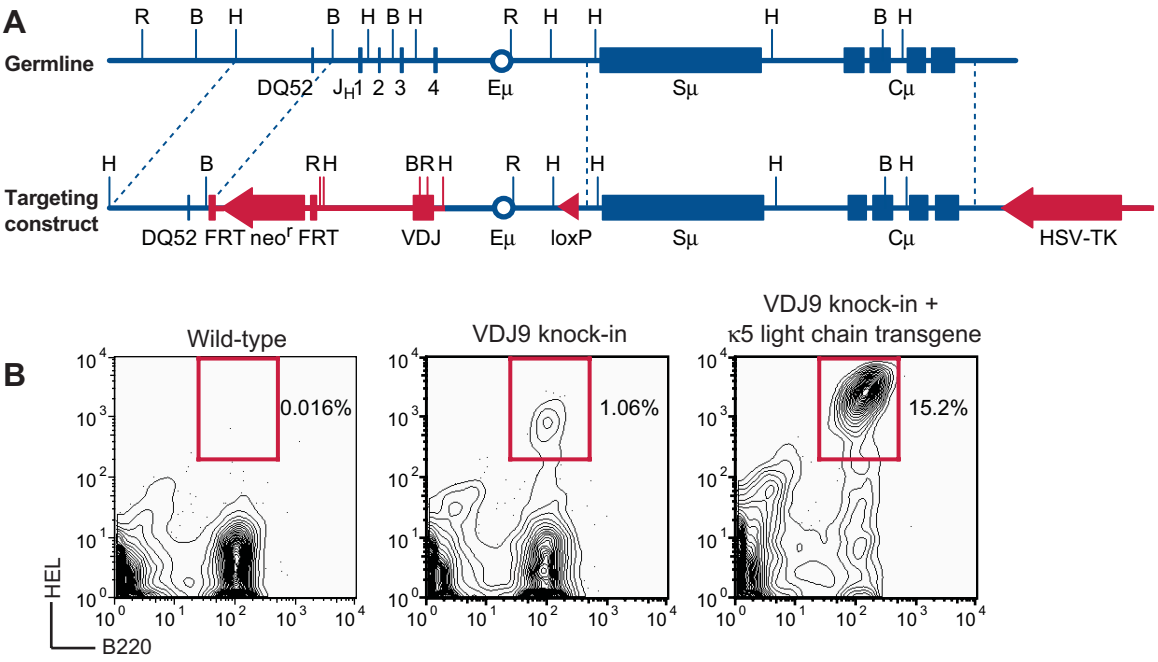

Fig. S1. Generation of HyHEL10 VDJ heavy-chain 'knock-in' mice. (A) The targeting construct and the corresponding region of the germline immunoglobulin heavy-chain locus containing DQ52, J_H1-4, the intronic heavy chain enhancer (Eμ), IgM switch (Sμ) and constant (Cμ) regions are depicted. Regions of homology are indicated with dashed lines. EcoRI (R), BamHI (B), and HindIII (H) restriction sites are shown. **(B)** Flow cytometric analysis of HEL-binding capability of scatter-gated peripheral blood cells in mice of the indicated genotypes.

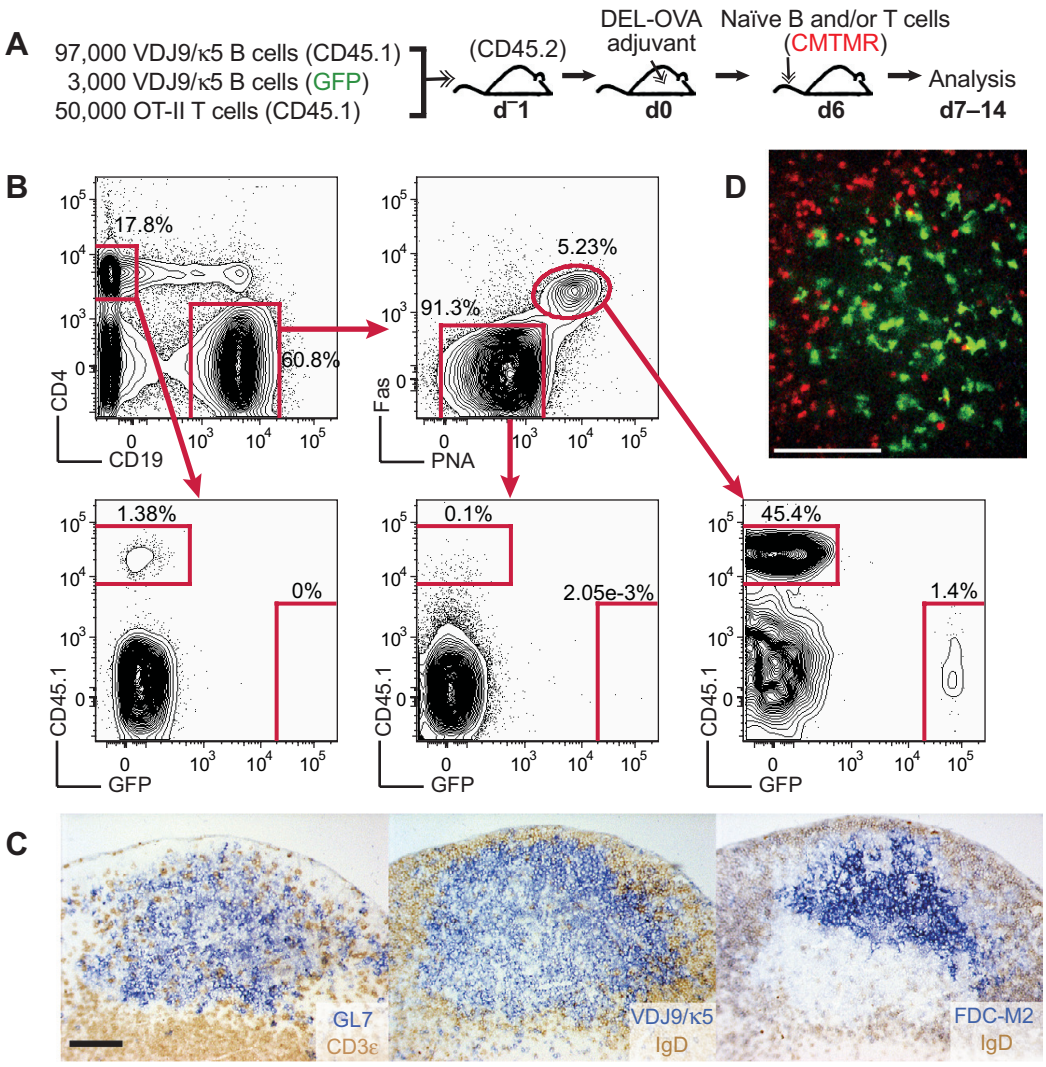

Fig. S2. A system for visualization of GC B cells by two-photon microscopy. Details of the system are described in the SOM Text. **(A)** Adoptive transfer and immunization scheme for imaging of GC B cells by two-photon microscopy. **(B)** Flow cytometric analysis of a draining brachial LN. Cells were pre-gated for scatter, singlets, and dead cell exclusion with propidium iodide (PI). **(C)** Immunohistochemistry of a draining facial LN, stained with the indicated markers, showing that transferred VDJ9/κ5 B cells cluster in germinal centers ($GL7^+$) with dark and light zone polarity (revealed by labeling of the light zone FDC network with FDC-M2). Middle panel, in order to specifically visualize VDJ9/κ5 B cells, the scheme in (A) was modified such that CD45.2 VDJ9/κ5 B cells were cotransferred with CD45.1 OT-II cells to CD45.1 recipients, and the section was stained with anti-CD45.2. **(D)** A maximum intensity projection from an 18 μm two-photon microscopy image stack of a draining brachial LN, showing GFP^+ GC B cells (green) and $CMTMR^+$ follicular mantle cells (red). Data in (B) to (D) were obtained 7 d after immunization. Scale bars, 100μm.

C). On average, about 1-2% of the GC B cells were GFP^+, although this frequency varied among individual GCs, suggesting that GCs were randomly seeded by as many as 50-100 precursors (fig. S2B and data not shown). The number of VDJ9/κ5 GC B cells reached a peak at day 7 after immunization and this time point was chosen for most of our analyses. By also transferring CMTMR-labeled naïve B and T cells to the recipients a day before analysis, we could identify GFP^+ cells in GCs and $CMTMR^+$ cells in the surrounding follicular mantle zones, respectively, by two-photon microscopy (fig. S2D).

We then tested whether the VDJ9/κ5 GC B cells could undergo class switching, affinity maturation, and somatic hypermutation. By flow cytometry, we found that class switching to $IgG_{2a}{}^a$ and IgG_{2b} was evident by day 7 after immunization, with the majority of cells switching to IgG_{2b} by day 14 after immunization (fig. S3A). Switching to $IgG_1{}^a$ was not observed (data not shown), and switching to other isotypes could not be reliably detected with the reagents available, however the low frequencies of IgM^{a+} cells at day 7 (≈15%) indicate that switching to other isotypes is also likely. The VDJ9/κ5 GC B cells also appeared to have acquired increased affinity for DEL by day 14, as assessed by binding to limiting amounts of DEL in a flow cytometric assay (fig. S3B), similar to an assay recently described for the binding of mutant forms of HEL to HyHEL10 (Phan *et al.*, 2006). By sequencing of the HyHEL10 VDJ heavy-chain segment in sorted VDJ9/κ5 GC B cells, we found an increase in the number of somatic mutations as the GC response progressed (fig. S4A), indicating that the somatic hypermutation process was active in these cells. Selection for particular somatic mutations was evident by day 14, at which time a high frequency of replacement mutations was observed in CDR2 (fig. S4B). Taken

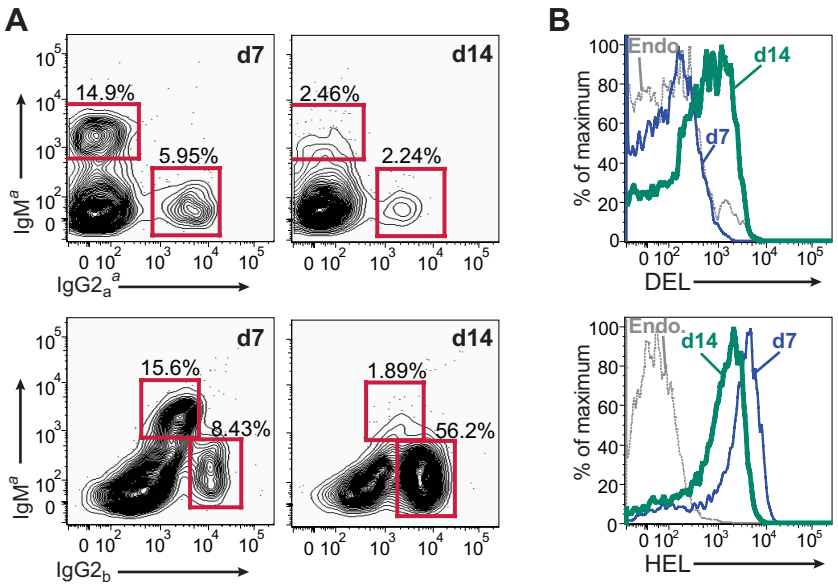

Fig. S3. VDJ9/κ5 GC B cells undergo immunoglobulin class switch recombination and affinity maturation. (A) Analysis of class switching of VDJ9/κ5 GC B cells by flow cytometry. Plots show immunoglobulin isotype surface expression on VDJ9/κ5 GC B cells (gated on scatter, singlets, PI^-, $CD4^-$, $CD19^+$, Fas^+, IgD^{lo}, $CD45.1^+$) from draining LNs 7 or 14 d after immunization. A similar pattern of isotype switching was observed in at least three mice. **(B)** Flow cytometric assay for affinity maturation of VDJ9/κ5 GC B cells (gated on scatter, singlets, PI^-, $CD4^-$, $CD19^+$, PNA^{hi}, Fas^+, $CD45.1^+$). Fluorescent DEL was applied at a concentration which was two-fold below the limit of detection for binding to naïve VDJ9/κ5 B cells ($K_a \approx 10^7\ M^{-1}$), thus binding by GC B cells at d14 indicates an increase in affinity for DEL. Binding to fluorescent HEL is shown to indicate that VDJ9/κ5 GC B cells at both d7 and d14 express a functional HyHEL10 BCR, therefore the differences observed in DEL-binding were not due to differences in BCR expression. For comparison, DEL- and HEL-binding to endogenous GC B cells ($CD45.2^+$) at d14 is overlaid with a dotted line. Data are representative of at least three mice.

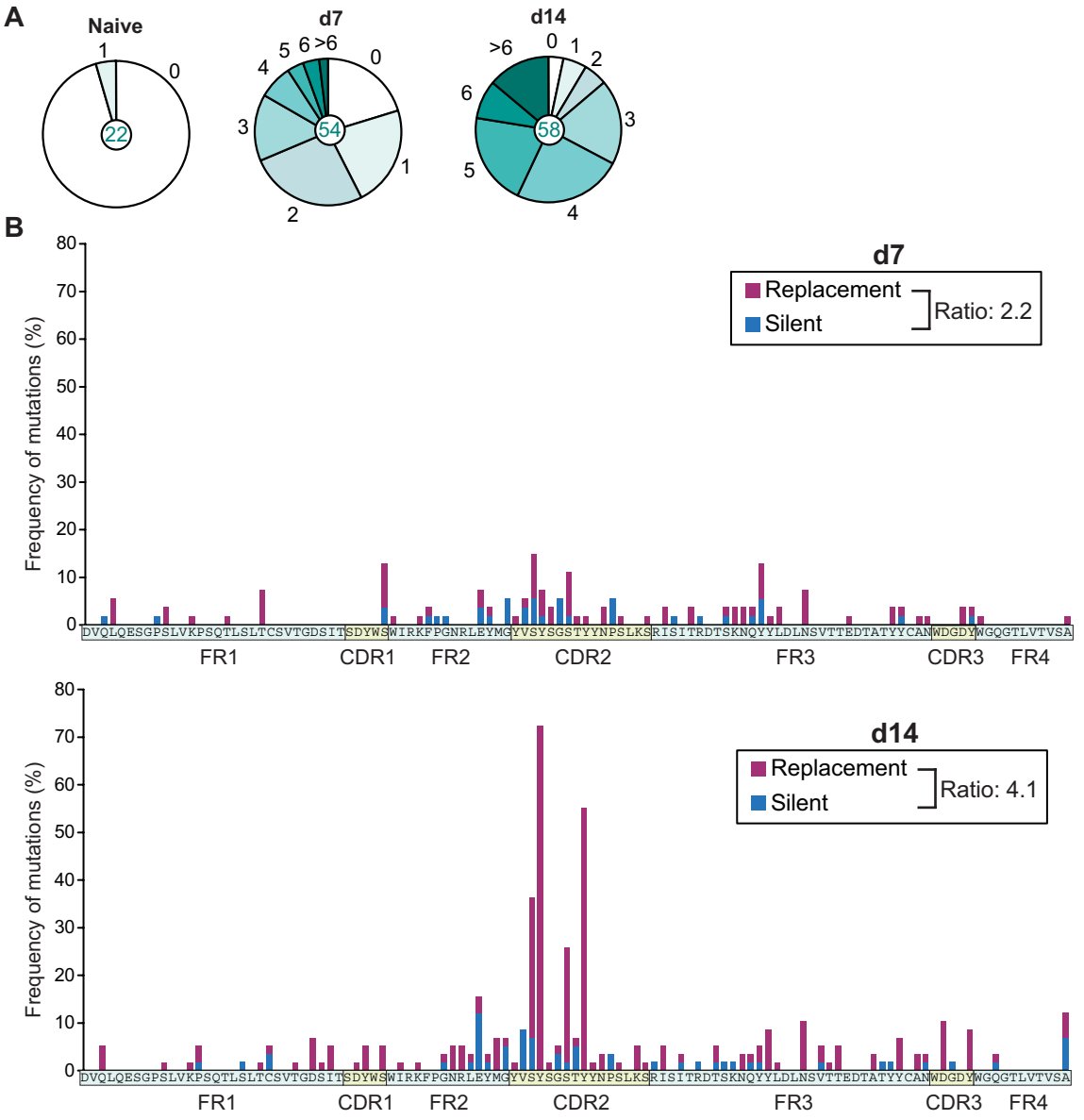

Fig. S4. Somatic hypermutation and selection occur in VDJ9/κ5 GCs. (A) Pie charts show the number of nucleotide mutations from the original HyHEL10 sequence in the VDJ heavy chain segments of individual VDJ9/κ5 GC B cells (sorted single cells based on gates for scatter, singlets, PI^{-}, $CD4^{-}$, $CD19^{+}$, $PNA^{hi,}$ Fas^{+}, IgD^{lo}, $CD45.1^{+}$). The numbers of sequences analyzed are indicated in the inner circles. **(B)** The frequency of nucleotide mutations that result in amino acid replacement or are silent are indicated for each amino acid in the HyHEL10 heavy-chain coding sequence. HyHEL10 heavy-chain framework regions (FR) and complementarity-determining regions (CDR) are shown.

together, these data indicate that VDJ9/κ5 GC B cells undergo the physiological processes of class switching, affinity maturation, and somatic hypermutation.

CXCL13 contributes to GC B cell motility

Previous work demonstrated that the chemokine CXCL13, which is highly expressed by FDCs in the GC light zone, and its receptor CXCR5 are involved in organizing the GC (Allen *et al.*, 2004; Ansel *et al.*, 2000; Voigt *et al.*, 2000). As some chemokines can promote random cell motility in addition to directional migration (Sozzani *et al.*, 1991; Stachowiak *et al.*, 2006), we tested the possibility that CXCL13 contributes to motility in the GC. We found that GC B cells in CXCL13-deficient mice moved with slower velocities (fig. S5, A and B) and with more circuitous paths, as measured by the turning angle between cell trajectories (fig. S5, C and D), compared with GC B cells in wild-type mice. This reduced motility led to significantly less mean displacement over time (fig. S5E). Although CXCL13 is required for correct polarization of the GC (Allen *et al.*, 2004), a comparison with our findings that dark and light zone GC B cells move at equivalent velocities (fig. S7A) shows that B cell motility in CXCL13$^{-/-}$ GCs is compromised compared to the motility of B cells in both light and dark zones of wild-type GCs. *In vitro* transwell assays showed that CXCL13 directly promoted GC B cell motility in the absence of a gradient, although the magnitude of the response was weaker than chemotaxis toward a CXCL13 gradient (fig. S5F). These data suggest that the functions of CXCL13 in the GC can be extended to include a role in promoting cell motility.

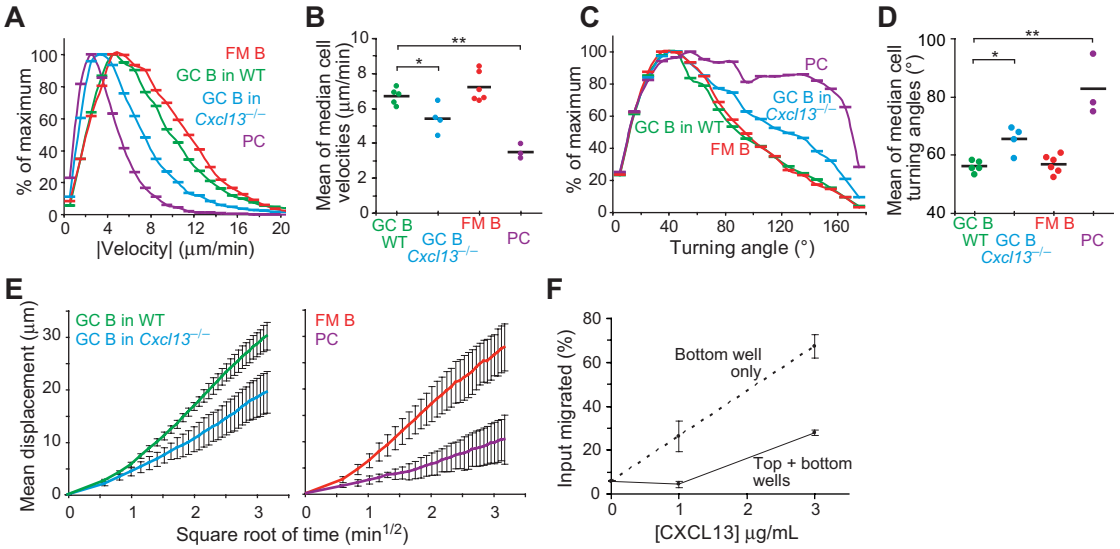

Fig. S5. Motility of GC B cells in wild-type (WT) and *Cxcl13*$^{-/-}$ mice, compared with follicular mantle (FM) B cells and plasma cells (PC). **(A)** Magnitudes of velocities measured at 20 s intervals. Horizontal bars indicate histogram bins. **(B)** Compiled magnitudes of velocities for cells in each imaging session. As cell velocities per 20 s interval show a non-Gaussian distribution, the median velocity for each cell was calculated, and the mean of the median cell velocities for each imaging session is shown as a dot. **(C)** Turning angles between cell trajectories measured at 20 s intervals. Horizontal bars indicate histogram bins. **(D)** Compiled turning angles for cells in each imaging session. As turning angles between 20 s trajectories show a non-Gaussian distribution, the median turning angle for each cell was calculated, and the mean of the median cell turning angles for each imaging session is shown as a dot. **(E)** Mean displacement versus the square root of time. Error bars, ± s.d. of the means of individual imaging sessions. The motility coefficients (M ± s.d.) of GC B cells in *Cxcl13*$^{-/-}$ (8.5 ± 3.5 µm^2 min^{-1}) and PC (2.5 ± 1.8 µm^2 min^{-1}) were significantly (P<0.01) reduced compared with GC B cells in WT (21.4 ± 4.2 µm^2 min^{-1}). Data in (A) to (E) are from tracking 465 GC B cells in WT, 442 GC B cells in *Cxcl13*$^{-/-}$, 365 FM B, and 200 PC. **(F)** *In vitro* transwell migration assay of GC B cells (gated on scatter, PI$^-$, CD19$^+$, GL7$^+$, Fas$^+$) from the spleens of immunized Eµ-*Bcl2*-22 transgenic mice. n=3; error bars, ± s.d. *, P<0.05, **, P<0.01

Visualization of plasma cells in LN medullary cords by two-photon microscopy

We characterized the morphology and motility of plasma cells, which are terminally differentiated B cells that secrete antibody, and are derived from both non-GC and GC pathways after immunization (Calame *et al.*, 2003). By flow cytometry, we found that after adoptive transfer and immunization (fig. S2A), a subset of VDJ9/κ5 GFP^+ cells expressed markers characteristic of antibody-secreting plasma cells in the draining LNs and that by microscopy a population of VDJ9/κ5 GFP^+ cells could be visualized in LN medullary cords, areas known to be rich in plasma cells (data not shown). These cells were imaged by two-photon microscopy and found to have a very round morphology, similar to that of naïve B cells (Fig. 1B). However, many of the plasma cells were sessile (Fig. 1C and movie S3), and those that moved did so with slower velocities and smaller displacements than follicular mantle B cells and GC B cells (fig. S5, A to E). To confirm these findings, we also visualized plasma cells in the *Blimp*^{gfp} mouse model, in which GFP expression is dependent on expression of Blimp, a transcription factor that is highly expressed in plasma cells. *Blimp*^{gfp} cells were relatively dim, but those that could be visualized in the superficial areas of the LN medulla showed even less motility than the VDJ9/κ5 GFP^+ plasma cells (movie S3), with slow velocities and minimal displacements over time (fig. S6).

Cell cycle analysis of GC B cells provides additional insight into GC dynamics

Imaging of the GC by two-photon microscopy demonstrated that GC B cells could transit between dark and light zones (Fig. 2, B and C) and divide in both zones (Fig. 3, A and B). However, a limitation of this technique was that individual cells could not be tracked

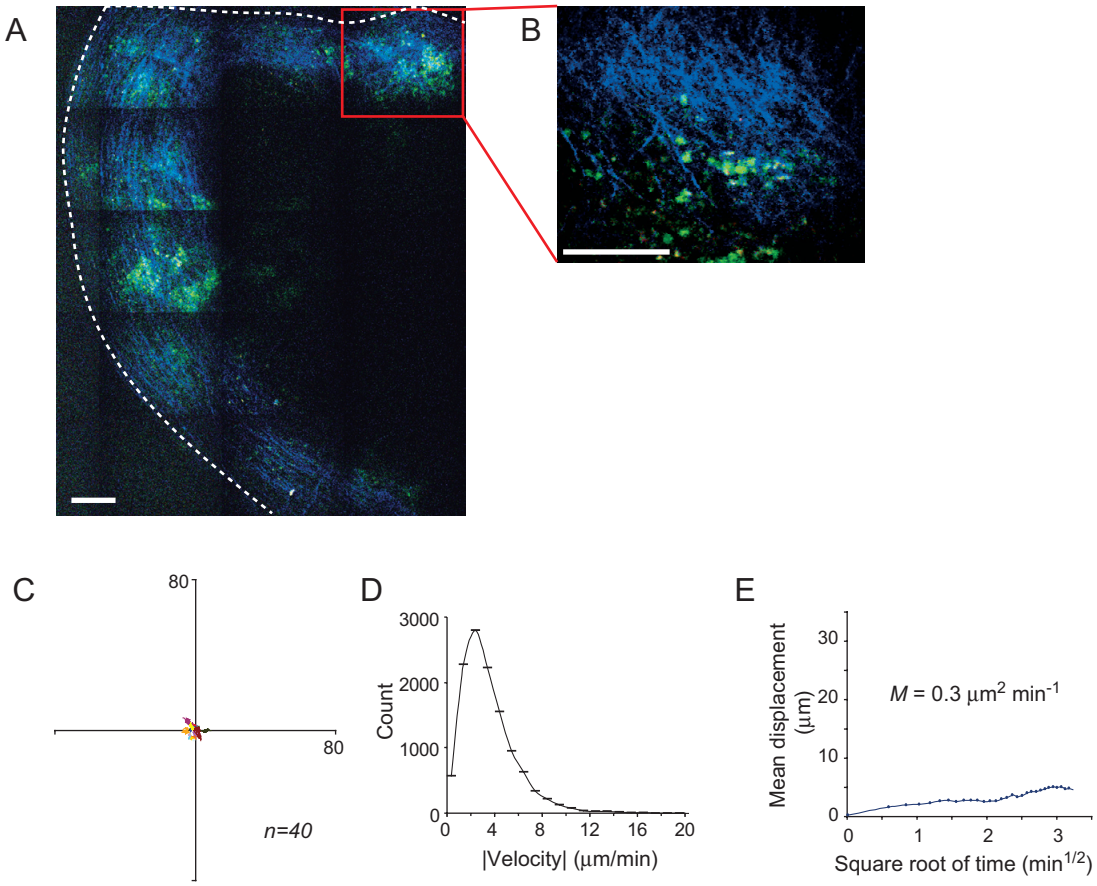

Fig. S6. **Plasma cells in LN medullary cords of *Blimp*^{gfp} mice are sessile. (A)** Multi-panel reconstruction of a LN medullary cord in a superficial cervical LN of a *Blimp*^{gfp} mouse, shown as a maximum intensity projection of a 105 µm two-photon image stack. Blue, collagen fibers; green, *Blimp*^{gfp} plasma cells; dashed line, the boundary of the LN. **(B)** A maximum intensity projection of a 12 µm two-photon image stack corresponding to the *x*-*y* region shown as an inset in (A). **(C)** Superimposed 15 min tracks in the *xy* plane of 40 randomly-selected *Blimp*^{gfp} cells, setting the starting coordinates to the origin. Units are in µm. **(D)** Magnitudes of velocities measured at 20 s intervals. Horizontal bars indicate histogram bins. **(E)** Mean displacement versus the square root of time. *M*, motility coefficient. Data in (C) to (E) were compiled from two imaging fields and a total of 154 cells were tracked. Scale bars, 100 µm.

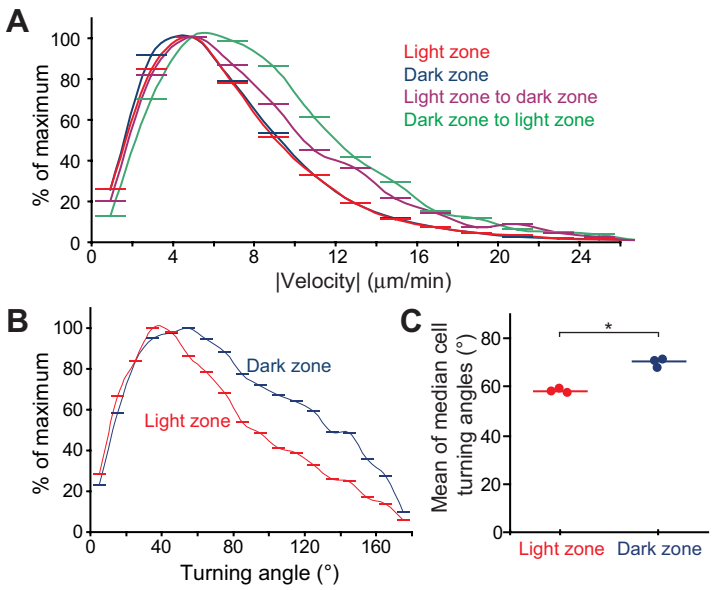

Fig. S7. Motility of GC B cells in dark and light zones and of cells that travel between zones. **(A)** Magnitudes of velocities measured at 20 s intervals. **(B)** Turning angles between cell trajectories measured at 20 s intervals. In (A) and (B), horizontal bars indicate histogram bins. **(C)** Compiled turning angles for cells in each imaging session. As turning angles between 20 s trajectories show a non-Gaussian distribution, the median turning angle for each cell was calculated, and the mean of the median cell turning angles for each imaging session is shown as a dot. *, P=0.011.

for periods greater than one hour due to movement beyond the imaging volume or in close proximity with other cells. Insight into GC B cell residence times in dark in light zones was obtained by cell cycle analysis. GC B cells in dark and light zones were identified by flow cytometry by gating based on the surface abundance of CXCR4 (Fig. 3C and fig. S9A), a chemokine receptor more highly expressed on dark zone than on light zone GC B cells (Allen *et al.*, 2004). Determination of the DNA content of GC B cells by flow cytometry (Fig. 3D) indicated that similar proportions of $CXCR4^{lo}$ and $CXCR4^{hi}$ GC B cells were in S phase of the cell cycle, and very few cells were in G2/M phases (Fig. 3E). These data were surprising, as studies examining GCs in rodents five hours after injection of the thymidine analog BrdU, which is incorporated into DNA during S phase, showed that BrdU-labeling was enriched in dark zone cells (Allen *et al.*, 2004; Liu *et al.*, 1991b).

We hypothesized that GC B cells in both dark and light zones were proliferating, but that after dividing in the light zone they do not stay resident there—perhaps returning to the dark zone, exiting the GC, or undergoing apoptosis—such that over time there might be an accumulation of BrdU-labeled cells in the dark zone. Consistent with this notion, BrdU-labeled cells appeared to be evenly distributed between dark and light zones 30 minutes after BrdU injection, but BrdU-labeled cells were concentrated in the dark zone five hours after injection (fig. S8). Similarly, the frequency of $CXCR4^{hi}$ cells that were $BrdU^{+}$ increased but the frequency of $CXCR4^{lo}$ cells that were $BrdU^{+}$ slightly decreased from 30 minutes to five hours (Fig. 3F and fig. S9B). Notably, after systemic injection most BrdU is lost from the blood within 15 minutes and is maximally absorbed in tissues within 90 minutes (Ryser *et al.*, 1999). Indeed, we found that after 30 minutes

all cells in S phase were labeled with BrdU, but that by five hours most of the labeled cells were in G1 phase (Fig 3G and fig. S9, C and D). Therefore, the increase of labeled cells in the dark zone after five hours can be attributed to a doubling of labeled cells, rather than additional BrdU labeling, and the vast majority of $CXCR4^{hi}$ cells in the dark zone are in the G1 phase of the cell cycle. By 12 hours, a substantial number of BrdU-labeled cells appeared in the light zone by immunohistochemistry, such that the dark and light zones again appeared equally labeled (fig. S8). Similarly, the frequency of $CXCR4^{lo}$ cells that were $BrdU^{+}$ increased whereas the frequency of $CXCR4^{hi}$ cells that were $BrdU^{+}$ decreased by 12 hours (Fig. 3F and fig. S9B). These data are consistent with direct observations by two-photon microscopy (Fig. 2, B and C) and previous evidence (MacLennan, 1994) that cells move from the dark zone to the light zone. After 12 hours, some of the BrdU-labeled cells were again in S phase (Fig. 3G and fig. S9, C and D), suggesting that the average time needed for GC B cells to complete one cell cycle is greater than 12 hours. This contrasts with the 5-7 hour cell cycle time suggested in studies that used less precise methods (Hanna, 1964; Zhang *et al.*, 1988) but is consistent with early reports that made estimates based on several quantification methods (Fliedner *et al.*, 1964; Zaitoun, 1980). Taken together, these data favor a model in which cell division can occur both in the dark and light zones, but that cells reside in the light zone only for several hours, and that the light zone is replenished by a constant influx of cells from the dark zone that recently completed a cell cycle.

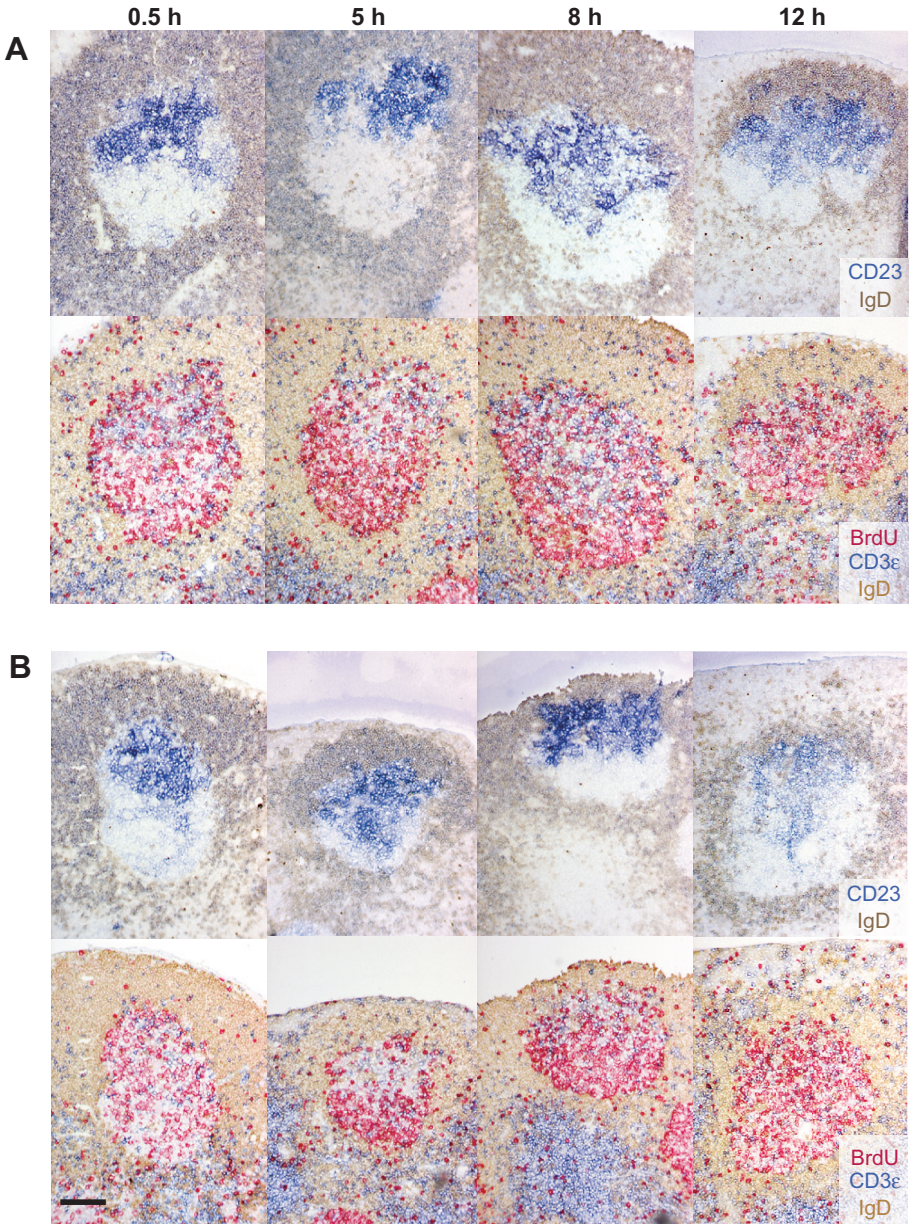

Fig. S8. Analysis of the light and dark zone localization of BrdU-pulsed GC B cells by immunohistochemistry. Two representative GCs (**A** and **B**) are shown at each indicated time point after BrdU injection. Cryostat sections of immunized LNs were stained with the indicated antibodies (bottom right). Serial cryostat sections show the position of the light zone FDC network ($CD23^+$, upper panel) and $BrdU^+$ GC B cells (lower panel). Scale bar, 100 µm.

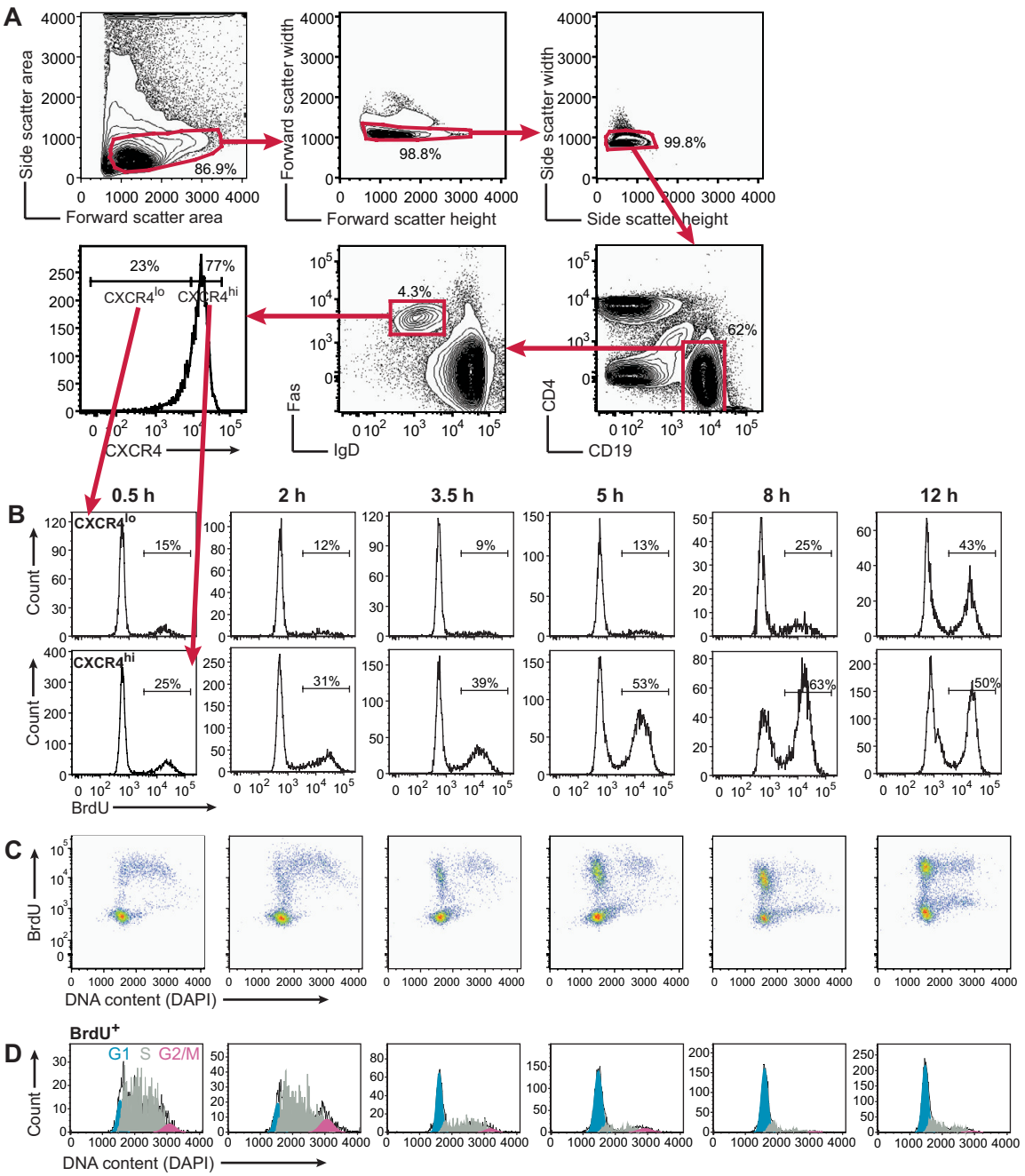

Fig. S9. Cell cycle analysis of light zone and dark zone GC B cells by flow cytometry. (A) Gating scheme for light zone ($CXCR4^{lo}$) and dark zone ($CXCR4^{hi}$) GC B cells from draining LNs, for combined analysis of BrdU incorporation and DNA content. Lymphocytes (including blast cells) were gated on forward and side scatter as shown, and then doublets were excluded with two singlet gates. GC B cells were identified as $CD4^{-}$ $CD19^{+}$ Fas^{+} IgD^{lo} cells. **(B)** Representative histograms for determination of the frequency of $CXCR4^{lo}$ or $CXCR4^{hi}$ GC B cells that were $BrdU^{+}$ at the indicated number of hours after BrdU injection. Data are compiled in Fig. 3F. **(C)** Plots of BrdU incorporation versus DNA content in GC B cells at the time points indicated in columns. **(D)** DNA histograms were analyzed by the Watson pragmatic method to resolve $BrdU^{+}$ GC B cells into G1, S, and G2/M stages of the cell cycle (indicated by shading). One example at each time point is shown; data are compiled in Fig. 3G.

Materials and Methods

Mice

B6 (000664; C57BL/6J), B6-CD45.1 (002014; *Ptprc*^{a} *Pepc*^{b}/BoyJ), UBC-GFP (004353; Tg(UBC-GFP)30Scha/J), and β-actin-CFP (004218; Tg(ACTB-ECFP)1Nagy/J) mice were from the Jackson Laboratory. OT-II mice were as described (Barnden *et al.*, 1998). *Blimp*^{gfp} mice (Kallies *et al.*, 2004) were a gift of S. Nutt. *Cxcl13*$^{-/-}$ (Ansel *et al.*, 2000) and Eμ-*Bcl2*-22 (Strasser *et al.*, 1991) mice were backcrossed for at least ten generations to the B6 strain.

VDJ9 HyHEL10 heavy chain knock-in mice were generated similarly to other immunoglobulin heavy chain knock-in mice (Cascalho *et al.*, 1996; Taki *et al.*, 1993). Upstream homology sequences were derived from a plasmid containing DQ52 along with flanking genomic sequences and a herpes simplex virus thymidine kinase gene (HSV-TK, gift of M. Cascalho (Cascalho *et al.*, 1996)). This plasmid was digested with BamHI and HindIII and ligated to a 50 bp polylinker with 5'-BamHI and 3'-HindIII overhangs (forward, 5'-GATCCGTTTAAACGTCGACCCCCCAAGCTTGTTAACAAGAATGCGGCCGC-3', reverse 3'-GCAAATTTGCAGCTGGGGGGTTCGAACAATTGTTCTTACGCCGGCGTCGA-5'). An FRT-flanked neomycin resistance cassette (a gift of N. Killeen) was then inserted in reverse orientation at a PmeI site in the polylinker. The heavy chain variable-diversity-joining (VDJ) segment of HyHEL10 and downstream sequences were obtained from a plasmid provided by C. Goodnow (Goodnow *et al.*, 1988). The heavy chain VDJ segment of HyHEL10 was isolated from this plasmid by SalI and partial HindIII digestion and inserted into corresponding sites in the polylinker. Downstream sequences, including the JH4 intron and enhancer, the μ-switch, and μ-constant regions, were attached from a

NaeI site in the JH4 intron to an HpaI site in the polylinker by blunt end ligation. A loxP site was also inserted at a SpeI site between the Igμ enhancer and the μ switch region, for use in future gene targeting. The targeting construct was linearized with PvuI and electroporated into JM1 129 mouse ES cells (a gift of N. Killeen). As the ES cells were derived from 129 mice, the immunoglobulin heavy chain locus is of the IgH^a allotype. G418 and gancyclovir resistant colonies were screened by Southern blots of a flanking 5' probe to EcoRI digested genomic DNA. Targeted clones were injected into B6 blastocysts. Chimeric males were mated to B6 females and germline transmission of the targeted allele was detected by flow cytometry of peripheral blood cells for binding to hen egg lysozyme (HEL) (e.g., fig. S1B).

To generate HyHEL10 light chain transgenic mice, a plasmid containing the VJ_κ exon of the HyHEL10 kappa light chain, the κ-constant region, and 3' flanking DNA including the κ enhancer elements was provided by C. Goodnow (Goodnow *et al.*, 1988). Pronuclear injection of the linearized HyHEL10 κ construct lacking vector sequences into fertilized B6.CBA F1 oocytes was performed according to standard procedures. One of three founder lines (κ5) was selected that carried 5-10 copies of the transgene.

VDJ9 HyHEL10 heavy-chain knock-in mice were then bred to κ5 HyHEL10 light chain transgenic mice. Mice carrying the heavy chain knock-in and light chain transgene of HyHEL10 were identified by flow cytometry of peripheral blood cells for HEL-binding (e.g., fig. S1B). VDJ9/κ5 mice were backcrossed to the B6 strain for at least 12 generations. For imaging studies, VDJ9/κ5 mice were repeatedly bred to homozygous UBC-GFP mice, and peripheral blood cells were screened for HEL-binding and homozygosity of the GFP transgene by flow cytometry. Homozygous UBC-GFP mice

were used for imaging experiments, as homozygous UBC-GFP cells were found to be significantly brighter by two-photon microscopy than hemizygous UBC-GFP cells. β-actin-CFP mice were backcrossed for nine generations to the B6 strain and then bred with OT-II mice. Mice hemizygous for the CFP transgene were identified by illumination of the hind paws with a hand-held UV lamp (UVL-56, VWR). All mice were maintained in transgenic barrier facilities and protocols were approved by the Institutional Animal Care and Use Committee of the University of California, San Francisco.

Adoptive transfers and PE immune complex deposition

For adoptive transfers, cells were isolated from spleens and/or LNs of donor mice by mechanical disruption on 40- or 70-μm nylon cell strainers (Falcon) in DMEM medium (Cellgro) containing 2% fetal bovine serum (FBS, HyClone), antibiotics (50 IU/mL of penicillin and 50 μg/mL of streptomycin; Cellgro) and 10 mM HEPES (Cellgro), and then were washed. Alternatively, when few donor cells were needed, such as in the transfer of 3000 VDJ9/κ5 GFP^+ B cells for GC imaging (Fig. S1C), 100-200 μL of blood was collected from the retro-orbital plexus of donor mice (anesthetized with isoflurane) into Microtainer tubes with EDTA (Becton Dickinson (BD)), and then erythrocytes were lysed by incubation in 1 mL of Tris-buffered NH_4Cl at 37°C for 12 min. As most transfers involved small numbers of donor cells, in many cases it was not necessary to purify donor cells prior to transfer; instead, the frequency of HEL-binding B cells isolated from donor VDJ9/κ5 mice or TCR-transgenic $CD4^+$ T cells isolated from donor OT-II mice were determined by flow cytometry, and total cell counts were measured on a Z1 Coulter Counter (Beckman Coulter), such that the overall cell number could be adjusted

to give the desired number of antigen-specific cells. For transfers of larger numbers of cells, B cells were purified as described (Allen *et al.*, 2004) or with directly conjugated anti-CD43 and anti-CD11c microbeads (Miltenyi Biotec). $CD4^+$ T cells were purified by labeling cells with the following biotinylated antibodies (at a 1:100 dilution) in DMEM media containing 2% FBS: rat anti-mouse CD8α (clone CT-CT8a, CALTAG Laboratories), rat anti-mouse CD11b (clone M1/70.15, CALTAG Laboratories), hamster anti-mouse CD11c (clone HL3, BD Pharmingen), rat anti-mouse CD45R/B220 (clone RA3-6B2, BD Pharmingen or CALTAG Laboratories), and rat anti-mouse Gr-1 (clone RB6-8C5, BD Pharmingen), then centrifuging cells in Tris-buffered NH_4Cl for lysis of erythrocytes, and then labeling cells for 20 min on ice with streptavidin microbeads (Miltenyi Biotec). Samples were depleted of labeled cells by autoMACS (Miltenyi Biotec) according to the manufacturer's instructions. B cell and T cell purities were typically greater than 95%.

For labeling with CellTracker Orange 5-(and-6)-(((4-chloromethyl)benzoyl)amino)tetramethylrhodamine (CMTMR, Invitrogen/Molecular Probes), cells were warmed to room temperature, washed, and resuspended in DMEM medium containing 1% FBS at a density of 1-2 x 10^7 cells per mL. A 1:1000 dilution of a 20 mM stock of CMTMR in DMSO was then added, and cells were incubated at 37°C for 20 min and then at room temperature for 5-10 min with occasional agitation. Cells were then washed with DMEM medium containing 2% FBS.

Cells were adoptively transferred by intravenous injection into the lateral tail vein or the retro-orbital plexus. For early B cell-T cell interaction imaging, purified B cells from VDJ9/κ5 UBC-GFP mice (3 x 10^6 HEL-binding B cells representing about 70% of

total B cells) and purified $CD4^+$ T cells from OT-II β-actin-CFP mice (3x 10^6 $V\alpha2^+$ $V\beta5^+$ T cells representing about 80% of total T cells), and 5 x 10^6 CMTMR-labeled, purified B or T cells from B6 mice were co-transferred into each recipient mouse, and then one day after transfer the mice were immunized as described below. Draining axillary, brachial, and facial LNs were isolated 36 to 48 hours after immunization. For GC imaging, adoptive transfers were as depicted in Fig. S1C, except that in some cases naïve B and T cells were from β-actin CFP mice rather than being labeled with CMTMR.

For generation of PE immune complexes *in vivo*, 2 d before analysis mice were given an intraperitoneal injection of 2 mg of rabbit IgG anti-B-PE (Rockland). Then, 1 d before analysis, mice were first anesthetized with an intraperitoneal injection of 100 mg/kg of ketamine (Sigma-Aldrich) and 20 mg/kg of xylazine (Sigma-Aldrich) in PBS, followed by an intraperitoneal injection of 0.15 mg/kg of isoproterenol (Sigma) in PBS to prevent anaphylaxis. A total of 75 μg of R-PE (Invitrogen) were then injected subcutaneously across multiple sites proximal to the original sites of immunization.

Immunizations and BrdU treatment

DEL was purified as described (Prager and Wilson, 1971) with the following modifications: 400 mL of pooled duck egg whites were diluted in 2L of 0.1*M* ammonium acetate (pH 9), homogenized in an Oster blender for 30 s on the frappé setting, and then filtered through two layers of Kimwipes (Fisher), followed by the addition of 4.5 g of CM Sephadex C-25 beads (Amersham Biosciences). Purified DEL was conjugated to OVA from chicken egg white (grade V, Sigma-Aldrich) by glutaraldehyde crosslinking (Garside *et al.*, 1998). A mixture containing 0.023% glutaraldehyde (grade II, Sigma-

Aldrich), 13.3 mg of DEL, and 13.3 mg of OVA, in a total volume of 4.2 mL in potassium phosphate buffer (65mM PO_4^{2-}, pH 7.5), was stirred at room temperature for 1 h. After the precipitate was removed by centrifugation, the solution was dialyzed against PBS (Slide-A-Lyzer 10K MWCO Dialysis Cassette, Pierce) overnight at 4°C. Coupled DEL-OVA was separated from free DEL and OVA by gel filtration on a Sephadex G-100 column. Purified DEL-OVA (0.66 mg/mL) in PBS was mixed with an equal volume of Ribi/MPL+TDM adjuvant (Corixa or Sigma-Aldrich), and mice were immunized subcutaneously in 3-4 sites with a total volume of 150 μL of this mixture (containing 50 μg DEL-OVA). For imaging of explanted axillary, brachial, and facial LNs, mice were immunized with DEL-OVA in the upper flanks and the scruff of the neck. For intravital imaging of inguinal LNs, mice were immunized with DEL-OVA in the lower flanks and near the base of the tail.

For cell cycle analysis, B6 mice were immunized subcutaneously in all 7 sites described above with a total of 100 μg of (4-hydroxy-3-nitrophenyl)acetyl-chicken gamma globulin (NP_{30}-CGG, Biosearch Technologies) emulsified in complete Freund's adjuvant (Sigma-Aldrich). Draining inguinal, axillary, brachial, and facial LNs were combined for analysis. 2.5 mg of BrdU (Sigma-Aldrich or BD Pharmingen) in PBS was administered by a single intraperitoneal injection at the indicated time period before analysis.

For transwell migration assays, Eμ-*Bcl2*-22 mice were immunized with an intraperitoneal injection of sheep red blood cells (Colorado Serum Company) as described (Shinall *et al.*, 2000) and spleen cells were assayed at d 7.

Flow cytometry and cell cycle analysis

Cell suspensions were prepared from LNs and stained with antibodies as described (Allen *et al.*, 2004), although in some cases 2 x 10^6 cells were stained in a volume of 50 μL in 96-well U-bottomed plates (BD Falcon). Data were collected on a BD FACS Calibur, BD LSRII, or BD FACS Aria and analyzed with FlowJo software (Tree Star). The following antibodies and reagents, conjugated to the indicated fluorophors, were used for cell staining (at a 1:100 dilution unless otherwise indicated): rat anti-mouse CD4 (clone RM4-5, Alexa Fluor 700, 1:200, BD Pharmingen), rat anti-mouse CD4 (clone GK1.5, allophycocyanin (APC)-Cy7, BD Pharmingen), rat anti-mouse CD19 (clone 1D3, APC and APC-Cy7, 1:75, BD Pharmingen), rat anti-mouse CD19 (clone 6D5, PE-Cy5.5, 1:50, CALTAG Laboratories), mouse anti-mouse CD45.1 (clone A20, APC and Pacific Blue, BioLegend), mouse anti-mouse CD45.2 (clone 104; fluorescein isothiocyanate (FITC), PE-Cy5.5, and APC-Cy5.5; BD Pharmingen, E-bioscience, and BioLegend, respectively), rat anti-mouse CD45R/B220 (RA3-6B2, PE, CALTAG Laboratories), hamster anti-mouse CD95/Fas (clone Jo2, PE and PE-Cy7, BD Pharmingen), rat anti-mouse CXCR4 (clone 2B11/CXCR4, biotin, BD Pharmingen), rat anti-mouse IgD (clone 11-26c.2a, PE, BioLegend), mouse anti-mouse $IgG_{2a}{}^{a}$ (clone 8.3, biotin, BD Pharmingen), rat-anti-mouse IgG_{2b} (clone RMG2b-1, biotin, BioLegend), mouse anti-mouse IgM^{a} (clone DS-1, FITC, BD Pharmingen), peanut agglutinin (PNA, biotin, 1:2000, Vector Labs), rat anti-mouse T- and B-cell activation antigen (clone GL7, FITC, 1:400, BD Pharmingen), rat anti-mouse Vα2 TCR (clone B20.1, PE, BD Pharmingen), mouse anti-mouse Vβ 5.1,5.2 TCR (clone MR9-4, FITC, BD Pharmingen), and streptavidin (APC and Qdot 605, 1:200, Invitrogen).

Routine enumeration of HEL-binding cells was by incubating cells with 200 ng/mL HEL (Sigma-Aldrich), washing, and then staining with HyHEL9 PE-Cy5.5 (1:300, custom conjugation by CALTAG Laboratories) together with other cell surface antibodies. For assessment of affinity maturation by flow cytometry, DEL and HEL in PBS were labeled with the Alexa Fluor 647 Microscale Protein Labeling Kit (Invitrogen) according to the manufacturer's instructions.

For analysis of DNA content by flow cytometry without BrdU (Fig. 3, D and E), cells were first surface stained as described above, except that 2×10^7 cells were stained in a volume of 0.5 mL. Cells were washed and then fixed in 0.5 mL of PBS that contained 1% paraformaldehyde (Sigma-Aldrich) and 0.5% Tween-20, for 30 min on ice and then 30 min at room temperature. Cells were resuspended in PBS containing 2% FBS and then 4',6-diamidino-2-phenylindole dihydrochloride (DAPI, Sigma-Aldrich) was added at a final concentration of 5 μM. Approximately 2×10^6 events were collected on the LO setting on a BD LSRII.

Combined BrdU and DNA content analysis was with a FITC BrdU flow kit (BD Pharmingen) according to the manufacturer's instructions, except that 3.5 x 10^6 cells were first surface stained in 96-well U-bottomed plates in a volume of 100 μL in PBS containing 3% FBS, washed, and then transferred to 5 mL polystyrene round-bottom tubes (BD Falcon) for the remainder of the procedure. Prior to acquisition, DAPI was added at a final concentration of 5 μM. At least 3 x 10^5 events were collected on the LO setting on a BD LSRII. Cells were resolved into G1, S, and G2/M stages of the cell cycle by applying the Watson pragmatic algorithm in the FlowJo cell cycle platform. The model was constrained by gating the location of the G1 peak, setting the G2 peak to be two times the G1 peak, and setting the G2 CV equal to the G1 CV.

Cell sorting and HyHEL10 heavy-chain sequence analysis

For fluorescence activated cell sorting, cell suspensions were first prepared in HBSS (UCSF Cell Culture Facility) that contained 1% FBS, 0.5% fatty-acid-poor, endotoxin-free bovine serum albumin (Calbiochem), 10 mM HEPES (Cellgro), and 2 mM EDTA (Teknova). Cells were labeled with antibodies at a density of 4 x 10^7 cells/mL for 30 min, washed, and filtered into polystyrene round-bottom tubes with cell-strainer caps (BD Falcon). Single cells were sorted on a BD FACS Aria equipped with an Automated Cell Deposition Unit into a volume of 10 μL containing 1X Taq buffer without $MgCl_2$ (Invitrogen), 0.5 mg/ml proteinase K (Fisher), 10 μg/mL yeast tRNA (Invitrogen), 0.1 mM EDTA (Teknova), and 0.1% Tween-20 (Sigma-Aldrich) in 96-well PCR plates (Optical PCR plates, Applied Biosystems or Thermo-Fast Skirted PCR plates, Abgene). After brief centrifugation, plates were stored at -70°C for several days. Proteinase K

digestion was then performed at 56°C for 40 min followed by inactivation at 95°C for 8 min. For the primary PCR, 15 μL were added to each well to achieve a final concentration of 1X Taq buffer (Invitrogen), 2 mM $MgCl_2$ (Invitrogen), 200 μM of each dNTP (PCR grade, Invitrogen), 0.15 μL of Taq DNA polymerase (Invitrogen), and 40 nM primers (forward, GTTGTAGCCTAAAAGATGATGGTG; reverse, GATAATCTGTCCTAAAGGCTCTGAG, Integrated DNA Technologies). Plates were then loaded onto a PTC-200 thermal cycler (MJ Research) with the following conditions: 94°C for 3 min, and then 35 cycles of 95°C for 15 s, 62°C for 1 min, and 72°C for 1 min, followed by 72°C for 5 min. For the secondary PCR, 2.5 μL of the primary PCR product were placed in a total volume of 25 μL containing 1X Taq buffer (Invitrogen), 2 mM $MgCl_2$ (Invitrogen), 200 μM of each dNTP (PCR grade, Invitrogen), 0.1 μL of Taq DNA polymerase (Invitrogen), and 400 nM nested primers (forward, TTGTAGCCTAAAAGATGATGGTGTTAAGTC; reverse, CTTGGGACAAAGGGGTTGAA, Integrated DNA Technologies, Inc.). Secondary PCR thermal cycler conditions were 94°C for 3 min, and then 35 cycles of 95°C for 15 s, 65°C for 30 s, and 72°C for 1 min. PCR amplification in each well was assessed by mixing 2 μL of the secondary PCR product with 2 μl of 2.5 μg/mL ethidium bromide (UCSF Cell Culture Facility) on parafilm (Fisher) with a multichannel pipette followed by examination under UV. The average efficiency of obtaining a PCR product was 81%. In order to remove primers and inactivate unincorporated nucleotides, 2.5 μL of the secondary PCR product were combined with 10.5 μL of water and 1 μL of ExoSap-IT (USB), followed by incubation at 37°C for 20 min and 80°C for 15 min. 1 μL of an 8 μM stock of the secondary PCR forward primer were then added for sequencing (Elim Biopharmaceuticals). Sequence

data were processed with Vector NTI (Invitrogen) and then analyzed in BioEdit (Tippmann, 2004) and by modifying the SAIVGeM package for Microsoft Excel (Messmer, 2005).

Transwell migration assays

Transwell migration assays were as described (Allen *et al.*, 2004) with some modifications. Cells and chemokines were first prepared at a 2X concentration. Then, 290 μL of chemokine and 290 μL of media were added to the bottom wells, and 50 μL cells and 50 μL of chemokine or media were added to the top wells, in order to achieve a uniform concentration or gradient of chemokine.

Immunohistochemistry and immunofluorescence

Immunohistochemistry of acetone-fixed, 7 μm cryostat sections was performed as described (Allen *et al.*, 2004). For identification of VDJ9/κ5 cells, sections were incubated with biotinylated mouse anti-mouse CD45.2 (clone 104, BD Biosciences) and polyclonal sheep anti-mouse IgD (1:300, The Binding Site) for 2-3 h, followed by streptavidin alkaline phosphatase (Jackson Immunoresearch) and peroxidase-conjugated donkey anti-sheep IgG H+L (Jackson Immunoresearch) for 1-2 h. Immunofluorescence analysis of cryostat sections was essentially identical to immunohistochemistry, except that the staining buffer contained phosphate buffered saline (PBS) instead of tris buffered saline, and coverslips were mounted with Fluoromount G (Southern Biotechnology). Sections were stained with purified FDC-M2 (1:200, ImmunoKontact) and sheep anti-mouse IgD for 2-3 h, followed by FITC-conjugated $F(ab')_2$ fragment donkey anti-rat IgG

H+L (1:100, Jackson Immunoresearch) and biotinylated donkey anti-sheep IgG H+L (1:300, Jackson Immunoresearch) for 1-2 h, and then with streptavidin AMCA (1:50, Vector Labs) for 1 h. Sections were viewed on a Leica DMRL fluorescence microscope equipped with a mercury arc lamp. Images were acquired on an Optronics MDE1580 cooled charge-coupled device video camera (Optronics Engineering). White balance, input levels, and sharpness were corrected by equivalent adjustments to all images in Adobe Photoshop 7.0 for Windows.

Two-photon microscopy

Explanted LNs were prepared for imaging as described (Okada *et al.*, 2005). Briefly, LNs were maintained in 36°C RPMI (Cellgro) bubbled with 95% O_2/5% CO_2, and imaged through the capsule in a region distal to the efferent lymphatic. Inguinal LNs were prepared for intravital microscopy as described (Lindquist *et al.*, 2004) with some modifications. After anesthetizing mice by intraperitoneal or intramuscular injection of 100 mg of ketamine and 20 mg of xylazine per kg in PBS, fur on the lower flank was shaved (Braintree Scientific). The mouse was then restrained on a Biotherm stage warmer at 37°C (Biogenics), an incision was made in the abdominal skin, and a skin flap containing the inguinal LN was separated from the abdominal muscle. The subdermal side of the skin flap was placed on a base consisting of an outer ring of Sylgard 184 silicone elastomer (Fisher) surrounding thermoconductive putty (T-putty 502, Thermagon) to conduct heat from the stage warmer. The cortical side of the inguinal LN was exposed through a small incision of epidermis and dermis by microsurgery. A nylon washer was placed with vacuum grease silicone (Beckman Coulter) over the skin flap,

surrounding the exposed LN, and was fixed to the silicone base with pins. The space inside the washer was filled with saline and sealed with a cover slip. Blood circulation was confirmed through all visible blood vessels in the LN. At the end of each imaging experiment, we confirmed that lymph flow was intact by assessing whether FITC-dextran (Invitrogen) injected subcutaneously reached the LN within one minute.

LNs were imaged with a custom two-photon microscope system that was constructed and maintained by M.F. Krummel. A 5-W MaiTai TiSapphire laser (Spectra-Physics) was tuned to provide an excitation wavelength of 910 nm. Each *xy* plane spanned 240 μm by 288 μm at a resolution of 0.6 μm per pixel and images of 35-37 *xy* planes with 3 μm *z* spacing were formed by averaging 10 video frames, detecting emission wavelengths of 455-485 nm (for CFP^+ cells and second harmonic emission of collagen fibers), 500-540 nm (for GFP^+ cells), and 567-640 nm (for CMTMR-labeled cells or PE immune complexes), every 20 s. Images were acquired by Video Savant software (IO Industries). The maximum intensity z-projection time-lapse image sequences were generated with MetaMorph software (Molecular Devices). 3-D rotations and time-lapse image sequences were generated in Imaris 5.01 x64 (Bitplane). Videos were processed with low pass or median noise filters. Annotation and final compilation of videos was in Adobe After Effects 7.0. Video files were converted to MPEG format with AVI to MPEG Converter for Windows 1.5 (FlyDragon Software). Semi-automated cell tracking in 3-D, verified and corrected manually, was with Imaris 4.2 or 5.0.1 x64. Tracking data were analyzed in Microsoft Excel with a custom macro written in Microsoft Visual Basic for Applications. The motility coefficient $M=x^2/6t$ (Sumen *et al.*,

2004) was calculated from the slope ($x/t^{1/2}$) obtained by regression analysis of the mean displacement (x) versus the square root of time ($t^{1/2}$) plots.

Tracks were manually classified based on their localization with respect to the PE^+ light zone as shown in Fig. 2 and movie S6. Cell tracks were classified as being in the light or dark zones if the entire track stayed within the PE^+ or PE^- region, respectively. Cell tracks were classified as representing movement between zones if the tracks originated in one zone, crossed an approximately 20 μm border between the zones, then entered at least 10 μm into the other zone, and stayed in that zone for the duration of the analysis. Some cell tracks could not be definitively classified by these criteria (≈32%), for example cell tracks that were too close to the border between the light and dark zones.

Statistical analysis

In comparisons of two groups, P values were calculated by the unpaired T-test in Microsoft Excel. For comparisons of multiple groups, P values were calculated by one-way ANOVA with Dunnett's post test in GraphPad Prism to reduce type I error.

Movie legends

Movie S1. GC B cells are motile and extend dendritic processes. A time-lapse sequence of 18 μm z-projection images shows the dynamics of GC B cells in an axillary lymph node explant 7 d after immunization. White arrowhead, a long process of a GC B cell; yellow arrowhead, cell depicted in Fig. 1B. Elapsed time is shown as hh:mm:ss.

Movie S2. Intravital imaging of GC B cells. A time-lapse sequence of 21 μm z-projection images of a GC in an inguinal lymph node of an anesthetized mouse 7 d after immunization. Cell division and death are annotated in the video. Also indicated is a blood vessel in which four CMTMR-labeled cells (arrowheads) appeared in the image stack within 20 s and disappeared within the next 20 s. Elapsed time is shown as hh:mm:ss.

Movie S3. Plasma cells move with slow velocities and minimal displacements. Time-lapse image sequences of plasma cells in lymph node medullary cords. Left, 36 μm z-projection of the medulla of an axillary lymph node explant in a recipient of VDJ9/κ5 B cells (3% GFP^+) and OT-II T cells (approximately 97% CFP^+) 7 d after immunization. Right, 30 μm z-projection of the medulla of a mesenteric lymph node explant in a *Blimp*^{gfp} mouse. Elapsed time is shown as hh:mm:ss.

Movie S4. The boundary between the follicular mantle (FM) and GC. Data are shown as 3-D rotations on the y-axis, and correspond to Fig. 1K. Note that tracks of GC B cells

(green) extend into the area occupied by FM B cells (red), and vice versa. The gridlines are separated by 20 μm.

Movie S5. Movement dynamics of cells in dark and light zones. Time-lapse image sequences show cells in the light zone (left panel, 18 μm z-projection) and dark zone (right panel, 33 μm z-projection) from the same GC in a facial lymph node explant 7 d after immunization. FDC in the light zone are labeled with PE immune complexes (IC). An arrowhead highlights a cell that is moving among processes of the FDC network. Elapsed time is shown as hh:mm:ss.

Movie S6. Tracks of cells traveling between light and dark zones. Data are shown as a 3-D rotation on the z-axis for the entire imaging volume analyzed from a GC in a brachial lymph node 7 d after immunization, and correspond to Fig. 2B and movie S8. The PE immune complexes deposited on the FDC network in the light zone are in red, and tracks indicate the path of GFP^+ GC B cells that transited from one zone to another. The gridlines are separated by 20 μm.

Movie S7. Cells migrating between dark and light zones. Time-lapse image sequences show maximum intensity projections of the entire 3-D imaging volume analyzed from a GC in a brachial lymph node 7 d after immunization, and correspond to Fig. 2B and movie S7. Tracks of cells moving between dark and light zones are color-coded according to the timescale shown in the bottom-right corner. Gray spheres show the positions of tracked cells over time. An arrowhead highlights a GC B cell moving from

the dark zone to the light zone that can easily be followed at this orientation of the imaging volume. The gridlines are separated by 20 μm. Elapsed time is shown as hh:mm:ss.

Movie S8. Most contacts between GC B cells and T cells are transient. A time-lapse sequence of 39 μm z-projection images shows the dynamics of GC B cells and T cells in a brachial lymph node explant 7 d after immunization. In this lymph node, 1-2% of GC B cells were GFP^+, and approximately 6% of OT-II T cells were CFP^+. Elapsed time is shown as hh:mm:ss.

Movie S9. Stable interactions between cognate antigen-specific B and T cells 36 h after immunization. A time-lapse sequence of 36 μm z-projection images show the dynamics of antigen-engaged B and T cells interacting each other in a facial lymph node. In this lymph node, nearly 100% of VDJ9/κ5 B cells were GFP^+ and approximately 97% of OT-II T cells were CFP^+. Elapsed time is shown as hh:mm:ss.

Movie S10. Example of a stable interaction between a GC B and T cell. A time-lapse sequence of 6 μm z-projection images shows a migratory conjugate of a GFP^+ VDJ9/κ5 B cell and CFP^+ OT-II T cell in a GC of an axillary lymph node explant 7 d after immunization. In this lymph node, 1-2% of GC B cells were GFP^+, and approximately 97% of OT-II T cells were CFP^+. Optimal 6 μm z-projection images capturing the conjugate within a 36 μm z-stack that the conjugate traveled through were used for the image sequence. The time-lapse image sequence is shown twice, first with and then

without a migration track of the conjugate. An arrowhead indicates the initial position of the conjugate. Elapsed time is shown as hh:mm:ss.

Movie S11. Fragmentation of GC B cells. Two time-lapse image sequences (30 μm and 54 μm z-projections in the order of appearance) show GFP^+ VDJ9/κ5 B cells that were dying and undergoing fragmentation. Fragments of each B cell were taken up by multiple macrophages outlined by dotted lines. Arrowheads indicate dying cells and fragments of dead cells. The last two arrows in the second image sequence indicate fragments that were not taken up by macrophages during imaging. Elapsed time is shown as hh:mm:ss.

Movie S12. GC B cell blebs are carried by GC T cells. Four time-lapse image sequences (45 μm, 39 μm, 36 μm and 24 μm z-projections in the order of appearance) show CFP^+ OT-II T cells migrating together with blebs from GFP^+ VDJ9/κ5 B cells in GCs. White dots show tracks of the T cell-attached blebs. Elapsed time is shown as hh:mm:ss.

Acknowledgments

We thank Y. Xu for excellent technical assistance; O. Lam for screening of mice; N. Killeen for help with gene targeting; M. Egeblad, S. Nutt, R.L. Reinhardt, and A.J. Tooley for providing mice; the Mt. Zion Animal Care Facility for animal husbandry; E. Passegue for advice on single cell sorting and for use of her cell sorter, and T.G. Phan and I.L. Grigorova for helpful discussions and critical reading of the text. C.D.C.A. is a predoctoral fellow and J.G.C. is an investigator of the Howard Hughes Medical Institute. This work was supported in part by grants from the NIH and by a Sandler New Technology Award.

CHAPTER 4

Conclusion

In the studies presented here, we have defined roles for the chemokine receptors CXCR4 and CXCR5 in GC B cell positioning and GC organization, and we have provided a set of observations about the movement dynamics of GC B cells *in vivo* and their interactions with other cells. These data address long standing questions about the mechanism by which GC compartmentalization is achieved and provide novel insights into the selection process during affinity maturation. In addition, these findings together with real-time imaging studies from other groups (Hauser *et al.*, 2007; Schwickert *et al.*, 2007) suggest that that the classical model of GC organization and function should be revisited and refined.

The classical model of GC compartmentalization into dark and light zones defined the dark zone as the site of proliferation (MacLennan, 1994). However, the work presented here and in other studies indicates that proliferation occurs in both dark and light zones (Hauser *et al.*, 2007; Rahman *et al.*, 2003; Wang and Carter, 2005). Cell division could be observed in both dark and light zones during real-time imaging of GCs, and no bias was seen for cell division in the dark zone, although these events were difficult to quantify as they occurred infrequently in recordings that typically lasted less than one hour. The proliferation rates in both zones were further quantified through cell cycle analysis by flow cytometry, which showed that a similar proportion of cells were in cycle in the dark and light zones, with a somewhat higher frequency of cells in G2/M phase in the dark zone.

It has been suggested that proliferation occurs in both dark and light zones in mice, but only in the dark zone in humans (Camacho *et al.*, 1998). This suggestion was primarily based on staining for the cell cycle antigen Ki67 that failed to show dark and

light zone polarity in mouse GCs (Camacho *et al.*, 1998), whereas this polarity is apparent in human GCs (Hardie *et al.*, 1993; Liu *et al.*, 1992). However, even in human GCs, it is evident that some $Ki67^+$ cells are present in the light zone as well, calling into question the strength of this argument (Hardie *et al.*, 1993; van Galen *et al.*, 2004). It is also difficult to compare existing data on mouse and human GCs because most mouse studies were performed on acute GCs in the spleen or lymph nodes that were induced by immunization, whereas most human studies were performed on chronic GCs in the tonsils, which are continually exposed to foreign antigens. Substantial differences were seen in the degree of GC compartmentalization between human lymph node GCs and human tonsil GCs (Brachtel *et al.*, 1996). For example, human tonsil GCs contain an outer zone rich in GC T cells, perhaps functioning to segregate GC B cell-T cell interactions in the outer zone from GC B cell-FDC interactions in the light zone. Recent studies also point to unique signaling requirements for chronic mouse GCs in mucosal lymphoid tissues (reviewed in Casola and Rajewsky, 2006). Further studies will be needed to understand how the additional levels of organization described for chronic GCs may contribute to the function of these structures in the immune responses induced by chronic foreign antigen exposure.

The notion that proliferation occurs only in the dark zone was also based on older studies that examined the frequency of mitotic figures by histological examination of a variety of secondary lymphoid organs in various species (reviewed in MacLennan, 1994). These studies indicated that a higher frequency of mitotic figures was seen in the dark zone than in the light zone. However, even in the 1930s it was apparent in GCs from various species, including humans, that mitotic figures were present in the light zone

(Kindred, 1938), a finding that was largely ignored in subsequent descriptions. A recent study has confirmed the presence of mitotic figures in the light zones of mouse GCs (Wang and Carter, 2005). When considering the frequency of mitotic figures in dark and light zones, it is important to consider that the density of B cells is much higher in the dark zone than in the light zone, because much of the light zone space is occupied by the processes of FDCs (referred to in the older literature as reticulum cells). Follicular helper T cells are also more abundant in the light zone than in the dark zone (Vinuesa *et al.*, 2005), and some naive follicular B cells are seen to enter the GC at the light zone pole (Schwickert *et al.*, 2007), perhaps accounting for the higher frequency of small lymphocytes seen in the light zone in older studies that were not undergoing mitosis. When the frequency of mitotic figures was considered only among medium sized lymphocytes, less than a two-fold difference was observed between dark and light zones (Kindred, 1938), consistent with the observations presented here.

Another classical distinction that was described between centroblasts and centrocytes was that centroblasts lacked surface Ig, whereas centrocytes reexpressed surface Ig (Liu *et al.*, 1992; Manser, 2004). It appears that this notion might have arisen from immunohistochemical analyses of GCs, in which more Ig was seen in the light zone. These studies must be interpreted with caution, however, as the FDCs in the light zone are known to capture large amounts of immune complexes containing various Ig isotypes (Kosco-Vilbois, 2003; Nieuwenhuis and Opstelten, 1984; Szakal *et al.*, 1989). In one study that fractionated GC cells from the rabbit appendix by size and density, it was noted that all GC cells expressed low amounts of surface Ig (Opstelten *et al.*, 1983). Cells expressing high amounts of Ig mRNA have been described at the base of the light zone;

however, these cells were relatively infrequent and expressed large amounts of cytoplasmic Ig protein, suggesting that these cells may have been undergoing differentiation into antibody-secreting plasma cells (Close *et al.*, 1990). It is interesting to note that no study to date has demonstrated by the routine quantitative method of flow cytometry that centroblasts and centrocytes differ in the amount of surface Ig. In mouse studies nearly all GC B cells have been described to express surface Ig by flow cytometry (Shinall *et al.*, 2000; Wang and Carter, 2005; Wolniak *et al.*, 2006), typically in low amounts compared with naïve B cells (Rossbacher *et al.*, 2006). Taken together with observations that Ig levels appear very low in the dark zone by immunohistochemistry (Kosco-Vilbois, 2003; Liu *et al.*, 1992; Opstelten *et al.*, 1982), these data suggest that all GC B cells express low levels of Ig and that the bright staining seen in the light zone is the result of Ig deposition on FDC instead of increased Ig expression by centrocytes. It is important to note that contamination of the GC B cell gate by some naïve follicular B cells might account for the bright population of surface Ig expressing cells seen in some studies. Through immunohistochemical analysis of splenic GCs induced by immunization with sheep red blood cells (SRBCs), it has recently been argued by Wang *et al.* (2005) that IgM^+ GC B cells are localized exclusively in the light zone, but it is unclear how this group excluded that IgM staining in the light zone resulted from the deposition of immune complexes containing IgM on FDC. Indeed, by flow cytometric analysis a large percentage of GC B cells have been reported to express IgM in the primary immune response to SRBCs (Kraal *et al.*, 1982; Shinall *et al.*, 2000; Wang and Carter, 2005), making it unlikely that these cells could be exclusively located in the light zone.

Therefore, it appears that all GC B cells express reduced surface Ig compared with naïve cells, but that this feature does not distinguish centroblasts from centrocytes.

It has also been suggested that somatic hypermutation occurs in the dark zone but not in the light zone (Zhang *et al.*, 1988). While this remains an attractive notion, it is currently supported by only limited direct evidence. Activation-induced cytidine deaminase (AID), a protein essential for somatic hypermutation and class switch recombination, was found to be expressed primarily in the dark zone in human tonsil GCs by immunohistochemistry (Cattoretti *et al.*, 2006; Moldenhauer *et al.*, 2006). A very small number of cells in the light zone were positive for AID, perhaps even fewer cells than were positive for Ki67, although no quantitative data were provided. Because of the low GC B cell density in the light zone compared with the dark zone, it is not clear what fraction of GC B cells in the light zone expressed AID. It is also not known whether such a polarized distribution occurs in the mouse, due to a lack of antibodies that can detect endogenous mouse AID by immunohistochemistry.

Recently several groups have performed microarray studies of gene expression in human B cell subsets that included centroblasts and centrocytes (Klein *et al.*, 2003; Nakayama *et al.*, 2006; Shaffer *et al.*, 2002). While these studies have shown a large number of genes differentially expressed between GC B cells and naïve B cells, relatively few differences were seen between centroblasts and centrocytes. The main differences observed were the expression of some plasma cell specific genes among centrocytes, suggesting that a fraction of centrocytes were differentiating into plasma cells. These microarray results suggest that centroblasts and centrocytes may be much more similar than previously thought. A caveat to these studies is that the centroblasts and centrocytes

were isolated based on the expression of CD77, a marker which shows a broad range of staining intensity on GC B cells and has been argued to be insufficient to discriminate between centroblasts and centrocytes (Feuillard *et al.*, 1995). However, when these microarray results are considered in light of the other data described above, one wonders whether the classical definitions of centroblasts and centrocytes are no longer valid and perhaps it would be better to think of GC B cells as a single cell type at various stages of a cycle. In addition, the microarray results suggest that most observed differences between centroblasts and centrocytes may be regulated at the protein level. Indeed, in samples from human tonsils, AID mRNA was expressed in both centroblasts and centrocytes (Shaffer *et al.*, 2002), yet AID protein was found primarily in the dark zone (Cattoretti *et al.*, 2006). Similarly, in our study of mouse GCs, CXCR4 protein was more abundant in centroblasts compared with centrocytes, yet similar amounts of CXCR4 mRNA were detected in these cells. Polycomb proteins have also been described to be differentially expressed in dark and light zones in human GCs, although it is unclear whether this expression is regulated at the mRNA or protein level (van Galen *et al.*, 2004). Further studies will be needed to define other differences in the proteins expressed by centroblasts and centrocytes.

Although the differences between centroblasts and centrocytes remain unclear, it appears that the localization of GC B cells in dark and light zones is tightly regulated. We demonstrated that CXCR4 was critical for the dark zone localization of centroblasts, as CXCR4-deficient cells were found to accumulate in the light zone and were absent from the dark zone. In contrast, CXCR5-deficient cells were found at the base of the dark zone and absent from the light zone, and CXCR5 was required for proper positioning of the

light zone. Consistent with these findings, the ligand for CXCR4, SDF-1, was found to be more abundant in the dark zone than in the light zone, whereas the ligand for CXCR5, CXCL13, was found to be more abundant in the light zone than in the dark zone. The opposing distribution of these chemokines suggests a mechanism for the positioning of centroblasts and centrocytes in the dark and light zones, respectively. However, both centroblasts and centrocytes expressed equivalent amounts of CXCR5, yet centroblasts expressed more CXCR4 than centrocytes, suggesting that regulation of CXCR4 protein levels may be the mechanism for determining the relative responsiveness of GC B cells to SDF-1 in the dark zone and CXCL13 in the light zone. The factors leading to the selective CXCR4 protein upregulation in centroblasts remain unknown and will be the subject of future studies. Some possibilities include regulation directly by the cell cycle or in response to additional cues such as BCR triggering or ongoing SDF-1 exposure. Further work will also be needed to elucidate the mechanism by which differential expression of SDF-1 and CXCL13 in dark and light zones, respectively, is achieved.

To further understand the relationship between the cell cycle and GC B cell trafficking between dark and light zones, we administered the thymidine analog BrdU to pulse-label cells in S phase. Strikingly, most cells that were BrdU-labeled in S phase in the light zone were found to be cleared from this compartment within five hours, although it remains unknown whether these cells returned to the dark zone, exited the GC, or underwent apoptosis. In contrast, BrdU-labeled cells were found to accumulate in the dark zone upon completing mitosis, resulting in a large number of BrdU-labeled cells in the dark zone in the G1 phase of the cell cycle five hours after BrdU injection. After several hours of the G1 phase of the cell cycle, however, a substantial fraction of the

BrdU-labeled cells were found to have returned to the light zone, such that by twelve hours an equivalent fraction of cells in dark and light zones were labeled with BrdU. This finding suggests that BrdU-labeled cells migrated from the dark zone to the light zone, consistent with previous reports. Importantly, this increase in the frequency of BrdU-labeled cells in the light zone cannot solely be attributed to cell division locally within the light zone as has been argued by one group (Hauser *et al.*, 2007). We observed a 2-fold increase in BrdU-labeled cells in the light zone from eight hours to twelve hours, yet at eight hours nearly all cells were in the G1 phase of the cell cycle and could not have completed a second round of cell division within this time frame. At the same time, we noted a decrease in the frequency of BrdU-labeled cells in the dark zone, consistent with the notion that these cells migrated to the light zone.

The migration of cells between dark and light zones was further assessed by real-time imaging. Based on strict criteria, we found that approximately 3-5% of total cell tracks showed cell movement from the dark zone to the light zone, whereas approximately 2-3% of total cell tracks showed cell movement from the light zone to the dark zone, within one hour. Recent reports of real-time imaging studies of the GC from other groups give slightly different estimates (Hauser *et al.*, 2007; Schwickert *et al.*, 2007), but taken together these data indicate that cells traffic between dark and light zones in both directions. It is important to note that all of these results lack precision due to technical limitations and are most likely an underestimate of the trafficking between dark and light zones. In our studies most cells could not be tracked for a full hour, and in many cases cells could only be tracked for approximately 20 minutes. For example, some cells came in too close proximity to other cells to reliably determine the total path of the

cells, and in other cases the cells exited the imaging volume in less than one hour. In addition, the dark and light zone boundary cannot be precisely defined, and thus we had to set stringent criteria for cells that were defined to have crossed from one zone into the other. One study has emphasized that most GC B cells recirculate within only dark or light zones and do not cross between zones during one hour imaging sessions (Hauser *et al.*, 2007); indeed, we also noted in our report that most cells that were in dark or light zones stayed resident in the respective zones. Over longer periods of time, however, it is clear from the results from all groups (Hauser *et al.*, 2007; Schwickert *et al.*, 2007) that substantial exchange occurs between dark and light zones. Together with our BrdU-labeling data presented above, it appears likely that a substantial fraction of cells within the light zone are turned over within hours of time and replenished by cells from the dark zone that recently completed a cell cycle. These global analyses do not exclude the possibility, however, that a small fraction of GC B cells might stay resident in one zone or another for longer periods of time.

One issue raised by recent studies relates to the cell cycle time of GC B cells. Previous studies had indicated a range of possible cell cycle times, with an estimate of five-seven hours becoming widely accepted over time (MacLennan, 1994). Our data suggested however that the average cell cycle time exceeds twelve hours, based on reentry of a fraction of BrdU pulse-labeled cells into S phase after twelve hours. In contrast, Hauser *et al.* (2007) observed reentry of BrdU labeled cells into S phase after eight hours. The factors that account for the differences between these studies remain unclear, and may be related to different experimental conditions; for example, we analyzed GCs at the peak of the response whereas Hauser *et al.* studied GC B cells early

after GCs reached maturity. It is important to note that our cell cycle analysis was performed on GCs derived from endogenous B cell responses in wild-type mice, whereas Hauser *et al.* immunized mice in which most B cells expressed a single rearranged immunoglobulin heavy chain and a large number of B cells were specific for the antigen, possibly affecting the competition among GC B cells. In both studies, however, what is evident is that only a fraction of the originally BrdU-labeled cells had reentered S phase at the indicated timepoints, suggesting that the cell cycles were not synchronous and that some cells would reenter S phase at a later time. Indeed, such a conclusion was made by an older study that carefully analyzed the fraction of labeled mitoses in the GC after administration of ^{3}H-thymidine (Zaitoun, 1980). Thus, these data can be interpreted to give the minimum cell cycle times, but not the average cell cycle times, which are likely to be longer and more difficult to determine.

The cell cycle times and trafficking of GC B cells are important to consider in the context of models for the selection of higher affinity cells. Hauser *et al.* (2007) conclude that the frequency of recirculation is insufficient to account for a selection mechanism that occurs only in the light zone, and therefore propose an intrazonal recirculation process in which most cells stay resident in dark or light zones and selection in the dark and light zones operate independently. Another group recently suggested that proliferation and selection occur independently in dark and light zones based on the study of CD19 signaling mutants (Wang and Carter, 2005). These studies raise the important issue that there is little if any evidence that selection occurs in the light zone but not in the dark zone. Much of the emphasis on selection in the light zone has emerged from the observation that large amounts of antigen are deposited in the form of immune complexes

on the processes of FDC in the light zone. These observations have not excluded that antigen may be available to cells in the dark zone below the limits of detection by standard methods such as immunohistochemistry. Arguing against a purely intrazonal recirculation and selection mechanism, however, our real-time imaging and BrdU pulse-labeling studies described above, together with other recent data, indicate that cells do transit between dark and light zones at a rate which would result in substantial exchange within twelve hours, which we estimate is less than the average cell cycle time of GC B cells. Similarly, based on real-time imaging, Schwikert *et al.* (2007) concluded that full exchange between dark and light zones occurs in less than 18 hours. Hauser *et al.* (2007) conclude that 100% exchange must occur in each cell cycle for selection to occur only in the light zone, and while our results are not inconsistent with this possibility, we also caution that this statement is based on theoretical modeling which cannot yet fully account for the complex cellular milieu and *in vivo* dynamics of the GC.

The light zone has several properties compared with the dark zone that may make it a unique site for selection. The classical model of GC organization and function was that selection depends on competition among centrocytes for firm adhesion to FDC based on the affinity of their B cell receptors for antigen held on the processes of the FDC in the form of immune complexes (MacLennan, 1994). However, several experimental results present challenges to this classical model. In mice deficient in serum immunoglobulin and therefore lacking immune complexes, GC size was not affected (Hannum *et al.*, 2000). Some evidence for selection was obtained in the absence of immune complexes, although the affinity maturation process could not be fully assessed in these studies due to the use of transgenic mice expressing multiple copies of a single immunoglobulin

heavy chain (Hannum *et al.*, 2000). Similarly, when FDC lacked the expression of complement receptors 1 and 2 and showed a marked decrease in the trapping of immune complexes, GC formation still occurred although sustained IgG responses were affected (Fang *et al.*, 1998). In addition, GCs were reported to form in the mesenteric lymph nodes of LTβ-deficient mice, which lack differentiated FDC (Koni *et al.*, 1997). It has also been difficult to explain based on the existing model how selection can operate efficiently in GCs derived from B cells that express B cell receptors with a wide range of starting affinities for a given antigen (Dal Porto *et al.*, 2002; Shih *et al.*, 2002). Perhaps the strongest evidence to date against this classical model, however, is that in the real-time imaging studies presented here and recently reported by other groups (Hauser *et al.*, 2007; Schwickert *et al.*, 2007), a common finding was that firm adhesion does not occur between GC B cells and the processes of FDCs. Schwickert *et al.* reported prolonged contacts between FDC-M1$^+$ cells and GC B cells, and Hauser *et al.* reported prolonged interactions between complement receptor 1-positive cell bodies and GC B cells, although it is not clear from these studies whether the cell bodies were tingible body macrophages or FDC. The significance of these interactions and whether or not they involve binding to cognate antigen remain unknown.

The light zone also forms the interface with naïve B cells in the follicular mantle zone. In our imaging experiments, we found that most follicular mantle B cells and GC B cells turned at the interface between the light zone and the follicular mantle and did not cross from one region into the other, although extensive overlap of the cell tracks in this region indicated that no physical boundary was present. Some cells clearly crossed this boundary however although their ultimate fate could not be ascertained. Schwickert *et al.*

(2007) proposed that the entry of follicular mantle B cells into the GC might allow new clones to participate in the GC response, and demonstrated that this can occur by the recruitment of adoptively transferred high affinity B cells into preexisting GCs. It remains unclear, however, whether such high affinity follicular mantle B cells would be present in a normal immune response, as it would be expected that such clones would have reacted early in the immune response and participated in the initial seeding of GCs. Perhaps over weeks of time, B cells with novel VDJ rearrangements might emerge from the bone marrow and contribute to GCs if of sufficiently high affinity for the immunizing antigen, or emigrants from one GC could enter another GC. A recent modeling study has argued that migration of cells between GCs may play a general role in achieving maximal affinity maturation (Or-Guil *et al.*, 2007). In this regard it is interesting to note that more sensitive techniques have demonstrated that antigen-specific GCs may be present for many weeks of time (Gatto *et al.*, 2007; Takahashi *et al.*, 2001), in contrast to the 2-3 week duration suggested by earlier studies (Liu *et al.*, 1991b; Takahashi *et al.*, 1998). In the immune response to the hapten nitrophenyl, selection occurs in GCs for a mutation of Trp33 to Leu in VH186.2 within the first 2-3 weeks giving an approximately 10-fold increase in affinity, but after 6 weeks a novel VH186.2 VDJ rearrangement emerges with Trp33 and Gly99 that exhibits even higher affinity (Furukawa *et al.*, 1999). It is unclear whether this novel rearrangement emerges because of the entry of additional cells into existing GCs or because of competition between cells that emerged from distinct GCs.

Another cell type enriched in the GC light zone is the GC T cell (MacLennan, 1994). GCs that are formed in response to T-independent antigens collapse shortly after compartmentalization into dark and light zones, suggesting that signals from T cells are

essential for maintaining the GC response (Manser, 2004; Vinuesa *et al.*, 2000). We found that few GC B cells were engaged in stable contacts with GC T cells that lasted for more than 5 minutes, in contrast to the prolonged interactions seen between activated B and T cells early in the immune response. In addition, although GC B cells have been estimated to be 5-20 times more abundant in the GC than GC T cells, and GC B cells and GC T cells are in close proximity in the light zone, less than a third of GC T cells were moving at velocities that indicated that they were interacting with GC B cells. These findings suggest that GC B cell interactions with GC T cells are tightly regulated. A high threshold for activation of GC T cells may provide a mechanism by which GC B cells can compete for the formation of stable conjugates with GC T cells. Some GC T cells were found to be engaged in stable interactions with blebs from apoptotic GC B cells, possibly contributing to the competition for T cell help.

Taken together, we suggest the following revised model for GC organization and function in selection. GC B cells are constantly in cycle and accumulate in the dark zone after undergoing mitosis. Growth during the early G1 phase of the cell cycle appears to occur in the dark zone, perhaps in response to dark zone-specific growth factors or simply to leave open space in the light zone for cells undergoing selection. Several hours after entering the G1 phase of the cell cycle, CXCR4 is downmodulated, perhaps regulated directly by the cell cycle or in response to additional cues such as B cell receptor triggering or ongoing SDF-1 exposure. CXCR4 downmodulation most likely occurs by defined mechanisms of internalization, ubiquitination, and proteolytic degradation. The GC B cells then respond less to SDF-1 in the dark zone causing the cells to migrate to the light zone in response to CXCL13. Within the light zone, the GC B

cells rapidly move about the FDC network and pick up antigen held on the processes of the FDC, providing B cell receptor-mediated survival signals. The GC B cells then internalize and process this antigen and present peptides on MHC Class II molecules. Higher affinity GC B cells may be able to capture more antigen than lower B affinity cells during rapid movement past the FDC processes by achieving greater shear force. In addition, as the GC B cells are in close proximity, higher affinity cells may be able to pick up antigen directly from the surface of lower affinity cells in direct cell-cell competition prior to antigen internalization. The GC B cells then compete with other GC B cells and dead B cell blebs for T cell help in the light zone. As T cells must polarize in a fashion that only allows interaction with one antigen presenting cell at a time, a single GC T cell will only form a stable interaction with the GC B cell that presents the highest number of antigen peptide-MHC Class II complexes compared with neighboring cells. The threshold for GC T cell activation may be higher than that of early activated T cells, possibly through intrinsic changes in cell signaling or through the action of negative costimulatory molecules. The time window for selection in the light zone is tightly regulated, such that all GC B cells must undergo apoptosis, exit the GC, or return to the dark zone within a few hours of entering the light zone. The signals that dictate the differentiation of GC B cells into plasma cells or memory B cells, versus return to the dark zone, need further definition but may be related to the stimulatory signals received from interactions with GC T cells or with other accessory cells (Casamayor-Palleja *et al.*, 1996; Liu *et al.*, 1991a).

REFERENCES

Allen, C. D., Ansel, K. M., Low, C., Lesley, R., Tamamura, H., Fujii, N., and Cyster, J. G. (2004). Germinal center dark and light zone organization is mediated by CXCR4 and CXCR5. *Nat Immunol* **5**: 943-952.

Amara, A., Lorthioir, O., Valenzuela, A., Magerus, A., Thelen, M., Montes, M., Virelizier, J. L., Delepierre, M., Baleux, F., Lortat-Jacob, H., and Arenzana-Seisdedos, F. (1999). Stromal cell-derived factor-1alpha associates with heparan sulfates through the first beta-strand of the chemokine. *J Biol Chem* **274**: 23916-23925.

Ansel, K. M., Ngo, V. N., Hyman, P. L., Luther, S. A., Forster, R., Sedgwick, J. D., Browning, J. L., Lipp, M., and Cyster, J. G. (2000). A chemokine-driven positive feedback loop organizes lymphoid follicles. *Nature* **406**: 309-314.

Ara, T., Itoi, M., Kawabata, K., Egawa, T., Tokoyoda, K., Sugiyama, T., Fujii, N., Amagai, T., and Nagasawa, T. (2003). A role of CXC chemokine ligand 12/stromal cell-derived factor-1/pre-B cell growth stimulating factor and its receptor CXCR4 in fetal and adult T cell development in vivo. *J Immunol* **170**: 4649-4655.

Bachmann, M. F., and Zinkernagel, R. M. (1997). Neutralizing antiviral B cell responses. *Annu Rev Immunol* **15**: 235-270.

Bajenoff, M., Egen, J. G., Koo, L. Y., Laugier, J. P., Brau, F., Glaichenhaus, N., and Germain, R. N. (2006). Stromal cell networks regulate lymphocyte entry, migration, and territoriality in lymph nodes. *Immunity* **25**: 989-1001.

Balogh, P., Aydar, Y., Tew, J. G., and Szakal, A. K. (2002). Appearance and phenotype of murine follicular dendritic cells expressing VCAM-1. *Anat Rec* **268**: 160-168.

Barnden, M. J., Allison, J., Heath, W. R., and Carbone, F. R. (1998). Defective TCR expression in transgenic mice constructed using cDNA-based alpha- and beta-chain genes under the control of heterologous regulatory elements. *Immunol Cell Biol* **76**: 34-40.

Batista, F. D., and Neuberger, M. S. (1998). Affinity dependence of the B cell response to antigen: a threshold, a ceiling, and the importance of off-rate. *Immunity* **8**: 751-759.

Benson, M. J., Erickson, L. D., Gleeson, M. W., and Noelle, R. J. (2007). Affinity of antigen encounter and other early B-cell signals determine B-cell fate. *Curr Opin Immunol* **19**: 275-280.

Berek, C., Berger, A., and Apel, M. (1991). Maturation of the immune response in germinal centers. *Cell* **67**: 1121-1129.

Bleul, C. C., Fuhlbrigge, R. C., Casasnovas, J. M., Aiuti, A., and Springer, T. A. (1996). A highly efficacious lymphocyte chemoattractant, stromal cell-derived factor 1 (SDF-1). *J Exp Med* **184**: 1101-1109.

Bleul, C. C., Schultze, J. L., and Springer, T. A. (1998). B lymphocyte chemotaxis regulated in association with microanatomic localization, differentiation state, and B cell receptor engagement. *J Exp Med* **187**: 753-762.

Blink, E. J., Light, A., Kallies, A., Nutt, S. L., Hodgkin, P. D., and Tarlinton, D. M. (2005). Early appearance of germinal center-derived memory B cells and plasma cells in blood after primary immunization. *J Exp Med* **201**: 545-554.

Bowman, E. P., Campbell, J. J., Soler, D., Dong, Z., Manlongat, N., Picarella, D., Hardy, R. R., and Butcher, E. C. (2000). Developmental switches in chemokine response profiles during B cell differentiation and maturation. *J Exp Med* **191**: 1303-1318.

Brachtel, E. F., Washiyama, M., Johnson, G. D., Tenner-Racz, K., Racz, P., and MacLennan, I. C. (1996). Differences in the germinal centres of palatine tonsils and lymph nodes. *Scand J Immunol* **43**: 239-247.

Cahalan, M. D., and Parker, I. (2006). Imaging the choreography of lymphocyte trafficking and the immune response. *Curr Opin Immunol* **18**: 476-482.

Calame, K. L., Lin, K. I., and Tunyaplin, C. (2003). Regulatory mechanisms that determine the development and function of plasma cells. *Annu Rev Immunol* **21**: 205-230.

Camacho, S. A., Kosco-Vilbois, M. H., and Berek, C. (1998). The dynamic structure of the germinal center. *Immunol Today* **19**: 511-514.

Casamayor-Palleja, M., Feuillard, J., Ball, J., Drew, M., and MacLennan, I. C. (1996). Centrocytes rapidly adopt a memory B cell phenotype on co-culture with autologous germinal centre T cell-enriched preparations. *Int Immunol* **8**: 737-744.

Casamayor-Palleja, M., Mondiere, P., Amara, A., Bella, C., Dieu-Nosjean, M. C., Caux, C., and Defrance, T. (2001). Expression of macrophage inflammatory protein-3alpha, stromal cell-derived factor-1, and B-cell-attracting chemokine-1 identifies the tonsil crypt as an attractive site for B cells. *Blood* **97**: 3992-3994.

Casamayor-Palleja, M., Mondiere, P., Verschelde, C., Bella, C., and Defrance, T. (2002). BCR ligation reprograms B cells for migration to the T zone and B-cell follicle sequentially. *Blood* **99**: 1913-1921.

Cascalho, M., Ma, A., Lee, S., Masat, L., and Wabl, M. (1996). A quasi-monoclonal mouse. *Science* **272**: 1649-1652.

Casola, S., and Rajewsky, K. (2006). B cell recruitment and selection in mouse GALT germinal centers. *Curr Top Microbiol Immunol* **308**: 155-171.

Cattoretti, G., Buttner, M., Shaknovich, R., Kremmer, E., Alobeid, B., and Niedobitek, G. (2006). Nuclear and cytoplasmic AID in extrafollicular and germinal center B cells. *Blood* **107**: 3967-3975.

Cinamon, G., Matloubian, M., Lesneski, M. J., Xu, Y., Low, C., Lu, T., Proia, R. L., and Cyster, J. G. (2004). Sphingosine 1-phosphate receptor 1 promotes B cell localization in the splenic marginal zone. *Nat Immunol*.

Close, P. M., Pringle, J. H., Ruprai, A. K., West, K. P., and Lauder, I. (1990). Zonal distribution of immunoglobulin-synthesizing cells within the germinal centre: an in situ hybridization and immunohistochemical study. *J Pathol* **162**: 209-216.

Congdon, C. C. (1962). Effect of injection of foreign bone marrow on the lymphatic tissues of normal mice. *J Natl Cancer Inst* **28**: 305-329.

Corcione, A., Ottonello, L., Tortolina, G., Facchetti, P., Airoldi, I., Guglielmino, R., Dadati, P., Truini, M., Sozzani, S., Dallegri, F., and Pistoia, V. (2000). Stromal cell-derived factor-1 as a chemoattractant for follicular center lymphoma B cells. *J Natl Cancer Inst* **92**: 628-635.

Corcione, A., Tortolina, G., Bonecchi, R., Battilana, N., Taborelli, G., Malavasi, F., Sozzani, S., Ottonello, L., Dallegri, F., and Pistoia, V. (2002). Chemotaxis of human tonsil B lymphocytes to CC chemokine receptor (CCR) 1, CCR2 and CCR4 ligands is restricted to non-germinal center cells. *Int Immunol* **14**: 883-892.

Cyster, J. G. (1999). Chemokines and cell migration in secondary lymphoid organs. *Science* **286**: 2098-2102.

Cyster, J. G., Ansel, K. M., Reif, K., Ekland, E. H., Hyman, P. L., Tang, H. L., Luther, S. A., and Ngo, V. N. (2000). Follicular stromal cells and lymphocyte homing to follicles. *Immunol Rev* **176**: 181-193.

Dal Porto, J. M., Haberman, A. M., Shlomchik, M. J., and Kelsoe, G. (1998). Antigen drives very low affinity B cells to become plasmacytes and enter germinal centers. *J Immunol* **161**: 5373-5381.

Dal Porto, J. M., Haberman, A. M., Kelsoe, G., and Shlomchik, M. J. (2002). Very low affinity B cells form germinal centers, become memory B cells, and participate in secondary immune responses when higher affinity competition is reduced. *J Exp Med* **195**: 1215-1221.

Deenen, G. J., Opstelten, D., and Nieuwenhuis, P. (1984). Homing of germinal-center cells into germinal centers of lymph node via afferent lymphatics. An autoradiographic study in rabbits. *Cell Tissue Res* **238**: 183-189.

Egawa, T., Kawabata, K., Kawamoto, H., Amada, K., Okamoto, R., Fujii, N., Kishimoto, T., Katsura, Y., and Nagasawa, T. (2001). The earliest stages of B cell development require a chemokine stromal cell-derived factor/pre-B cell growth-stimulating factor. *Immunity* **15**: 323-334.

Eisen, H. N., and Siskind, G. W. (1964). Variations in Affinities of Antibodies During the Immune Response. *Biochemistry (Mosc)* **3**: 996-1008.

Estes, J. D., Keele, B. F., Tenner-Racz, K., Racz, P., Redd, M. A., Thacker, T. C., Jiang, Y., Lloyd, M. J., Gartner, S., and Burton, G. F. (2002). Follicular dendritic cell-mediated up-regulation of CXCR4 expression on CD4 T cells and HIV pathogenesis. *J Immunol* **169**: 2313-2322.

Fang, Y., Xu, C., Fu, Y. X., Holers, V. M., and Molina, H. (1998). Expression of complement receptors 1 and 2 on follicular dendritic cells is necessary for the generation of a strong antigen-specific IgG response. *J Immunol* **160**: 5273-5279.

Ferguson, A. R., Youd, M. E., and Corley, R. B. (2004). Marginal zone B cells transport and deposit IgM-containing immune complexes onto follicular dendritic cells. *Int Immunol* **16**: 1411-1422.

Feuillard, J., Taylor, D., Casamayor-Palleja, M., Johnson, G. D., and MacLennan, I. C. (1995). Isolation and characteristics of tonsil centroblasts with reference to Ig class switching. *Int Immunol* **7**: 121-130.

Fliedner, T., Kesse, M., Cronkite, E. P., and Robertson, J. S. (1964). Cell Proliferation in Germinal Centers of the Rat Spleen. *Ann N Y Acad Sci* **113**: 578-594.

Forster, R., Mattis, A. E., Kremmer, E., Wolf, E., Brem, G., and Lipp, M. (1996). A putative chemokine receptor, BLR1, directs B cell migration to defined lymphoid organs and specific anatomic compartments of the spleen. *Cell* **87**: 1037-1047.

Forster, R., Kremmer, E., Schubel, A., Breitfeld, D., Kleinschmidt, A., Nerl, C., Bernhardt, G., and Lipp, M. (1998). Intracellular and surface expression of the HIV-1 coreceptor CXCR4/fusin on various leukocyte subsets: rapid internalization and recycling upon activation. *J Immunol* **160**: 1522-1531.

Freedman, A. S., Munro, J. M., Rice, G. E., Bevilacqua, M. P., Morimoto, C., McIntyre, B. W., Rhynhart, K., Pober, J. S., and Nadler, L. M. (1990). Adhesion of human B cells to germinal centers in vitro involves VLA-4 and INCAM-110. *Science* **249**: 1030-1033.

Furukawa, K., Akasako-Furukawa, A., Shirai, H., Nakamura, H., and Azuma, T. (1999). Junctional amino acids determine the maturation pathway of an antibody. *Immunity* **11**: 329-338.

Futterer, A., Mink, K., Luz, A., Kosco-Vilbois, M. H., and Pfeffer, K. (1998). The lymphotoxin beta receptor controls organogenesis and affinity maturation in peripheral lymphoid tissues. *Immunity* **9**: 59-70.

Garside, P., Ingulli, E., Merica, R. R., Johnson, J. G., Noelle, R. J., and Jenkins, M. K. (1998). Visualization of specific B and T lymphocyte interactions in the lymph node. *Science* **281**: 96-99.

Gatto, D., Martin, S. W., Bessa, J., Pellicioli, E., Saudan, P., Hinton, H. J., and Bachmann, M. F. (2007). Regulation of memory antibody levels: the role of persisting antigen versus plasma cell life span. *J Immunol* **178**: 67-76.

Goodnow, C. C., Crosbie, J., Adelstein, S., Lavoie, T. B., Smith-Gill, S. J., Brink, R. A., Pritchard-Briscoe, H., Wotherspoon, J. S., Loblay, R. H., Raphael, K., Trent, R. J., and Basten, A. (1988). Altered immunoglobulin expression and functional silencing of self-reactive B lymphocytes in transgenic mice. *Nature* **334**: 676-682.

Guinamard, R., Signoret, N., Ishiai, M., Marsh, M., Kurosaki, T., and Ravetch, J. V. (1999). B cell antigen receptor engagement inhibits stromal cell-derived factor (SDF)-1alpha chemotaxis and promotes protein kinase C (PKC)-induced internalization of CXCR4. *J Exp Med* **189**: 1461-1466.

Haberman, A. M., and Shlomchik, M. J. (2003). Reassessing the function of immune-complex retention by follicular dendritic cells. *Nat Rev Immunol* **3**: 757-764.

Hanna, M. G., Jr. (1964). An Autoradiographic Study of the Germinal Center in Spleen White Pulp During Early Intervals of the Immune Response. *Lab Invest* **13**: 95-104.

Hannum, L. G., Haberman, A. M., Anderson, S. M., and Shlomchik, M. J. (2000). Germinal center initiation, variable gene region hypermutation, and mutant B cell selection without detectable immune complexes on follicular dendritic cells. *J Exp Med* **192**: 931-942.

Hardie, D. L., Johnson, G. D., Khan, M., and MacLennan, I. C. (1993). Quantitative analysis of molecules which distinguish functional compartments within germinal centers. *Eur J Immunol* **23**: 997-1004.

Hargreaves, D. C., Hyman, P. L., Lu, T. T., Ngo, V. N., Bidgol, A., Suzuki, G., Zou, Y. R., Littman, D. R., and Cyster, J. G. (2001). A coordinated change in chemokine responsiveness guides plasma cell movements. *J Exp Med* **194**: 45-56.

Hauser, A. E., Junt, T., Mempel, T. R., Sneddon, M. W., Kleinstein, S. H., Henrickson, S. E., von Andrian, U. H., Shlomchik, M. J., and Haberman, A. M. (2007). Definition of germinal-center B cell migration in vivo reveals predominant intrazonal circulation patterns. *Immunity* **26**: 655-667.

Hernandez, P. A., Gorlin, R. J., Lukens, J. N., Taniuchi, S., Bohinjec, J., Francois, F., Klotman, M. E., and Diaz, G. A. (2003). Mutations in the chemokine receptor gene CXCR4 are associated with WHIM syndrome, a combined immunodeficiency disease. *Nat Genet* **34**: 70-74.

Jacob, J., Kassir, R., and Kelsoe, G. (1991a). In situ studies of the primary immune response to (4-hydroxy-3-nitrophenyl)acetyl. I. The architecture and dynamics of responding cell populations. *J Exp Med* **173**: 1165-1175.

Jacob, J., Kelsoe, G., Rajewsky, K., and Weiss, U. (1991b). Intraclonal generation of antibody mutants in germinal centres. *Nature* **354**: 389-392.

Jacob, J., and Kelsoe, G. (1992). In situ studies of the primary immune response to (4-hydroxy-3-nitrophenyl)acetyl. II. A common clonal origin for periarteriolar lymphoid sheath-associated foci and germinal centers. *J Exp Med* **176**: 679-687.

Kallies, A., Hasbold, J., Tarlinton, D. M., Dietrich, W., Corcoran, L. M., Hodgkin, P. D., and Nutt, S. L. (2004). Plasma cell ontogeny defined by quantitative changes in blimp-1 expression. *J Exp Med* **200**: 967-977.

Kelsoe, G. (1996). Life and death in germinal centers (redux). *Immunity* **4**: 107-111.

Kepler, T. B., and Perelson, A. S. (1993). Cyclic re-entry of germinal center B cells and the efficiency of affinity maturation. *Immunol Today* **14**: 412-415.

Kindred, J. E. (1938). A quantitative study of the lymphoid organs of the albino rat. *Am J Anat* **62**: 453-473.

Klein, U., Tu, Y., Stolovitzky, G. A., Keller, J. L., Haddad, J., Jr., Miljkovic, V., Cattoretti, G., Califano, A., and Dalla-Favera, R. (2003). Transcriptional analysis of the B cell germinal center reaction. *Proc Natl Acad Sci U S A* **100**: 2639-2644.

Koburg, E. (1966). Cell Production and Cell Migration in the Tonsil. Paper presented at: Germinal Centers in Immune Responses (University of Bern, Switzerland, Springer-Verlag New York Inc.).

Koni, P. A., Sacca, R., Lawton, P., Browning, J. L., Ruddle, N. H., and Flavell, R. A. (1997). Distinct roles in lymphoid organogenesis for lymphotoxins alpha and beta revealed in lymphotoxin beta-deficient mice. *Immunity* **6**: 491-500.

Koni, P. A., and Flavell, R. A. (1999). Lymph node germinal centers form in the absence of follicular dendritic cell networks. *J Exp Med* **189**: 855-864.

Koopman, G., Parmentier, H. K., Schuurman, H. J., Newman, W., Meijer, C. J., and Pals, S. T. (1991). Adhesion of human B cells to follicular dendritic cells involves both the lymphocyte function-associated antigen 1/intercellular adhesion molecule 1 and very late antigen 4/vascular cell adhesion molecule 1 pathways. *J Exp Med* **173**: 1297-1304.

Koopman, G., Keehnen, R. M., Lindhout, E., Newman, W., Shimizu, Y., van Seventer, G. A., de Groot, C., and Pals, S. T. (1994). Adhesion through the LFA-1 (CD11a/CD18)-ICAM-1 (CD54) and the VLA-4 (CD49d)-VCAM-1 (CD106) pathways prevents apoptosis of germinal center B cells. *J Immunol* **152**: 3760-3767.

Kosco, M. H., Pflugfelder, E., and Gray, D. (1992). Follicular dendritic cell-dependent adhesion and proliferation of B cells in vitro. *J Immunol* **148**: 2331-2339.

Kosco-Vilbois, M. H. (2003). Are follicular dendritic cells really good for nothing? *Nat Rev Immunol* **3**: 764-769.

Kraal, G., Weissman, I. L., and Butcher, E. C. (1982). Germinal centre B cells: antigen specificity and changes in heavy chain class expression. *Nature* **298**: 377-379.

Krug, A., Uppaluri, R., Facchetti, F., Dorner, B. G., Sheehan, K. C., Schreiber, R. D., Cella, M., and Colonna, M. (2002). IFN-producing cells respond to CXCR3 ligands in the presence of CXCL12 and secrete inflammatory chemokines upon activation. *J Immunol* **169**: 6079-6083.

Lavoie, T. B., Drohan, W. N., and Smith-Gill, S. J. (1992). Experimental analysis by site-directed mutagenesis of somatic mutation effects on affinity and fine specificity in antibodies specific for lysozyme. *J Immunol* **148**: 503-513.

Li, L., and Choi, Y. S. (2002). Follicular dendritic cell-signaling molecules required for proliferation and differentiation of GC-B cells. *Semin Immunol* **14**: 259-266.

Lindquist, R. L., Shakhar, G., Dudziak, D., Wardemann, H., Eisenreich, T., Dustin, M. L., and Nussenzweig, M. C. (2004). Visualizing dendritic cell networks in vivo. *Nat Immunol* **5**: 1243-1250.

Liu, Y. J., Cairns, J. A., Holder, M. J., Abbot, S. D., Jansen, K. U., Bonnefoy, J. Y., Gordon, J., and MacLennan, I. C. (1991a). Recombinant 25-kDa CD23 and interleukin 1 alpha promote the survival of germinal center B cells: evidence for bifurcation in the development of centrocytes rescued from apoptosis. *Eur J Immunol* **21**: 1107-1114.

Liu, Y. J., Zhang, J., Lane, P. J., Chan, E. Y., and MacLennan, I. C. (1991b). Sites of specific B cell activation in primary and secondary responses to T cell-dependent and T cell-independent antigens. *Eur J Immunol* **21**: 2951-2962.

Liu, Y. J., Johnson, G. D., Gordon, J., and MacLennan, I. C. (1992). Germinal centres in T-cell-dependent antibody responses. *Immunol Today* **13**: 17-21.

Luther, S. A., Gulbranson-Judge, A., Acha-Orbea, H., and MacLennan, I. C. (1997). Viral superantigen drives extrafollicular and follicular B cell differentiation leading to virus-specific antibody production. *J Exp Med* **185**: 551-562.

Ma, Q., Jones, D., Borghesani, P. R., Segal, R. A., Nagasawa, T., Kishimoto, T., Bronson, R. T., and Springer, T. A. (1998). Impaired B-lymphopoiesis, myelopoiesis, and derailed cerebellar neuron migration in CXCR4- and SDF-1-deficient mice. *Proc Natl Acad Sci U S A* **95**: 9448-9453.

MacLennan, I. C. (1994). Germinal centers. *Annu Rev Immunol* **12**: 117-139.

MacLennan, I. C., Gulbranson-Judge, A., Toellner, K. M., Casamayor-Palleja, M., Chan, E., Sze, D. M., Luther, S. A., and Orbea, H. A. (1997). The changing preference of T and B cells for partners as T-dependent antibody responses develop. *Immunol Rev* **156**: 53-66.

Maeda, K., Burton, G. F., Padgett, D. A., Conrad, D. H., Huff, T. F., Masuda, A., Szakal, A. K., and Tew, J. G. (1992). Murine follicular dendritic cells and low affinity Fc receptors for IgE (Fc epsilon RII). *J Immunol* **148**: 2340-2347.

Manser, T. (2004). Textbook germinal centers? *J Immunol* **172**: 3369-3375.

Marchese, A., and Benovic, J. L. (2001). Agonist-promoted ubiquitination of the G protein-coupled receptor CXCR4 mediates lysosomal sorting. *J Biol Chem* **276**: 45509-45512.

Martin, C., Burdon, P. C., Bridger, G., Gutierrez-Ramos, J. C., Williams, T. J., and Rankin, S. M. (2003). Chemokines acting via CXCR2 and CXCR4 control the release of neutrophils from the bone marrow and their return following senescence. *Immunity* **19**: 583-593.

Martin, F., Oliver, A. M., and Kearney, J. F. (2001). Marginal Zone and B1 B Cells Unite in the Early Response against T-Independent Blood-Borne Particulate Antigens. *Immunity* **14**: 617-629.

Martinez-Pomares, L., Kosco-Vilbois, M., Darley, E., Tree, P., Herren, S., Bonnefoy, J. Y., and Gordon, S. (1996). Fc chimeric protein containing the cysteine-rich domain of the murine mannose receptor binds to macrophages from splenic marginal zone and lymph node subcapsular sinus and to germinal centers. *J Exp Med* **184**: 1927-1937.

Matsumoto, M., Lo, S. F., Carruthers, C. J., Min, J., Mariathasan, S., Huang, G., Plas, D. R., Martin, S. M., Geha, R. S., Nahm, M. H., and Chaplin, D. D. (1996). Affinity maturation without germinal centres in lymphotoxin-alpha-deficient mice. *Nature* **382**: 462-466.

McHeyzer-Williams, L. J., Malherbe, L. P., and McHeyzer-Williams, M. G. (2006). Checkpoints in memory B-cell evolution. *Immunol Rev* **211**: 255-268.

McHeyzer-Williams, M. G., and Ahmed, R. (1999). B cell memory and the long-lived plasma cell. *Curr Opin Immunol* **11**: 172-179.

Messmer, B. T. (2005). SAIVGeM: spreadsheet analysis of immunoglobulin VH gene mutations. *Biotechniques* **39**: 353-358.

Meyer-Hermann, M. E., Maini, P. K., and Iber, D. (2006). An analysis of B cell selection mechanisms in germinal centers. *Math Med Biol* **23**: 255-277.

Miller, M. J., Wei, S. H., Parker, I., and Cahalan, M. D. (2002). Two-photon imaging of lymphocyte motility and antigen response in intact lymph node. *Science* **296**: 1869-1873.

Millikin, P. D. (1966). Anatomy of germinal centers in human lymphoid tissue. *Arch Pathol* **82**: 499-505.

Moldenhauer, G., Popov, S. W., Wotschke, B., Bruderlein, S., Riedl, P., Fissolo, N., Schirmbeck, R., Ritz, O., Moller, P., and Leithauser, F. (2006). AID expression identifies interfollicular large B cells as putative precursors of mature B-cell malignancies. *Blood* **107**: 2470-2473.

Mond, J. J., Lees, A., and Snapper, C. M. (1995). T cell-independent antigens type 2. *Annu Rev Immunol* **13**: 655-692.

Nakayama, Y., Stabach, P., Maher, S. E., Mahajan, M. C., Masiar, P., Liao, C., Zhang, X., Ye, Z. J., Tuck, D., Bothwell, A. L., Newburger, P. E., and Weissman, S. M. (2006). A limited number of genes are involved in the differentiation of germinal center B cells. *J Cell Biochem* **99**: 1308-1325.

Ngo, V. N., Tang, H. L., and Cyster, J. G. (1998). Epstein-Barr virus-induced molecule 1 ligand chemokine is expressed by dendritic cells in lymphoid tissues and strongly attracts naive T cells and activated B cells. *J Exp Med* **188**: 181-191.

Nieuwenhuis, P., and Opstelten, D. (1984). Functional anatomy of germinal centers. *Am J Anat* **170**: 421-435.

Okada, T., Ngo, V. N., Ekland, E. H., Forster, R., Lipp, M., Littman, D. R., and Cyster, J. G. (2002). Chemokine requirements for B cell entry to lymph nodes and Peyer's patches. *J Exp Med* **196**: 65-75.

Okada, T., Miller, M. J., Parker, I., Krummel, M. F., Neighbors, M., Hartley, S. B., O'Garra, A., Cahalan, M. D., and Cyster, J. G. (2005). Antigen-engaged B cells undergo chemotaxis toward the T zone and form motile conjugates with helper T cells. *PLoS Biol* **3**: e150.

Opstelten, D., Stikker, R., Deenen, G. J., Bos, L., and Nieuwenhuis, P. (1981). Germinal centers and the B-cell system. VI. Migration pattern of germinal-center cells of the rabbit appendix. *Cell Tissue Res* **218**: 59-73.

Opstelten, D., Stikker, R., Deenen, G. J., and Nieuwenhuis, P. (1982). Germinal centers and the B-cell system. VII. Complement receptors, antigen receptors, immunoglobulin and alkaline phosphatase in germinal centers of the rabbit appendix and popliteal lymph nodes. *Cell Tissue Res* **224**: 505-516.

Opstelten, D., Deenen, G. J., Stikker, R., Bos, L., and Nieuwenhuis, P. (1983). Germinal centers and the B cell system. VIII. Functional characteristics and cell surface markers of germinal center cell subsets differing in density and in sedimentation velocity. *Immunobiology* **165**: 1-14.

Or-Guil, M., Wittenbrink, N., Weiser, A. A., and Schuchhardt, J. (2007). Recirculation of germinal center B cells: a multilevel selection strategy for antibody maturation. *Immunol Rev* **216**: 130-141.

Pape, K. A., Catron, D. M., Itano, A. A., and Jenkins, M. K. (2007). The humoral immune response is initiated in lymph nodes by B cells that acquire soluble antigen directly in the follicles. *Immunity* **26**: 491-502.

Paus, D., Phan, T. G., Chan, T. D., Gardam, S., Basten, A., and Brink, R. (2006). Antigen recognition strength regulates the choice between extrafollicular plasma cell and germinal center B cell differentiation. *J Exp Med* **203**: 1081-1091.

Petrasch, S. G., Kosco, M. H., Perez-Alvarez, C. J., Schmitz, J., and Brittinger, G. (1991). Proliferation of germinal center B lymphocytes in vitro by direct membrane contact with follicular dendritic cells. *Immunobiology* **183**: 451-462.

Phan, T. G., Paus, D., Chan, T. D., Turner, M. L., Nutt, S. L., Basten, A., and Brink, R. (2006). High affinity germinal center B cells are actively selected into the plasma cell compartment. *J Exp Med*.

Plotkin, J., Prockop, S. E., Lepique, A., and Petrie, H. T. (2003). Critical role for CXCR4 signaling in progenitor localization and T cell differentiation in the postnatal thymus. *J Immunol* **171**: 4521-4527.

Prager, E. M., and Wilson, A. C. (1971). Multiple lysozymes of duck egg white. *J Biol Chem* **246**: 523-530.

Qi, H., Egen, J. G., Huang, A. Y., and Germain, R. N. (2006). Extrafollicular activation of lymph node B cells by antigen-bearing dendritic cells. *Science* **312**: 1672-1676.

Rahman, Z. S., Rao, S. P., Kalled, S. L., and Manser, T. (2003). Normal induction but attenuated progression of germinal center responses in BAFF and BAFF-R signaling-deficient mice. *J Exp Med* **198**: 1157-1169.

Reichert, R. A., Gallatin, W. M., Weissman, I. L., and Butcher, E. C. (1983). Germinal center B cells lack homing receptors necessary for normal lymphocyte recirculation. *J Exp Med* **157**: 813-827.

Röhlich, K. (1930). Beitrag zur Cytologie der Keimzentren der Lymphknoten. *Z Mikrosk Anat Forsch* **20**: 287-297.

Röhlich, K. (1933). Struktur und Blutgesfässversorgung der Keimzentren. *Anat Anz* **76**: 215-222.

Rossbacher, J., Haberman, A. M., Neschen, S., Khalil, A., and Shlomchik, M. J. (2006). Antibody-independent B cell-intrinsic and -extrinsic roles for CD21/35. *Eur J Immunol* **36**: 2384-2393.

Roy, M. P., Kim, C. H., and Butcher, E. C. (2002). Cytokine control of memory B cell homing machinery. *J Immunol* **169**: 1676-1682.

Ryser, J. E., Blauenstein, P., Remy, N., Weinreich, R., Hasler, P. H., Novak-Hofer, I., and Schubiger, P. A. (1999). [76Br]Bromodeoxyuridine, a potential tracer for the measurement of cell proliferation by positron emission tomography, in vitro and in vivo studies in mice. *Nucl Med Biol* **26**: 673-679.

Schwickert, T. A., Lindquist, R. L., Shakhar, G., Livshits, G., Skokos, D., Kosco-Vilbois, M. H., Dustin, M. L., and Nussenzweig, M. C. (2007). In vivo imaging of germinal centres reveals a dynamic open structure. *Nature* **446**: 83-87.

Secord, E. A., Edington, J. M., and Thorbecke, G. J. (1995). The Emu-bcl-2 transgene enhances antigen-induced germinal center formation in both BALB/c and SJL mice but causes age-dependent germinal center hyperplasia only in the lymphoma-prone SJL strain. *Am J Pathol* **147**: 422-433.

Shaffer, A. L., Lin, K. I., Kuo, T. C., Yu, X., Hurt, E. M., Rosenwald, A., Giltnane, J. M., Yang, L., Zhao, H., Calame, K., and Staudt, L. M. (2002). Blimp-1 orchestrates plasma cell differentiation by extinguishing the mature B cell gene expression program. *Immunity* **17**: 51-62.

Shih, T. A., Meffre, E., Roederer, M., and Nussenzweig, M. C. (2002). Role of BCR affinity in T cell dependent antibody responses in vivo. *Nat Immunol* **3**: 570-575.

Shinall, S. M., Gonzalez-Fernandez, M., Noelle, R. J., and Waldschmidt, T. J. (2000). Identification of murine germinal center B cell subsets defined by the expression of surface isotypes and differentiation antigens. *J Immunol* **164**: 5729-5738.

Smith, K. G., Light, A., O'Reilly, L. A., Ang, S. M., Strasser, A., and Tarlinton, D. (2000). bcl-2 transgene expression inhibits apoptosis in the germinal center and reveals differences in the selection of memory B cells and bone marrow antibody-forming cells. *J Exp Med* **191**: 475-484.

Sozzani, S., Luini, W., Molino, M., Jilek, P., Bottazzi, B., Cerletti, C., Matsushima, K., and Mantovani, A. (1991). The signal transduction pathway involved in the migration induced by a monocyte chemotactic cytokine. *J Immunol* **147**: 2215-2221.

Stachowiak, A. N., Wang, Y., Huang, Y. C., and Irvine, D. J. (2006). Homeostatic lymphoid chemokines synergize with adhesion ligands to trigger T and B lymphocyte chemokinesis. *J Immunol* **177**: 2340-2348.

Strasser, A., Whittingham, S., Vaux, D. L., Bath, M. L., Adams, J. M., Cory, S., and Harris, A. W. (1991). Enforced BCL2 expression in B-lymphoid cells prolongs antibody responses and elicits autoimmune disease. *Proc Natl Acad Sci U S A* **88**: 8661-8665.

Sumen, C., Mempel, T. R., Mazo, I. B., and von Andrian, U. H. (2004). Intravital microscopy: visualizing immunity in context. *Immunity* **21**: 315-329.

Szakal, A. K., Holmes, K. L., and Tew, J. G. (1983). Transport of immune complexes from the subcapsular sinus to lymph node follicles on the surface of nonphagocytic cells, including cells with dendritic morphology. *J Immunol* **131**: 1714-1727.

Szakal, A. K., Kosco, M. H., and Tew, J. G. (1989). Microanatomy of lymphoid tissue during humoral immune responses: structure function relationships. *Annu Rev Immunol* **7**: 91-109.

Takahashi, Y., Dutta, P. R., Cerasoli, D. M., and Kelsoe, G. (1998). In situ studies of the primary immune response to (4-hydroxy-3-nitrophenyl)acetyl. V. Affinity maturation develops in two stages of clonal selection. *J Exp Med* **187**: 885-895.

Takahashi, Y., Ohta, H., and Takemori, T. (2001). Fas is required for clonal selection in germinal centers and the subsequent establishment of the memory B cell repertoire. *Immunity* **14**: 181-192.

Taki, S., Meiering, M., and Rajewsky, K. (1993). Targeted insertion of a variable region gene into the immunoglobulin heavy chain locus. *Science* **262**: 1268-1271.

Tamamura, H., Hiramatsu, K., Mizumoto, M., Ueda, S., Kusano, S., Terakubo, S., Akamatsu, M., Yamamoto, N., Trent, J. O., Wang, Z., Peiper, S. C., Nakashima, H., Otaka, A., and Fujii, N. (2003). Enhancement of the T140-based pharmacophores leads to the development of more potent and bio-stable CXCR4 antagonists. *Org Biomol Chem* **1**: 3663-3669.

Tarlinton, D. (2006). B-cell memory: are subsets necessary? *Nat Rev Immunol* **6**: 785-790.

Tarlinton, D. M., and Smith, K. G. (2000). Dissecting affinity maturation: a model explaining selection of antibody-forming cells and memory B cells in the germinal centre. *Immunol Today* **21**: 436-441.

Tippmann, H. F. (2004). Analysis for free: comparing programs for sequence analysis. *Brief Bioinform* **5**: 82-87.

van Galen, J. C., Dukers, D. F., Giroth, C., Sewalt, R. G., Otte, A. P., Meijer, C. J., and Raaphorst, F. M. (2004). Distinct expression patterns of polycomb oncoproteins and their binding partners during the germinal center reaction. *Eur J Immunol* **34**: 1870-1881.

Vinuesa, C. G., Cook, M. C., Ball, J., Drew, M., Sunners, Y., Cascalho, M., Wabl, M., Klaus, G. G., and MacLennan, I. C. (2000). Germinal centers without T cells. *J Exp Med* **191**: 485-494.

Vinuesa, C. G., and Cook, M. C. (2001). The molecular basis of lymphoid architecture and B cell responses: implications for immunodeficiency and immunopathology. *Curr Mol Med* **1**: 689-725.

Vinuesa, C. G., Tangye, S. G., Moser, B., and Mackay, C. R. (2005). Follicular B helper T cells in antibody responses and autoimmunity. *Nat Rev Immunol* **5**: 853-865.

Voigt, I., Camacho, S. A., de Boer, B. A., Lipp, M., Forster, R., and Berek, C. (2000). CXCR5-deficient mice develop functional germinal centers in the splenic T cell zone. *Eur J Immunol* **30**: 560-567.

Vonderheide, R. H., and Hunt, S. V. (1990). Does the availability of either B cells or CD4+ cells limit germinal centre formation? *Immunology* **69**: 487-489.

Wang, Y., Huang, G., Wang, J., Molina, H., Chaplin, D. D., and Fu, Y. X. (2000). Antigen persistence is required for somatic mutation and affinity maturation of immunoglobulin. *Eur J Immunol* **30**: 2226-2234.

Wang, Y., and Carter, R. H. (2005). CD19 regulates B cell maturation, proliferation, and positive selection in the FDC zone of murine splenic germinal centers. *Immunity* **22**: 749-761.

Wehrli, N., Legler, D. F., Finke, D., Toellner, K. M., Loetscher, P., Baggiolini, M., MacLennan, I. C., and Acha-Orbea, H. (2001). Changing responsiveness to chemokines allows medullary plasmablasts to leave lymph nodes. *Eur J Immunol* **31**: 609-616.

Wolniak, K. L., Noelle, R. J., and Waldschmidt, T. J. (2006). Characterization of (4-hydroxy-3-nitrophenyl)acetyl (NP)-specific germinal center B cells and antigen-binding B220- cells after primary NP challenge in mice. *J Immunol* **177**: 2072-2079.

Zaitoun, A. M. (1980). Cell population kinetics of the germinal centres of lymph nodes of BALB/c mice. *J Anat* **130**: 131-137.

Zhang, J., MacLennan, I. C., Liu, Y. J., and Lane, P. J. (1988). Is rapid proliferation in B centroblasts linked to somatic mutation in memory B cell clones? *Immunol Lett* **18**: 297-299.

Zou, Y. R., Kottmann, A. H., Kuroda, M., Taniuchi, I., and Littman, D. R. (1998). Function of the chemokine receptor CXCR4 in haematopoiesis and in cerebellar development. *Nature* **393**: 595-599.

UCSF LIBRARY RELEASE FORM

Publishing Agreement

It is the policy of the University to encourage the distribution of all theses and dissertations. Copies of all UCSF theses and dissertations will be routed to the library via the Graduate Division. The library will make all theses and dissertations accessible to the public and will preserve these to the best of their abilities, in perpetuity.

Please sign the following statement:

I hereby grant permission to the Graduate Division of the University of California, San Francisco to release copies of my thesis or dissertation to the Campus Library to provide access and preservation, in whole or in part, in perpetuity.

Christyn D.C. Alm
Author Signature

June 15, 2007
Date